A STUDY ON THE METRICS OF NEUTRON INDUCED PRIMARY RADIATION DAMAGE IN STRUCTURAL MATERIALS USING THE RECENT BASIC EVALUATED NUCLEAR DATA LIBRARIES

By

UTTIYOARNAB SAHA

(Enrolment No. PHYS 02 2014 04 007)

INDIRA GANDHI CENTRE FOR ATOMIC RESEARCH

KALPAKKAM

A Thesis Submitted to the

Board of Studies in Physical Sciences

In the Partial Fulfillment of the Requirements for the Degree of

DOCTOR OF PHILOSOPHY

of

HOMI BHABHA NATIONAL INSTITUTE

MAY, 2019

Homi Bhabha National Institute[1]

Recommendations of the Viva Voce Committee

As members of the Viva Voce Committee, we certify that we have read the dissertation prepared by Uttiyoarnab Saha entitled "*A Study on the Metrics of Neutron Induced Primary Radiation Damage in Structural Materials using the Recent Basic Evaluated Nuclear Data Libraries*" and recommend that it may be accepted as fulfilling the thesis requirement for the award of Degree of Doctor of Philosophy.

Chairman- Dr. B. Venkataraman		**Date:** 22/11/19
Guide / Convener- Dr. K. Devan		**Date:** 22/11/2019
Examiner- Dr. Antony Joseph		**Date:** 22/11/2019
Member 1- Dr. M.T. Jose		**Date:** 22/11/2019
Member 2- Dr. N.V. Chandra Shekar	N.V. Chandra Shekar	**Date:** 22/11/2019
Member 3- Dr. Umasankari Kannan	Umasankari Kannan	**Date:** 22/11/2019

Final approval and acceptance of this thesis is contingent upon the candidate's submission of the final copies of the thesis to HBNI.

I hereby certify that I have read this thesis prepared under my direction and recommend that it may be accepted as fulfilling the thesis requirement.

Date: 22/11/2019

Place: Kalpakkam

Guide: Dr. K. Devan

[1] This page is to be included only for final submission after successful completion of viva voce.

STATEMENT BY AUTHOR

This dissertation has been submitted in partial fulfillment of requirements for an advanced degree at Homi Bhabha National Institute (HBNI) and is deposited in the Library to be made available to borrowers under rules of the HBNI.

Brief quotations from this dissertation are allowable without special permission, provided that accurate acknowledgement of source is made. Requests for permission for extended quotation from or reproduction of this manuscript in whole or in part may be granted by the Competent Authority of HBNI when in his or her judgment the proposed use of the material is in the interests of scholarship. In all other instances, however, permission must be obtained from the author.

Uttiyoarnab Saha

Uttiyoarnab Saha

DECLARATION

I, hereby declare that the investigation presented in the thesis has been carried out by me. The work is original and has not been submitted earlier as a whole or in part for a degree / diploma at this or any other Institution / University.

Uttiyoarnab Saha

Uttiyoarnab Saha

To motherland India and my family

List of publications arising from the thesis

Journals

1) **Uttiyoarnab Saha**, K. Devan, Abhitab Bachchan, G. Pandikumar and S. Ganesan, Neutron radiation damage studies in the structural materials of a 500 MWe fast breeder reactor using DPA cross-sections from ENDF/B-VII.1, *Pramana – J. Phys.* (2018) 90:46.
2) **Uttiyoarnab Saha**, K. Devan, S. Ganesan, A study to compute integrated dpa for neutron and ion irradiation environments using SRIM-2013, *Journal of Nuclear Materials* 503 (2018) 30 – 41.
3) **Uttiyoarnab Saha**, K. Devan, S. Ganesan, Propagation of uncertainties in basic nuclear reaction data to uncertainties in the parameters of primary radiation damage by neutrons, *Journal of Nuclear Materials*510 (2018) 43 – 60.
4) **Uttiyoarnab Saha**, K. Devan, S. Ganesan, An estimation of neutron-induced production of gases with propagation of uncertainties in nuclear data for structural materials of fission and fusion reactors, *Journal of Nuclear Materials*519 (2019) 88 – 103.
5) **Uttiyoarnab Saha**, K. Devan, S. Ganesan, Application of arc-dpa model to estimate the primary radiation damage of structural materials by neutrons and the necessity of rescaling dpa versus final experimental damage correlations, *Journal of Nuclear Materials* 522 (2019) 86 – 96.
6) **Uttiyoarnab Saha**, K. Devan, An Estimation of the Neutron Heating Rates in Structural Materials and their Uncertainties due to Basic Evaluated Nuclear Data, *(under review in Progress in Nuclear Energy).*

International / National Conference Proceedings

1) **Uttiyoarnab Saha**, K. Devan, The effect of anisotropy of elastic scattering of neutrons in the dpa cross sections of light and medium mass nuclei, *Proceedings of the DAE-BRNS Symp. on Nucl. Phys*. 61 (2016) 644 – 645.
2) **Uttiyoarnab Saha**, K. Devan, The computation of displacement damage cross sections of silicon, carbon and silicon carbide for high energy applications, *Materials Today: Proceedings* 5 (2018) 16501–16508.

3) **Uttiyoarnab Saha**, K. Devan, Quantifying neutron radiation damage in structural elements from evaluated nuclear data using an indigenous computer code – CRaD, *Proceedings of the DAE Symp. on Nucl. Phys.* 62 (2017)1142 – 1143.
4) **Uttiyoarnab Saha**, K. Devan, The estimation of neutron kerma coefficients from evaluated nuclear data by using the CRaD code, *Proceedings of the DAE Symp. on Nucl. Phys.* 63 (2018) 1116 – 1117.

International / National Conferences / Seminars

1) **Uttiyoarnab Saha**, K. Devan, "Computation of DPA Cross Sections from Evaluated Nuclear Data Libraries", *4th. National Conference on Condensed Matter Physics and Applications*, MIT, Manipal University, Karnataka, (2016),(Best oral presentation award).
2) **Uttiyoarnab Saha**, K. Devan, "The Effect of Anisotropy of Elastic Scattering of Neutrons in the DPA Cross Sections of Light and Medium Mass Nuclei, *61st. DAE-BRNS Symposium on Nuclear Physics*, SINP, West Bengal, (2016).
3) **Uttiyoarnab Saha**, K. Devan, "The computation of displacement damage cross sections of silicon, carbon and silicon carbide for high energy applications", *First International Conference on Advanced Materials (SCICON 16)*, Amrita University, Tamil Nadu, (2016).
4) **Uttiyoarnab Saha**, K. Devan, S. Ganesan, "Covariance matrices of DPA cross sections from TENDL-2015 for structural elements with NJOY-2016 and CRaD codes", *The Fourth DAE-BRNS Theme Meeting on Generation and Use of Covariance Matrices in the Applications of Nuclear Data*, Manipal Academy of Higher Education, Karnataka, (2017).
5) **Uttiyoarnab Saha**, K. Devan, "Quantifying Neutron Radiation Damage in Structural Elements from Evaluated Nuclear Data Using an Indigenous Computer Code – CRaD", *62nd. DAE-BRNS Symposium on Nuclear Physics*, Thapar University, Punjab, (2017).
6) **Uttiyoarnab Saha**, K. Devan, "Neutron heating and gas production rates in structural materials", *Homi Bhabha National Institute Research Scholars Meet on Material Science*

and Engineering of Nuclear Materials(RSM-MSENM-2018), IGCAR, Tamil Nadu, (2018).

Reports

1) **Uttiyoarnab Saha**, K. Devan, "Processing of gas production cross sections of isotopes of Fe from ENDF/B-VIII.0 using CRaD, NJOY-2016.31 and NJOY21 codes", *Report: IGC-RDG/RND/CPS/192*, Indira Gandhi Centre for Atomic Research, 2019.
2) **Uttiyoarnab Saha**, K. Devan, "Gas production in structural materials used in PFBR and their nuclear data uncertainties computed from basic evaluated nuclear data libraries by using the CRaD code", *Report: IGC-RDG/RND/CPS/194*, Indira Gandhi Centre for Atomic Research, 2019.
3) **Uttiyoarnab Saha**, K. Devan, "Validation of Neutron DPA Cross Sections, Heating Cross Sections and PKA Spectra computed using the CRaD code ", *Report: IGC-RDG/RND/CPS/198*, Indira Gandhi Centre for Atomic Research, 2019.
4) **Uttiyoarnab Saha**, K. Devan, "CRaD: A Computer Code to Calculate the Metrics of Primary Radiation Damage, User's Manual to Version 1.0", Indira Gandhi Centre for Atomic Research, 2019.

Workshops / Schools

School cum First Collaboration Meeting on Computational Nuclear Structure and Reactions (CMNSR2018), SINP, West Bengal, (2018).

UttiyoArnabSaha

Acknowledgement

I take this opportunity to appreciate, acknowledge and thank the well wishers whose constant support and benevolence have helped me complete the thesis work in a timely manner. My words are never sufficient to conduct my feeling of gratitude.

I gratefully acknowledge the guidance of Dr. K. Devan, my PhD supervisor, in all the aspects of this study. I feel fortunate that I have got the opportunity to understand the subject better from his immense knowledge and experience. I shall be ever indebted to his invaluable contributions and encouragement towards completing this study.

I shall be ever grateful to Dr. S. Ganesan (ex-Raja Ramanna Fellow, BARC) for his valuable advices towards improving the work and maintaining the motivation to carry out the study. I gratefully acknowledge sir for giving numerous insightful suggestions throughout the work. I also thank Dr. V. Gopalakrishnan (formerly associated to RDG) for giving certain initial directions of the work and encouragement.

I am thankful to Dr. M. Sai Baba (ex-Director, RMG) for referring me to Dr. K. Devan for the selection of the project of my PhD.

I am thankful to the members in my doctoral committee: Dr. B. Venkataraman, Dr. N.V. Chandrasekhar, Dr. M.T. Jose, Dr. Umasankari Kannan, Dr. S. Sivakumar (ex-member) and Dr. John Arul (ex-member) for their valuable time and sincere efforts towards evaluating my progress after every academic year.

My first exposure to a nuclear physics research laboratory was at the Saha Institute of Nuclear Physics, Kolkata, where I have worked as a M.Sc. dissertation student under the guidance of Prof. Maitryee Saha Sarkar. I am thankful to madam for the valuable suggestions and continuous encouragement towards pursuing the research work. I want to thank all my teachers who have taught me in the B. Sc and M. Sc degrees for their valuable training and guidance while pursuing science.

I gratefully acknowledge the Department of Atomic Energy of India for providing research scholarship.

The stay at Research Scholar Enclave has been funny, humorous and inspiring all the way because of my *expert at everything* friends. I shall keep recollecting some of their jokes and supportive gestures. I thank all my friends for their support, many helpful discussions and the joyous moments and wish them successful careers ahead. Especially, I am thankful to Harimohan, Dr. Radhikesh, Suman Saurav.

I also thank all the distinguished instructors of the HBNI-Physics PhD course work for their valuable lectures under the curriculum and all the distinguished colleagues in the department, especially S.C. Ravichander sir, Vedharathinam sir and Anuraj sir, for their much timely help and cooperation.

I gratefully acknowledge the reviewers of the manuscripts and examiners of the thesis for their valuable suggestions and comments which have helped me to understand the subject better and improve the quality of the work. I am also thankful to the audience and the experts in various conferences for their valuable feedback and encouragement.

My family inculcates a feeling in me that the earth and the work I do are beautiful. They inspire me by teaching the usefulness and goodness of every small piece of work. Their encouragement and support are pillars of my being. I am used to discuss about the mathematical and computing techniques with my parents and elder brother, whose contributions are fundamental and have profound impact on my work. Their encouragement and mentoring guides me through as I complete developing a computer code, writing the manuscripts and the thesis.

I am thankful to all those whom I am forgetting but because of whom I sustain.

Humbly yours,

Uttiyoarnab Saha

Uttiyoarnab Saha

Abstract

The primary radiation damage due to interaction of neutrons in structural materials of nuclear systems is quantified through the estimation of the four metrics viz. primary knock-on atom (PKA) spectra, displacements per atom (dpa) cross sections, gas production cross sections and heating cross sections by using the basic evaluated nuclear data libraries. There has been a significant improvement in the evaluation of nuclear data and modeling of the primary radiation damage phenomena in the recent times. An indigenous computer code CRaD (Computation of Radiation Damage) is developed to study the effects of these improvements on the estimation of primary radiation damage. The dependence of the damage metrics on the incident neutron spectrum is investigated by estimating the corresponding spectrum-integrated quantities such as PKA rate, dpa, concentration of gas, heating rate, etc. The application of improved nuclear data and atom-displacement damage models may necessitate rescaling of the observed damage in materials with the improved values of dpa. It is justified that such a rescaling can be done in order to be consistent with the improved estimations and it will not affect the design time limits of operations of the materials in the radiation environment. A new method is proposed to compute dpa in polyatomic materials using the self-ion simulations in SRIM-2013, where the PKAs estimated by CRaD code are considered as the incident ions on the target. The advantages of this method towards more realistic estimations are discussed and it is shown that the dpa in both neutron and ion irradiation environments can be determined equivalently. The use of different basic evaluated nuclear data libraries give rise to differences in the estimated values of the damage metrics. The nuclear data uncertainties in the damage metrics are quantified by using the Total Monte Carlo methodology of uncertainty propagation. The damage metrics are often found to be correlated and exhibit non-Gaussian distributions. A number of future directions of the study are also outlined.

List of figures

List of tables

Contents

Chapter1

Introduction

1.1 Primary radiation damage and its metrics

The structural materials in nuclear systems such as fission and fusion reactors face high levels of irradiation doses from different kinds of particles such as neutrons, protons, gammas, electrons, etc. during the period of their operation. The incident radiation induces a phenomenon of continuous dislodging of atoms from the pristine structures of these materials. A long-term endurance of this state of extreme condition leads to detrimental changes in the physical and mechanical properties of the materials. This is generally referred as the radiation damage of structural materials. Therefore, it is vital to estimate the radiation damage in these structural materials, during design stage itself of such systems. Among all other particles, due to the high flux of neutrons involved in fission and fusion reactors, the major concern is about the radiation damage induced by these particles. Especially in fusion reactors, the radiation damage phenomena and their quantifications are more complex with the increased chances for the production of different particles via threshold reactions of neutrons.

The radiation damage of materials involves phenomena which are multi-scale in both length and time. It starts from the interaction of a particle like neutron with a material nucleus creating a primary knock-on atom (PKA) within a few femtoseconds, the primary displacement damage evolving in the material up to a few hundreds of picoseconds and finally the displacements-induced microstructures develop within the material from nanoseconds to longer times [1]. The effects of these microstructures can be observed in millimeter and larger lengths after a period of irradiation time. The evolution of damage subsequent to the primary

displacement processes depends strongly on the environment and operating conditions of the material. Hence the radiation damage phenomena can be divided into two main stages depending on the time scale of its observation. The phenomena from its initiation, i.e. from the impingement of the radiation on the material, its interactions with the material atoms and up to the formation of stable vacancy-interstitial (Frenkel) defects due to the displacements and replacements of the atoms in the collision cascades is called primary radiation damage (~ 10^{-10}s). The evolution of the primary defects into microstructures under the influence of various external conditions which lead to the changes in the structural properties of the materials comes under the study of secondary effects of radiation damage (> 10^{-9}s). The occurrences of these phenomena with approximate time scales are presented in Table 1.1 [1, 2].

Table 1.1: Production of defects in metals upon particle irradiation with approximate time scales

Time (s)	Event	Result
10^{-18}	Energy transfer from incident particle	Creation of a PKA
10^{-13}	Displacement of lattice atoms by PKA	Displacement cascade
10^{-11}	Energy dissipation, spontaneous recombination and clustering	Stable Frenkel pairs (single interstitial atoms (SIA) and vacancies) and defect clusters
$>10^{-8}$	Defect reactions by thermal migration	SIA and vacancy recombination, clustering, trapping, defect emission

The primary radiation damage due to interactions of neutrons in structural materials is quantified through the estimation of four metrics, namely, spectra of primary knock-on atoms (PKAs), cross sections for displacements of atoms, production of transmutation gases and deposition of heat by the charged reaction products. The primary damage caused due to displacements of atoms is quantified by the first two metrics, i.e. PKA spectra and displacements per atom (dpa) cross section. The unit dpa is defined as the average number of times each atom

has been displaced from its lattice site during the period of irradiation [3]. The metric, gas production, deals with the estimation of gas species such as hydrogen, deuterium, tritium, helium-3 and helium which are accumulated in the material due to the creation of light charged particles such as proton, deuteron, triton, ^{3}He and alpha respectively, via the transmutation reactions of neutrons with the target nuclei. These gas species can interfere with the formed defects, thereby affecting the evolution of microstructures and are known to lead to the degradation of materials through phenomena such as void swelling, grain-boundary embrittlement, etc. The fourth quantifying parameter of primary radiation damage deals with the estimation of the energy that is deposited locally in the material by the charged products formed in the neutron reactions and it is referred as neutron heating, in short. The determination of heating of materials due to radiation is essential in order to ensure their safe operation and efficient thermo-mechanical performance.

There exist well established experimental techniques and measured data to quantify the gases produced [4-7] and the heating of the materials [8-11] as a result of interactions with neutrons of some distinct energies. However, rigorous quantification of primary radiation damage phenomena occurring due to the displacements of atoms in terms of parameters such as dpa cross sections and PKA spectra depends on their estimation by theoretical calculations, as there is lack of well-proven experimental techniques and measured data for the required completeness. Nevertheless, prior to establishing an experimental setup to perform irradiation programs for varied nuclear researches, it is necessary to have the knowledge of the parameters of primary radiation damage for efficient and safe designing of the structural materials. The correct prediction of these parameters helps to decide the maximum permissible irradiation dose on the materials and the effective time available for their useful operation in the system.

1.2 A short survey of literature

The present study has been made possible only by the understanding acquired from a large set of research works carried out by different groups and individual researchers. An account of the survey of the related literature is presented here. This survey is not complete and plenty of important literatures exist which could not be covered in this part. However, it is ensured that all the literatures that formed the background of the present study are noted at relevant stages in the subsequent chapters.

The initial attempts to quantify primary damage of materials due to the displacements of atoms upon interactions by energetic particles have been made by Seitz [12], Snyder and Neufeld [13]. Kinchin and Pease [14] have developed the first analytical model (came to be known as K-P model) to calculate the dpa in target elements. This model is based on the assumption that the kinetic energy is transferred from PKA to lattice atoms by hard sphere collisions and there would be displacements if this energy is above threshold lattice displacement energy. A high energy limit of the PKA (called cutoff energy) is assumed beyond which energy would be dissipated in electronic excitations, not causing displacements of atoms. Lindhard et al. [15, 16] have calculated the sharing of PKA energy between electronic (ionization) processes and nuclear interactions during the atomic collision phenomena. The PKA energy, excluding that which goes into electronic processes, is expended in displacing further atoms in the lattice. This fraction of the PKA energy is called as damage energy. Robinson [17], based on the energy-partition theory of Lindhard et al., has formulated the concise analytical expressions to compute this damage energy, by using computer simulations. Subsequently, Norgett, Robinson and Torrens [18] have proposed an improved version of atom-displacement model (came to be known as NRT model) that included the correction for the damage energy of PKA instead of the simple kinetic energy

transfer mechanism given by K-P model. As improvements, NRT model also considered realistic potentials rather than hard sphere potential in atomic collisions and removed the sharp cut-off energy (used in K-P model) between nuclear and electronic energy losses. The NRT model is currently accepted as ASTM (American Society for Testing and Materials) [19] standard in assessing the dpa. The measured radiation damage (like the change in hardness, electrical properties, swelling, etc.) in the structural materials after being subjected to irradiations is correlated to the NRT dpa [2] for design purposes.

However, it has been observed [[20] and related references therein] that the NRT dpa over-predicts the primary damage (in metals and other materials).It is inadequate to capture the observations as made in realistic Monte Carlo (MC) [21] and molecular dynamics (MD) simulations [20], where the in-cascade behavior viz. formation of heat spike zone, recombination of defects, replacements of atoms, etc. occurring within the picoseconds time range are very important in order to have a more complete description of the primary displacement damage phenomena. Nordlund et al. [20, 22, 23] have reviewed a large number of works on MD simulations and irradiation experiments to present the nature of displacement damage cascades and the defects produced in metals, semiconductors, ionic materials and carbon-based materials. One of the important outcomes of their study is the improved atom-displacement model called athermal recombination corrected – dpa (arc-dpa). The arc-dpa model has been introduced with an additional damage efficiency term which is parameterized such that the nonlinear nature of defect production, their recombination and saturation behavior are adequately described. In a recent work, the limitations of simulations and analytical models are discussed and further improvements of the arc-dpa model are also provided [23]. Broeders et al. [24] have evaluated the Frenkel pair resistivity for metals by deriving the systematics of the resistivity values based

on the available data and experimental damage resistivity rates. They have also calculated the efficiencies of defect production for various neutron spectra by using the binary collision approximation (BCA) model. Based on this work, Konobeyev et al. [25] have estimated the parameters of arc-dpa model for a large number of elements from $_{3}$Li to $_{92}$U by deriving systematics for threshold energies in materials from the compiled data on various physical quantities. These developments in the modeling of primary displacement damage beyond the NRT formalism genuinely inspire a researcher to review their effects in the designing of structural materials for nuclear reactors.

Several computer codes have been developed to estimate primary radiation damage by using the evaluated nuclear data. Gabriel et al. [26] have developed the RECOIL code; Greenwood et al. [27] have developed the SPECTER code and Greenwood [28] has developed the SPECOMP code to estimate primary damage in materials. The SPECOMP code has been developed to compute displacement damage in polyatomic materials. The RECOIL and SPECTER codes work on the in-built databases from ENDF/B-IV and ENDF/B-V libraries to compute the dpa cross sections. The SPECTER code also computes gas production and PKA spectra for incident neutron spectra. MacFarlane et al. [29] have developed the NJOY-2016 code system, and Harada et al. [30] have developed the PHITS code to process basic evaluated nuclear data and estimate the metrics of primary radiation damage, among many other diverse applications. Gilbert et al. [31] have developed the code SPECTR-PKA which reads the output of GROUPR module of NJOY code to give the PKA spectra in required energy group structure and also computes the dpa in materials for any facility neutron spectra [32]. Sublet et al. [33] have developed the FISPACT-II code system to perform the detail nuclear inventory calculations among many other useful capabilities like estimation of primary radiation damage, activation and

transmutation radio-nuclide prediction, uncertainty propagation, etc. Abdou et al. [34] have investigated the calculation of nuclear heating (neutron fluence-to-kerma coefficients) from the available nuclear data by developing a computer code called MACK. They have also examined the validity of the calculated kerma coefficients by checking the conservation of energy between basic neutron interaction and gamma-ray production data. Zhang et al. [35] have developed a computer code called MAZE to estimate neutron and gamma kerma coefficients from both energy balancing and energy-momentum balancing principles. They have compared the computed kerma coefficients with measurements carried out using a 14 MeV D-T neutron source and generated a library, called MAZE-LIB containing kerma coefficients for many fusion-related materials. The results from these modern codes from various research units form the sources for validation and benchmarking exercises towards developing a suitable computational tool to estimate the primary radiation damage in structural materials for the Indian fast nuclear reactors.

Mazey [36] and Abromeit [37] have critically surveyed the methodologies to simulate neutron radiation damage using ion irradiations, their advantages and disadvantages, nature of the damages produced by these two types of irradiations and how to correlate them. David et al. [38] and Was et al. [39] have performed the simultaneous implantation of helium ions along with heavy or self-ion irradiation to simulate the effects of helium that is produced in the operating conditions of a nuclear reactor and determine its role in the micro-structural evolution of the radiation induced material. The SRIM code [40], employing MC simulations of displacement cascades of radiation particles in materials, is widely used by experimentalists to obtain the estimates required for planning these irradiation experiments. Stoller et al. [41] have given the guidelines for using the SRIM code to estimate NRT dpa in materials. Devanathan et al. [42] have performed MD simulations in SiC to investigate the threshold displacement energies for C

and Si PKAs. Their study suggests that the effective displacement energy in SiC averaged over both sub-lattices is about 25 eV. Heinisch et al. [43] have estimated the total displacement cross sections due to irradiation of SiC with neutrons in hundred energy group structure by using the SPECOMP code and computed the dpa for various reactor spectra. The SPECOMP code solves the Parkin-Coulter coupled integro-differential equations [44-47] to find the number of displacements in the interactions among different sub-lattices of the polyatomic material. There is a limitation on the maximum number of elements (up to four) in the polyatomic target for which the SPECOMP can compute the dpa cross sections by this method. It is hence worthwhile to search for a suitable method to estimate the dpa in multi-component alloys.

Greenwood [48] has calculated the displacement damage occurring due to reactions of thermal neutrons in ^{59}Ni, i.e. ^{59}Ni (n, α) ^{56}Fe, where very high energy (~ 340 keV) ^{56}Fe recoils produced can increase the number of displacements significantly in the nickel-bearing materials used in thermal neutron fluences above 10^{20} n/cm^{2}and mixed-spectrum reactors like HFIR. Greenwood et al. [49] have calculated the helium produced in nickel using the cross sections from ENDF/B-VI and compared the estimated values with the measured data obtained from irradiations performed in various reactors. The calculations and measurements in this work have shown quite accurate agreements. Gopalakrishnan et al. [50] have theoretically investigated the production of helium in two different samples of steel by using cross sections from different evaluated nuclear data libraries (ENDL/84-V [51], ENDF/B-IV [52], KEDAK-4 [53], ENDF/B-VI [54] and JENDL-2 [55]). They have also compared these estimations with an earlier experiment by Nandedkar et al. [5], which has shown differences by factors of 2 to 3 due to both limitations in the accuracy of measurements and knowledge of accurate cross sections for ^{59}Ni. Mansur et al. [56] have illustrated the possibility to manipulate the ratio of helium production to

the displacements of atoms by artificially altering the relative isotopic abundances of the stable isotopes of Ni. This would help to tailor-make the alloys with necessary requirements for applications in fusion reactors. The incident neutron spectrum plays an important role on the integrated damage metrics which are obtained by performing neutron spectrum-averaging of the PKA spectra, dpa cross sections, gas production cross sections and heating cross sections. It is always intriguing to investigate the final effects of the newly modeled and evaluated primary radiation damage cross sections on the structural materials under the neutron spectra at the exact locations of applications.

There have been recently significant efforts towards making the nuclear data more complete and improving the estimations of nuclear data covariances [57, 58]. Koning et al. [59] have used the TALYS [60] nuclear reaction code (a part of T6 code package) to generate the new evaluated nuclear data library called TENDL. Smith [61] and Koning et al. [62] have developed the Total Monte Carlo (TMC) methodology to propagate the uncertainties in nuclear data to the uncertainties in the derived parameters of reactor physics. They have introduced this concept to determine the uncertainties in the derived parameters by using the knowledge of the uncertainties in nuclear physics model parameters [63] and experimental data [64]. Using the information on theoretical and experimental uncertainties on the nuclear model parameters and neutron interaction cross sections in the T6 code system, they have generated a large number of random evaluated nuclear data files so as to propagate the uncertainties in nuclear data to the uncertainties in derived parameters. Rochman et al. [65-69] have applied the TMC methodology to estimate the nuclear data uncertainties in the parameters of nuclear reactors such as sodium void reactivity coefficient, k_{eff}, radio-toxicity, etc and compared these results with the uncertainties calculated by the traditional perturbation method [70]. It has been observed that due

to ignoring various possible correlations among nuclear reaction variables, the perturbation method often underestimates the uncertainties in nuclear data and the TMC approach is more suitable for the non-linear propagation of uncertainties by including correlations among various parameters. Griffin et al. [71] have estimated the uncertainties in the damage metrics of Si which arise due to both nuclear data and material physics model parameters associated with the calculation of damage energy and number of displacements in materials. Simakov et al. [72] have demonstrated the use of TMC methodology in the estimation of uncertainties in dpa, gas production and kerma coefficients of ^{56}Fe. The uncertainties contributed by material physics model parameters to the displacement damage are also quantified in their study by following a similar methodology. The IAEA-CRP [73] has presented numerous recent developments by various research groups on the modeling and experiments performed to determine primary radiation damage in materials. In particular, new databases of dpa cross sections (JEFF-3.3 dpa data base [74]) have been generated by applying the improved modeling techniques such as combined MD-BCA and arc-dpa models alongside the NRT dpa cross sections; the PKA spectra, dpa and heating cross sections due to neutron and charged particle radiation have been compared with available experimental data; and advantages and short comings of different codes, modeling techniques and basic evaluated nuclear data libraries have been identified through extensive comparisons among different estimations. The works presented in this CRP have formed one of the major sources of information and motivation for the present study. Along with the above mentioned reasons for its suitability, the TMC methodology has been found to be feasible also in the present study because it is simple to apply within a well-framed approach requiring lesser number of specialized codes and in-between steps as compared to the requirements in the perturbation method of uncertainty propagation.

1.3 Objectives of the thesis

The needs and the areas requiring investigations are identified from the above survey of literature. The following objectives are hence set for the present study:

The metrics of primary radiation damage due to neutrons are estimated by using the data for their interactions with the material nuclei from the basic evaluated nuclear data libraries [75], such as ENDF/B-VIII.0 [58], JENDL-4.0 [76], TENDL-2017 [59], etc. In the recent times, there has been a significant advancement in the evaluation of basic nuclear data with the development of state-of-the-art experimental facilities and theoretical modeling and improvement in the measured values of the nuclear reaction variables. Particular emphasis has been given towards making the evaluations more complete and general purpose, including also the effect of covariances of nuclear model parameters as well as the experimental data. The aim of the present study is to investigate the effects of improved nuclear data on the metrics of primary radiation damage.

Apart from the neutron reaction data in basic evaluated nuclear data libraries, the estimated dpa cross sections depend on the application of different models of atom-displacement damage [14, 18, 22] which are derived from simulations and experiments in materials physics. The present study aims to apply and investigate the effects of recent atom-displacement damage models [18, 22] in the predictions of primary radiation damage in materials. It also aims to provide a solution to the problem of rescaling the measured damage with dpa that can naturally arise as a result of the improvements in nuclear data, atom-displacement models and computer codes.

The dpa cross sections in polyatomic target materials are generally computed by weighted addition of dpa cross sections for each of the constituent elements [77, 78] and also by using the Parkin-Coulter method [44-47]. The first method may not be realistic sometimes, but there is no alternative way when the target material is an alloy of several elements. The second method treats the problem more realistically by considering physical parameters in terms of different stopping powers, sub-lattice interactions of the constituent elements, etc., but it has some limitations and can be applied for materials with a less number of elements [28]. The present study aims to investigate the calculation of displacement damage in polyatomic materials through feasible computational means which can be easily extended for any number constituent elements.

The metrics of primary radiation damage generally differ when different basic evaluated nuclear data are used for their estimations. This is due to the spread in the data obtained from different basic evaluated nuclear data libraries. These derived parameters are uncertain due to the uncertainties in evaluated nuclear data, which arise due to the uncertainties in the parameters of nuclear physics models [63] and experimental nuclear data [64] and differences in the subjective assessment and various computational tools used in the evaluation procedure. The present study aims to determine the mean values of the parameters of primary radiation damage and quantify their nuclear data uncertainties by following the TMC methodology, which should be useful to achieve the desired target accuracy in the designing of structural materials for reactor systems.

1.4 Major challenges and motivation of the thesis

The diverse nature and demand of versatility of the set objectives indicate that a dedicated computational tool is the primary requirement to perform such a study. This code

should have the capability to handle the improvements of nuclear data formats and data representations in the recent ENDF-6 [79] libraries. The computer codes that have been developed by researchers to compute the parameters of primary radiation damage from evaluated nuclear data libraries can be listed as follows: RECOIL, SPECTER, NJOY-2016, SPECOMP, PHITS, FISPACT-II, etc. The RECOIL code is based on an in-built database from ENDF/B-IV (1974) library and the SPECTER code from ENDF/B-V (1979) library. These codes can calculate the production of gases, PKA spectra and dpa cross sections in energy multigrouped formats. These codes perform satisfactorily and although they are continued to be used at IGCAR [80] for estimating neutron primary radiation damage, they have limitations with respect to handling the newer, state-of-the-art evaluations of nuclear data and versatility of energy group structures of the calculated results as per requirement. The SPECOMP code is popularly used among the radiation research community; but still has the drawback of being limited to using data based on only ENDF/B-V and in certain pre-defined energy group structures. The NJOY-2016 is a versatile code system to process the latest ENDF-6 format nuclear data libraries and can calculate all four metrics of primary radiation damage in elemental targets in both point (energy-cross section) data form and in any chosen energy-group structure for applications. However, at present there is less flexibility with regard to applying different models of atom-displacements damage to compute dpa cross sections using NJOY-2016. This code has been made available as open-source [81] for the users only in February, 2017. The earlier versions of NJOY nuclear data processing code system were not licensed to India. PHITS is also a general-purpose Monte Carlo particle transport simulation system that can calculate the radiation dose in materials due to a large variety of particles and has wide applications. It has been applied to predict material damage due to very high energy radiations which are of importance in the

accelerator driven systems [82]. FISPACT-II, as mentioned earlier, also has versatile capabilities for transmutation, activation and damage calculations. However, these two codes are also not licensed to India. Hence, a long-standing need has been identified to develop a computer code for the estimation of primary radiation damage in the structural materials that will be used in the upcoming fast breeder reactors (FBRs) in India. The foremost aim of this study is consequently outlined from this necessity and a code, named as CRaD (Computation of Radiation Damage) [78, 83, 84], is developed to estimate the four metrics of primary radiation damage occurring due to irradiation of neutrons on the structural materials of fast reactors, by using neutron reaction data from the latest evaluated nuclear data libraries. Even though NJOY-2016 has been released as open source software, the development of the indigenous code CRaD is continuously pursued in order to have better understanding of the procedures of estimation of primary radiation damage, and also, it is believed that, by this way we shall be able to develop the methods for processing evaluated nuclear data and verify the uses of the traditional processing systems.

1.5 Works performed and organization of the thesis

The works performed in this study are organized into six chapters as follows:

In *Chapter 2*, the methodologies adapted towards the development of the indigenous computer code, CRaD (Computation of Radiation Damage), to estimate the PKA spectra, dpa cross sections, gas production cross sections and heating cross sections in the structural materials by using the neutron interaction cross sections from basic evaluated nuclear data libraries are described. The salient working description of the CRaD code is also given.

In *Chapter 3*, the results of CRaD code on the neutron induced primary damage metrics in structural materials obtained using different ENDF-6 [79] files are discussed, including its

validation. The cross sections of dpa, neutron heating and gas production from CRaD code are compared with the NJOY-2016, NJOY21 [85] codes and the discrepancies observed are also discussed. The neutron spectrum dependence of PKAs, dpa, gas production and heating rates in structural materials are estimated using the CRaD code. The neutron spectra-integrated quantities such as the dpa, concentrations of gases and heating rates are compared with available codes and literature. The arc-dpa model is implemented in CRaD code and the results are compared with the predictions from the NRT model. The necessity to rescale the measured radiation damage with the improved values of dpa, which are estimated using improved data and models, without affecting the irradiation time limits of the materials, is discussed. The productions of gas species such as hydrogen, deuterium, tritium, helium-3 and helium in various materials is investigated by applying the single-step and two-step processes of transmutations in fission and fusion spectra. The transmutation of ^{58}Ni to ^{59}Ni and the consequent production of gases are investigated in detail by using different basic evaluated nuclear data libraries and in different neutron spectra. The spectra-integrated neutron heating rates in structural materials are determined by the direct method and the differences observed with respect to the heating values from the energy balance method (NJOY-2016) are discussed.

In *Chapter 4*, a novel method to compute dpa from NRT model in elemental and polyatomic target materials and from arc-dpa model in elemental target materials, based on the estimation of average energies of the PKAs with CRaD code and simulating self-ion irradiations with the SRIM-2013 [40] software is described, with examples in Fe, SiC, etc. The potential of this method to compute dpa cross sections in other polyatomic materials and the usefulness of the PKA energies estimated by the CRaD code to perform more realistic simulations using the MD and BCA methods are also highlighted. The self-ion simulated integrated dpa in various

materials are compared with the values obtained by the standard method and it is shown that dpa can be equivalently determined in both the methods.

In *Chapter 5*, the propagation of nuclear data uncertainties to the metrics of primary radiation damage is discussed. The metrics of primary radiation damage estimated using different sources of nuclear data are found to be non-unique and sometimes show significant variations. The uncertainties of nuclear data in these derived parameters are quantified by applying the TMC methodology [61, 62] of uncertainty propagation in the CRaD code. A large number (~ 300 to 500) of random ENDF-6 files available in TENDL-2015 and TENDL-2017 nuclear data libraries are used to determine the mean values, uncertainties, nature of the resulting random distributions, covariance and correlation matrices of each these parameters. The mean values of these parameters along with their uncertainties obtained using the random files are also compared with the estimates obtained using other basic evaluated nuclear data libraries.

In *Chapter 6*, the salient conclusions of this study are summarized and the possible works that can be performed in future are outlined.

Chapter 2

Methodologies to Compute the Primary Radiation Damage Metrics

2.1 Introduction

In this chapter, the methodologies used in the CRaD code to compute the metrics of primary radiation damage induced by the interactions of neutrons in structural materials viz. PKA spectra, dpa cross sections, gas production cross sections and heating cross sections are discussed in detail. The ENDF-6 [79] basic evaluated nuclear data files containing the information on the neutron-nucleus interactions form the starting point in the quantification of these metrics. In the first part of this chapter, the data in a basic evaluated nuclear data file which are necessary to compute these metrics shall be described briefly. In the second part of this chapter, the general methodologies that are applied to estimate these metrics by using the ENDF-6 nuclear data shall be described. The third part is devoted to a short working description of the indigenously developed code CRaD, where an overview of the code shall be given to illustrate how it performs the estimations of these metrics by using the ENDF-6 files.

2.2 Necessary data from ENDF-6 files to quantify primary radiation damage

The full information of interaction of a neutron with a target nucleus is represented by the cross sections; multiplicity, energy and angle of emission of secondary particles and recoil nucleus; excited levels of the compound nucleus; the emission of γ-rays from excited nucleus and various other data in the ENDF-6 files. These data are arranged in various Files (denoted by MF), sections and subsections of the ENDF-6 data file for the target nucleus. The relevant data in

an ENDF-6 file for a structural nucleus which are necessary for the estimation of primary radiation damage due to neutrons are discussed in the subsequent sections.

2.2.1 Cross sections of neutron interaction in File 3

The energy-wise neutron interaction cross sections are given in File 3 (MF = 3) of the ENDF file for the material. There are various possible ways by which a neutron can interact with a target nucleus. The mode of interaction depends on the energy of the neutron and the target nucleus. The cross sections of interaction via different channels are given in different sections (MT) of the ENDF file. For example, the cross sections for elastic scattering (n, n) are given MT = 2, total inelastic scattering (n, n′) in MT = 4, radiative capture (n, γ) in MT = 102, one proton production in exit channel (n, p) in MT = 103, etc. The (n, n′) cross sections in MT = 4 are sum of the cross sections for discrete / resolved inelastic levels (MT = 51 to 90) and the continuum (MT = 91). Likewise, there can also be discrete level plus continuum cross sections for reactions where only one charged particle is produced in the exit channel, like (n, p) in MT = 600 – 648 and 649; (n, d) in MT = 650 – 698 and 699; (n, t) in MT = 700 – 748 and 749; (n, ^{3}He) in MT = 750 – 798 and 799 and (n, α) in MT = 800 – 848 and 849. The energy-wise sum of all the cross sections which are not given explicitly under any particular neutron reaction MT is given in MT = 5. The neutron interaction cross sections are dependent on the temperature of the target nucleus and are represented in various parameterized forms in an evaluated nuclear data file. The evaluated cross sections are always given at 0 K temperature of the target nucleus. The temperature-dependent point cross sections can be generated with the help of nuclear data pre-processing codes, like NJOY-2016 [29], PREPRO [86], etc. These are then referred to as the pre-processed point cross sections, which are arranged in specific ENDF-6 formats [79] with

increasing neutron energy. The data for each reaction is given against their particular MT number and the reactions are arranged in an increasing order of the MT.

In addition to the energy and cross section data, the other important information given in File 3 and used in the calculation of the energy transfer kernels for various reactions are the Q-values. These are QM, known as the mass-difference Q-value and QI, known as the reaction Q-value. QM is defined as the total mass of the target and the neutron (projectile) minus the total mass of the residual nucleus in ground state and all the other products of reaction. QI value is given in case of a simple two-body reaction or a breakup reaction, for the lowest energy state that is defined by the reaction MT number. It is defined as the QM for the ground state of the residual nucleus (or the intermediate system before breakup) minus the energy of the excited level in this system. The value of QI is equal to QM, if there are no intermediate states in the residual nucleus for a reaction and, also if the reaction proceeds without complex breakup.

2.2.2 Angular distribution data of secondary particles in File 4

The angular distribution of secondary particles in the exit channel of neutron reactions are given in MF = 4 of the basic ENDF-6 data file. These distributions are usually given for discrete level reactions where a neutron or a charged particle is produced in the exit channel. These may also be given for other neutron emitting continuum reactions like (n, $n'_{continuum}$), (n, 2n), etc. For a particular reaction (MT), the angular distributions are given for a series of incident neutron energies, in order of increasing energy. The data for different reactions are given in the increasing order of MT.

The angular distributions of the scattered particles are expressed as normalized probability distributions given by $f(\mu, E)$ such that

$$\int_{-1}^{1} f(\mu, E)d\mu = 1 \quad . \tag{2.1}$$

Here, E is the energy of the incident neutron and μ is the cosine of the scattering angle of the emitted particle. $f(\mu, E)d\mu$ is the probability that a reaction initiated by a neutron of energy E will lead to emission of the secondary particle in the angular range $d\mu$ about the angle whose cosine is μ. It is assumed that the angular distribution of the emitted particles is azimuthally symmetric. So it can be represented as series of Legendre polynomials $P_l(\mu)$ as follows:

$$f(\mu, E) = \sum_{l=0}^{NL} \frac{2l+1}{2} a_l(E) P_l(\mu) \quad . \tag{2.2}$$

Here, $a_l(E)$ is the $l^{th.}$ Legendre polynomial coefficient and NL is the highest order of Legendre polynomial.

For different incident energies, the angular distribution data are given either in the form of tabulated μ vs. $f(\mu, E)$distributions or in terms of the Legendre polynomial coefficients [79], in MF = 4. These data have to be processed correctly to take into account the energy transferred to the target nucleus due to reactions proceeding through the emission of particles at various angles.

2.2.3 Energy distribution data of secondary particles in File 5

The energy distribution data of secondary particles are given as normalized probability distributions in File 5 [79]. The data for (n, $n'_{continuum}$), (n, xn), MT = 649, 699, etc. reactions can be given in this File, if they are not given in File 6. The data can be represented in different forms indicated by the distribution law. Among the several possible laws [79], the arbitrary tabulated function and evaporation spectrum are implemented in the present study. The energy

distributions of all the products are represented preferably by the use of File 6 when several charged particles are emitted and also when the angular and energy distributions of the particle are strongly correlated.

2.2.4 Angular and energy distribution data of products in File 6

The energy and angular distribution data of the reaction products, i.e. neutrons, photons, charged particles and residual nuclei are given in MF = 6. The data for a particular reaction are given in this file when it is necessary to couple the energy and angular information of the emitted particles and when a concurrent description of the scattered neutrons, emitted particles and the residual nucleus are important. Data are given for some incident neutron energies in an increasing order. For a given incident energy, the information on the distribution of the product is also arranged in increasing order of its energy. The data for each product is given in separate sub-sections in the following sequence:

a) Particles (n, p, d, t, ^{3}He, α) are arranged in increasing order of their ZAP and LIP values. The ZAP is called product identifier, defined as $1000 \times Z + A$, with Z = 0 for photons and A= 0 for electrons and positrons. The LIP is called product modifier flag, mainly used to identify the isomeric state of a product nucleus. In this case, LIP = 0 identifies the ground state, LIP = 1 for the first isomeric state, etc. This flag may also be used to distinguish subsections with same value of ZAP for light particles, for example, in case of sequence of neutron emission, LIP = 0 can denote the first emitted neutron, LIP = 1 the second neutron and so on.
b) The residual nuclei and isomers in order of increasing ZAP and LIP. The average recoil energy and spectrum for an elemental target can be represented in a subsection with A = 0.
c) Photons
d) Electrons

The energy-angle distribution in each sub-section is represented in different forms based on the flag LAW. There are eight different representations that can be identified from the value of LAW [79]. The most common LAW dependent structures that are dealt with in this study are as follows:

1: Continuum energy-angle distributions – By this law, the data can be represented in the following ways [79]: Legendre coefficients representation; Kalbach-Mann systematics representation; tabulated function representation.

2: Discrete two-body reaction angular distributions – By this law, the two-body scattering data is represented in terms of the coefficients of Legendre polynomials [79].

3: Isotropic discrete emission – By this law, the data is given for isotropic angular distribution in the centre of mass system [79].

The details of these and the remaining LAW dependent structures can be found in Ref. [79].

2.2.5 Energy distribution data of emitted photons in Files 12 and 15

The calculation of energy of the recoil nucleus in (n, γ) reaction requires the knowledge of the energy distribution of the photons with incident neutron energy. For this, Files 12 and 15 together provide complete information on the discrete as well as the continuous photons. The production of discrete photons (for the corresponding cross sections in File 3) is represented in File 12 by giving the multiplicities / yields of the photons at different neutron energies. The yields for continuum photons at various neutron energies may be given in File 12 and / or File 15. If these yields are present, then the energy distributions of continuum photons at different neutron energies are always given in File 15 as normalized probability distributions. As

mentioned in previous Section, File 6 also has provisions for giving the energy spectra of emitted photons in (n, γ) reaction. In that case, the discrete and continuum photons are represented in a more compact manner [79].

2.3 Computation methodologies of the metrics

2.3.1 The spectra of primary knock-on atoms

The energy spectra of the primary knock-on atoms (PKAs), produced after a lattice atom is knocked off its lattice position by the impingement of the energetic neutron, is a fundamental quantity in the estimation of primary radiation damage. The PKA spectra give quantitative information on the energy distribution of the PKAs formed as a result of different kinds of neutron interactions. The PKA spectra are computed from the models developed within nuclear physics and applying the kinematics of nuclear reactions. These spectra form the basis for the estimations of dpa and neutron heating cross sections.

The PKA spectra can be defined as the probability to form a PKA in the energy range of E_R to $E_R + dE_R$ after the interaction of a neutron of energy E. It is expressed as follows:

$$\frac{d\sigma(E, E_R)}{dE_R} = \sum_i \sigma^i(E) K^i(E, E_R) . \qquad (2.3)$$

Here, $\sigma^i(E)$ is the cross section for interaction of the neutron of energy E via reaction channel i. $K^i(E, E_R)$ is called the kernel of reaction i which proceeds with the transfer of energy E to E_R from the neutron to the recoil nucleus. The total PKA spectrum is obtained by adding the contributions from all partial interactions of neutron with the nucleus, such as, elastic scattering (n, n), inelastic scattering reaction (n, n′), (n, 2n), (n, p), (n, α), etc. In the present study, the PKA spectra have been calculated from all the reactions based on the kinematics relations of the energy and angular distributions of emitted secondary particles and the recoiling nucleus by

using the data given in the ENDF-6 file for the target material. However, the PKA spectra resulting in the radiative capture of neutrons are not determined explicitly in the study. The energy of the nucleus recoiling after (n, γ) reaction is calculated by using the ENDF-6 data given in Files 3, 6, 12 and 15.

2.3.1.1 Elastic scattering (n, n)

The kernel in (n, n) reaction is defined by Eq. (2.2), along with the condition given in Eq. (2.1). The angular distribution of elastically scattered neutron given in File 4 ensures that the total scattering probability over full scattering angular range is unity, i.e. Eq. (2.1) holds. The value of μ corresponding to specific (pre-defined) incident and recoil energies (E and E_R) is calculated by solving Eq. (2.4):

$$E_R = \frac{2AE}{(A+1)^2}(1-\mu). \tag{2.4}$$

Here, A is the target mass with respect to neutron mass. Once the value of μ is obtained, the distribution $f(\mu, E)$ for the particular μ is calculated by performing interpolations from the given data. The distribution $f(\mu, E)$ thus obtained is multiplied with the neutron cross section at energy E to get the value of the PKA spectrum for this pair of incident and recoil energies. Similarly, the PKA spectra for all possible recoil energies are obtained for this particular neutron energy.

2.3.1.2 Inelastic scattering (n, n′)

The total (n, n′) reaction is defined by two parts: discrete or resolved level (n, n′) scattering and continuum (n, n′) scattering. For the resolved level inelastic scattering, the calculations are done in a similar way as in the (n, n) scattering, from the following equation [79]:

$$E_R = \frac{AE}{(A+1)^2}\left(\gamma^2 + 1 - 2\gamma\mu\right), \tag{2.5a}$$

where, γ is given by

$$\gamma = \left(1 + \frac{A+1}{A}\frac{Q}{E}\right)^{\frac{1}{2}}. \tag{2.5b}$$

Here Q is the reaction Q-value. Eq. (2.5a) reduces to Eq. (2.4) if the value of Q is set to 0. For a given E_R, the value of μ is obtained using Eq. (2.5a). The PKA spectrum is calculated for this μ from the angular distributions of the (n, n′) scattered neutrons given in either File 4 or File 6 of the ENDF-6 data file.

The PKA spectrum for inelastic scattering in the continuum energies is calculated in the most accurate way if the data for energy distribution of the recoil nucleus, calculated based on the models of nuclear reactions are given in the ENDF-6 file. Then these can be obtained from the 'residual nucleus' sub-section given in File 6. If such data are not available, then approximate calculations are performed assuming neutron evaporation model [2]. This is expressed through the following equations:

$$K(E,\ E_R) = \int_0^{E'_{\max}} dE' \frac{f(E,E')}{4\frac{1}{A+1}(E\,E')^{1/2}}, \tag{2.6a}$$

where, E' is the energy of the secondary neutron. The maximum value of E' is given by

$$E'_{\max} = \frac{A}{A+1}\left(Q + \frac{A}{A+1}E\right), \tag{2.6b}$$

where, Q is the Q-value for the lowest resolved level. The distribution function $f(E,E')$ represents the probability that a neutron of energy E' in the centre of mass frame is evaporated from the compound nucleus. In the centre of mass frame it is given as the Maxwellian of nuclear temperature $E_D = kT$:

$$f(E,E') = \frac{E'}{I(E)} e^{-E'/E_D}, \tag{2.6c}$$

$$\text{where, } I(E) = E_D^2 \left[1 - \left(1 + \frac{E'_{max}}{E_D} \right) e^{-E'_{max}/E_D} \right] \tag{2.6d}$$

is a normalization factor such that

$$\int_0^{E'_{max}} dE' \, f(E,E') = 1. \tag{2.6e}$$

The recoil energy due to continuum inelastic reaction is found by using the following equation:

$$E_R(E,E',\mu) = \frac{1}{A}(E - 2\mu\sqrt{EE'} + E'), \tag{2.7}$$

where, μ is the cosine of the laboratory angle of emission of secondary neutron. The PKA spectrum due to inelastic scattering (MT = 4) is obtained completely by adding the contributions from all the discrete levels as well as the inelastic continuum.

2.3.1.3 (n, xn) reactions

Similar to the inelastic continuum, the spectrum of the PKA resulting after an (n, 2n) reaction is most accurately determined if the data for recoil energy distribution are available in

the ‘recoil section’ of File 6. In case when these data are not available, the PKA spectrum is calculated based on the evaporation model as given below:

$$K(E,E_R)=\int_0^{E'_{\max}}\frac{E'}{I(E)}e^{-E'/E_D}\int_0^{E-E'}\frac{E''}{I(E,E')}e^{-E''/E_D}\,dE'\,dE'', \tag{2.8}$$

where, $I(E)$ is given by Eq. (2.6d) with $E'_{max}= E$ and $I(E, E')$ is given by Eq. (2.6d) with E'_{max} replaced by $E''_{max}= E–E'$. The energy of the recoil nucleus is found from Eq. (2.7). The PKA spectra for (n, 3n) and (n, 4n) reactions are only estimated if the recoil data are present in File 6.

2.3.1.4 (n, charged particle) reactions

The neutron reactions where one charged particle is emitted in the exit channel are generally called as charged particle out (CPO) reactions. The exit channel, in addition to the heavy recoiling nucleus, may consist of only one charged particle (like (n, p), (n, d), etc. reactions) or multiple charged particles and also secondary neutrons (like (n, p α), (n, n p α), etc. reactions). The CPO reactions like (n, p), (n, d), (n, t), (n, ^{3}He) and (n, α) with one emitted charged particle is represented in the ENDF-6 file in terms of discrete levels plus a continuum or in terms of only one continuum representation. The other kinds of CPO reactions can have only a continuum representation. When the discrete level data for the angular distribution of charged particles are given in File 4 or File 6, the calculation of PKA spectra for these reactions follows a similar procedure as described in case elastic scattering and resolved level inelastic scattering. The angle of scattering is first obtained from the known incident and recoil energies by solving the following relation [79]:

$$E_R=E\frac{(A+1-A')}{(A+1)^2}(\gamma^2-2\gamma\mu+1), \tag{2.9}$$

where, μ is the cosine of the centre of mass scattering angle. A and A' are respectively the target-to-neutron and emitted particle-to-neutron mass ratios. Here γ is defined as

$$\gamma = \frac{A'}{A+1-A'}\left[\frac{A(A+1-A')}{A'}\left(1+\frac{A+1}{A}\frac{Q}{E}\right)\right]^{\frac{1}{2}}. \tag{2.10}$$

Here Q is the reaction Q-value, defined for the discrete excited level of the residual nucleus to which the reaction takes place. The other possible way by which the recoil energy distributions can be represented is by giving the data for only the total continuum CPO reaction in File 6. If neither of the above data is given in the ENDF-6 file, then the PKA spectra for CPO reactions are estimated by CRaD code in an approximate way by assuming isotropic emission of the recoil nucleus. Then the minimum and maximum energies that are possible to be transferred are calculated from the following kinematics relation [29]:

$$E_R = \frac{1}{A+1}\left(E^* - 2\sqrt{A'E^*E_p}\,\mu + A'E_p\right), \tag{2.11}$$

where, $E^* = \frac{(A+1-A')}{A+1}E$ (2.12)

and energy of the emitted particle, Ep is taken as the smaller value by comparing between the available energy, which is

$$Q + \frac{AE}{A+1} \tag{2.13}$$

and the Coulomb barrier energy, which is

$$\frac{1.029\times10^{6}\,zZ}{A'^{1/3}+A^{1/3}}\ \ in\ eV\,, \tag{2.14}$$

where, z and Z are charges of the emitted particle and target respectively. The kernel of energy transfer in this case (considering isotropic emission of recoil atom) is calculated as [87]

$$K(E,E_R)=\frac{1}{E_{R\max}(E)-E_{R\min}(E)}\,. \tag{2.15}$$

2.3.2 Displacements per Atom (dpa) cross sections

The displacements per atom (dpa) cross sections of neutrons are measures of the probabilities for the displacements of the atoms from their original positions in the target material due to the impingements of neutrons on them. An energetic neutron can interact with the target nucleus in any of the different reaction channels that are energetically possible for the particular neutron-nucleus pair. The cross sections for different reaction channels vary with the energy of the neutron. The elastic scattering takes place at all energies and the radiative capture of the neutrons producing gamma rays is generally significant at low neutron energies. In general, the inelastic scattering and CPO reactions are of threshold nature. However, in many nuclei the CPO reactions are exothermic and take place with significantly high cross sections at low energies of neutrons. The well-known examples of this type are the (n, α) reactions in ^{10}B nucleus and the transmuted nucleus ^{59}Ni. After neutron interaction has occurred, it is the recoiling nucleus which predominantly produces the damage in the material by displacing the lattice atoms. The recoil energies in different neutron reactions are determined from the reaction kinematics and by using the energy and angle information in the evaluated nuclear data files. In the CRaD code, the kinematics relations along with the data obtained from the ENDF-6 files (as discussed in previous sections) are used to compute the recoil energies.

2.3.2.1 Damage energy

In encounters with energetic neutrons a target atom gets displaced from its original position if the energy transferred to it is greater than the threshold lattice displacement energy, E_d. This displaced atom is called primary knock-on atom (PKA), which creates further displacements in the medium by producing higher order knock-on atoms. It is only a part of the initial PKA energy (recoil energy of the nucleus after neutron interaction) that goes in the phenomena of atom-displacements. This fraction of the recoil energy is called damage energy, T_{dam}, which is responsible for displacement damage of the material. Another part of the recoil energy is expended in exciting the electrons in the medium and in ionization process. This partitioning of energy between displacements of atoms and electronic excitation processes is given by the theory of Lindhard et al. [15, 16]. The energy partitioning theory of Lindhard et al. has been concisely formulated by Robinson and Torrens through simulations based on the BCA method [17]. The damage energy of the PKA is estimated from the recoil energy as follows:

$$T_{dam}(E_R) = \frac{E_R}{1 + FG(\varepsilon)}\ , \tag{2.16a}$$

where F, ε and G are defined as

$$F = \frac{0.0793 Z_1^{2/3} Z_2^{1/2} (A_1 + A_2)^{3/2}}{(Z_1^{2/3} + Z_2^{2/3})^{3/4} A_1^{3/2} A_2^{1/2}}$$

$$\varepsilon = \frac{E_R}{30.724 Z_1 Z_2 (Z_1^{2/3} + Z_2^{2/3})^{1/2} (A_1 + A_2)/A_2} \tag{2.16b}$$

$$G(\varepsilon) = 3.4008\varepsilon^{1/6} + 0.40244\varepsilon^{3/4} + \varepsilon$$

Here Z_1 and A_1 are atomic and mass numbers of the PKA and Z_2 and A_2 are those of the atom in the target with which the PKA interacts. F is constant for a given PKA-target combination

obtained from the description of Thomas-Fermi atomic interactions [15]. ε describes the nuclear stopping of the PKA, where the denominator was introduced in Ref. [16] to make this parameter a dimensionless quantity. $G(\varepsilon)$ is the universal function obtained using a numerical approximation by Robinson to calculate the inelastic energy loss according to the theory of Lindhard et al.

The T_{dam} of the PKA thus determined is responsible for the primary radiation damage caused due to the displacements of the atoms in the target material. The next important quantity that needs to be determined in order to compute the dpa cross sections is the number of displacements that the atoms in the target material has undergone. It is estimated from the damage energy with the help of an atom-displacement damage model. A few of these models that have been developed in various pioneering works are discussed in the following subsection.

2.3.2.2 Models of atom-displacements damage

The quantification of displacement damage due to interactions of energetic particles in matter was initially attempted during the late 1940s [12, 13]. The first analytical model to calculate the dpa was developed by Kinchin and Pease [14, 88] based on the transfer of kinetic energy above the threshold lattice displacement energy. This is known as the KP model after the names of the developers. Thereafter, a number of models have been developed [18, 22]. The presently accepted standard to predict the primary radiation damage employs the NRT model, developed by Norgett, Robinson and Torrens [18]. The NRT model and the arc-dpa model, recently developed by Nordlund et al. [22], are only discussed here.

Norgett-Robinson-Torrens (NRT) model

The NRT model is an improvement over the KP model. It is given as follows:

$$\nu_{NRT}(T_{dam}) = \begin{cases} 0, & T_{dam} < E_d \\ 1, & E_d \le T_{dam} < 2E_d / 0.8 \\ 0.8\,T_{dam} / 2E_d, & T_{dam} \ge 2E_d / 0.8 \end{cases} . \quad (2.17)$$

The NRT model is different from the KP model in two important ways. The first is the factor 0.8, which is included in the NRT model in order to account for the interactions of the PKA with more realistic interatomic potentials, rather than assuming hard sphere scattering. The second important aspect is the inclusion of the concept of damage energy, where the two modes of sharing of the PKA energy between nuclear and electronic stopping can be considered in a more realistic approach by using the energy partitioning theory of Lindhard et al. Consequently, the assumption of sharp energy cut-off (as in K-P model) is not required. The NRT model has been derived for mono-atomic target materials; the replacement collisions and variation of the threshold lattice displacement energy E_d with crystalline orientations have not been accounted. It provides a useful basis to calculate the number of displaced atoms by a PKA and has been accepted as the international standard to model and compare primary radiation damage in materials.

The NRT model, however, has been found to overestimate the number of displaced atoms compared to more realistic observations and thus provides an upper limit to the prediction of primary radiation damage in a material [20 and related references there]. The actual number of defects that remain in the target material is far less compared to that predicted by the NRT model. This happens due to a large number of self-assisted recombination that takes place during the displacement damage event. Based on the results of advanced simulations and irradiation experiments, an improved atom-displacement damage model, called the arc-dpa model, has been derived [20, 22] to capture the phenomena more realistically.

Athermal recombination corrected – dpa (arc-dpa) model

The recently developed arc-dpa model [22] captures the physical phenomena undergoing in materials just after the formation of PKA (time ~ 10^{-12}s) in greater detail and more realistically compared to the earlier models. In general, there are uncertainties on the results of MD simulations due to the choice of various interatomic potentials, but MD simulations of displacement damage cascades in metals have consistently shown closeness to the experimentally observed damage recombination [89]. The results of such simulations and experiments [24, 90-95] have suggested that the defect production efficiency ξ, which is the ratio of the true number of existing defects to that predicted by NRT model, is much less than 1 for recoil energies above ~ 1 keV. For a number of interatomic potentials used to simulate cascades in dense metals like Iron, ξ is found to vary as a function of energy and reach a saturation value between 0.2 and 0.5 [95]. Mostly, this saturation value is found to be around 0.3, in agreement with experiments.

For the first about 200 fs of PKA interactions, the atoms get displaced in ballistic collisions (the number of these displaced atoms corresponds closely to the NRT model) and after this, the cascade becomes a heat spike [20, 22]. The interior of this heat spike region is less dense compared to the outskirts and it lasts only for a few picoseconds, quenching rapidly and tending towards a perfect crystal. This is called cooling down phase, where many of the displaced atoms regain the lattice positions (original or another lattice site) and many of the vacancies and interstitials initially created during the ballistic phase recombine. This recombination process takes place as a result of natural migrations of atoms due to the kinetic energy introduced by the PKA in the medium. It requires no external thermal assistance and is independent of the ambient temperature of the target. Hence, it is referred as an athermal recombination process. The arc-dpa

model, as obtained after analyzing the MD simulations and experimental results in Ref. [20, 22], is given by Eq. (2.18a) and (2.18b).

$$\nu_{arc-dpa}(T_{dam}) = \begin{cases} 0; & T_{dam} < E_d \\ 1; & E_d \le T_{dam} < 2E_d/0.8 \\ 0.8\,T_{dam}\,\xi(T_{dam})/2E_d; & T_{dam} \ge 2E_d/0.8 \end{cases}, \quad (2.18a)$$

where,

$$\xi(T_{dam}) = \frac{1-c_{ad}}{\left(\frac{2E_d}{0.8}\right)^{b_{ad}}} T_{dam}^{\,b_{ad}} + c_{ad} \quad . \quad (2.18b)$$

The energy dependent damage efficiency term ξ in the arc-dpa model is the ratio of number of actually remaining defects to that predicted by the NRT model. The arc-dpa model depends on three material specific parameters: E_d, b_{ad} and c_{ad}. The b_{ad} and c_{ad} parameters give the dependence of the function ξ on the behavior of the cascade with damage energy. At low and intermediate energies, the number of defects follows a power law with energy and at high energies (~ 100 keV), the production of damage becomes linearly dependent on the energy as the cascades divide into subcascades. At this point of division of cascade into subcascades, there is a saturation of defect formation and ξ attains a constant value. The parameter b_{ad} is negative as the damage efficiency reduces with damage energy. The saturation value is given by the parameter c_{ad}. It is positive and indicates the extent to which the recombination of vacancies within the displacement cascades can be effective in reducing the number of remaining defects. It is lower for dense close packed metals like Fe, Ni, etc. and higher for relatively less dense and open structured elements like Si, C, etc. It is observed that the effect of vacancy recombination is higher in dense metals, which lowers the value of the saturation parameter in them. The

additional b_{ad} and c_{ad} parameters in the arc-dpa model are systematically determined from MD simulations and irradiation experiments by using their correlations with different properties of the materials, like melting temperature, Frenkel pair resistivity, minimum lattice displacement energy, etc [24, 25].

2.3.2.3 Computation of displacements per atom cross sections

The reaction-wise recoil energies and the number of displacement defects ν for the corresponding damage energies are computed. Then the dpa cross sections are calculated as follows:

$$\sigma_D^t(E) = \sum_i \sigma_i(E) \int_0^{E_{R\max}} dE_R K^i(E, E_R) \nu[T_{dam}(E_R)] \quad . \tag{2.19}$$

For any reaction i, the kernel of energy transfer is integrated along with the number of atom-displacements over the full energy range of the recoil atoms and multiplied with the basic neutron interaction cross section σ_i to obtain the dpa cross section. The total dpa cross section is the sum of partial dpa cross sections. The energy-group averaged dpa cross sections are calculated from the point data as follows:

$$\sigma_{D,g}^t = \frac{\int_{E_{g(\min)}}^{E_{g(\max)}} \sigma_D{}^t(E)\varphi(E)dE}{\int_{E_{g(\min)}}^{E_{g(\max)}} \varphi(E)dE} \quad . \tag{2.20}$$

Here, total dpa cross section in neutron energy group *g* is calculated from the point cross sections and the limits of the integration are the boundaries of group *g*.

2.3.3 Gas production cross sections

The light charged products of neutron reactions, i.e. p, d, t, ^{3}He and α, accumulate as gases, i.e. hydrogen, deuterium, tritium, 3 helium and helium, respectively, in the bulk medium. The CPO and other neutron induced reactions that lead to the activation of the target nucleus are considered in the estimation of the gases produced in the target materials. A target nucleus gets transmuted by an incident neutron in all types of reactions, except by elastic scattering (n, n) and by inelastic scattering (n, n′) reaction processes. Therefore, the total activation cross section at the neutron energy *E* can be defined as follows:

$$\sigma_{act}(E) = \sigma_{n,\gamma}(E) + \sum_{x} \sigma_{n,x\,n}(E) + \sum_{cpo} \sigma_{(n,particle)}(E) \quad . \tag{2.21}$$

The first term on the right-hand side of Eq. (2.21) represents the cross section for the radiative capture of neutron. The symbol *x* in the suffix of the second term on right hand side can be 2, 3, 4, etc., representing multiple neutron emission cross sections, (n, xn). Generally, the (n, 2n) reaction is sufficiently probable to occur within 20 MeV limit of neutrons, encountered in fission and fusion systems and the (n, 3n), (n, 4n), etc. reactions are more probable in fusion related and accelerator driven subcritical systems. The third term is the sum of all the cross sections where one or more light charged particles are emitted. In order to correctly predict a particular gas species produced by neutron induced reactions using the basic evaluated nuclear data all the reactions where the corresponding charged particle is present in the exit channel are taken into account. This is because there can be non-negligible contributions from reactions where more

than one particles are emitted such as (n, n α), (n, p α), (n, 2n α), etc, in addition to the (n, p), (n, d), (n, α), reactions where a single particle is emitted.

The sum of all the neutron reaction cross sections producing proton, deuteron, triton, ^{3}He and alpha are estimated separately to give the corresponding gas production cross sections. All the cross sections of CPO reactions contributing to the production of various charged species are often not disentangled separately in the evaluation of nuclear data by using the nuclear model codes like EMPIRE [96], TALYS [60], etc. A significant part of the charged particle production cross sections can be sometimes given in lumped form in a single section (reaction MT = 5) [79]. In such cases, these cross sections are taken into account to compute the total production of various light charged particles, by using the data for the yields of the respective charged species which are given in File 6 (MT = 5).

2.3.4 Neutron heating cross sections

The light charged species such as proton, deuteron, alpha, etc. and the heavy recoiling nucleus after neutron interactions deposit their kinetic energy almost entirely while travelling through the medium. The charge neutral products of nuclear reactions, i.e. neutrons and photons are assumed not to deposit their energy at least locally in the medium, but may do so after travelling over large distances. It is the kinetic energy of a charged reaction product which is estimated in order to determine the heating due to neutrons, so the phenomenon has an acronym as ‘kerma’ expanding as ‘kinetic energy release in materials’.

The kinetic energies of secondary particles and recoil nucleus are calculated by applying the laws of conservation of energy and momentum and by using their energy and angular distributions data from a basic evaluated nuclear data file. The sum of the energies of recoiling

nucleus and other charged products of a neutron-induced reaction gives the estimate of the total heat energy likely to be deposited locally in the medium. This energy, multiplied with the cross section for the respective reaction process, gives the neutron heating cross section (kerma coefficient). The total kerma coefficient for a material *p* at the neutron energy *E* is defined as follows:

$$k_p(E) = \sum_q \sum_r \overline{E}_{pqr}(E)\sigma_{pq}(E) \quad . \tag{2.22}$$

The quantity$\bar{E}$ in the RHS of Eq. (2.22) denote the average kinetic energy carried away by the r^{th} secondary charged species and σ is the cross section of the q^{th} reaction process ((n, n), (n, n′), (n, γ), (n, p), (n, 2n), (n, p α), (n, nα), etc.). This is called the 'direct method' of computing kerma coefficient.

Another way of estimating the neutron heating is by the energy balance method. In this method, the energies of the outgoing neutrons and emitted photons are subtracted from the available energy in order to get the energy which will heat the medium. The total kerma coefficient of material *p*in this method is obtained by adding over all the neutron reactions *q* as follows [29]:

$$k_p(E) = \sum_q \left(E + Q_{pq} - \overline{E}_{pq,n} - \overline{E}_{pq,\gamma}\right)\sigma_q(E) \quad . \tag{2.23}$$

Here, Q_{pq} is the mass-difference Q-value of material nucleus *p* for reaction *q* and the quantities $\bar{E}_{pq,n}$ and $\bar{E}_{pq,\gamma}$ are average energies of the secondary neutrons and photons respectively.

The direct method is followed in the present study. In different reactions, the energy of the recoil nucleus is calculated as discussed above and the energies of light charged particles are calculated as follows [79]:

$$E_{particle} = E\frac{A'}{(A+1)^2}(\beta^2 + 2\beta\mu + 1) \quad . \tag{2.24}$$

Here, β is defined as

$$\beta = \left[\frac{A(A+1-A')}{A'}\left(1+\frac{A+1}{A}\frac{Q}{E}\right)\right]^{\frac{1}{2}} \quad . \tag{2.25}$$

Here A, A', Q and μ are defined in the same way as in Eq. (2.9) and Eq. (2.10). In elastic scattering, $Q = 0$ and $A' = 1$ in elastic scattering and inelastic scattering reaction. In some cases when recoil and / or outgoing charged particle data are not present in the basic evaluated nuclear data file, Eqs. (2.7), (2.11) – (2.14) are used to compute their energies.

2.4 Salient working description of CRaD code

The CRaD code is written in FORTRAN programming language in the Lahey / Fujitsu FORTRAN 95 (LF95) [97]. A block diagram of the code is presented in Fig. 2.1. A meticulous investigation of the neutron reaction data in ENDF-6 files has been carried out in order to develop the methodologies of computing the four metrics of primary radiation damage by using the CRaD code [78, 83-84, 98-101]. The basic requirements of this code are the unprocessed evaluated nuclear data file and a pre-processed neutron interaction cross section data file. The CRaD code does not pre-process the cross sections from tabulated cross sections (File 3) or from the resonance parameters (File 2) and one of the nuclear data processing codes like NJOY-2016 [29], PREPRO [86], etc. is required to pre-process these files to produce temperature-dependent point basic cross sections. The post-processing and computations using CRaD code requires the

data in Files 1, 3, 4, 5, 6, 12 and 15. The information in File 1 is used to check if the cross sections for a particular reaction (MT) are present or not.

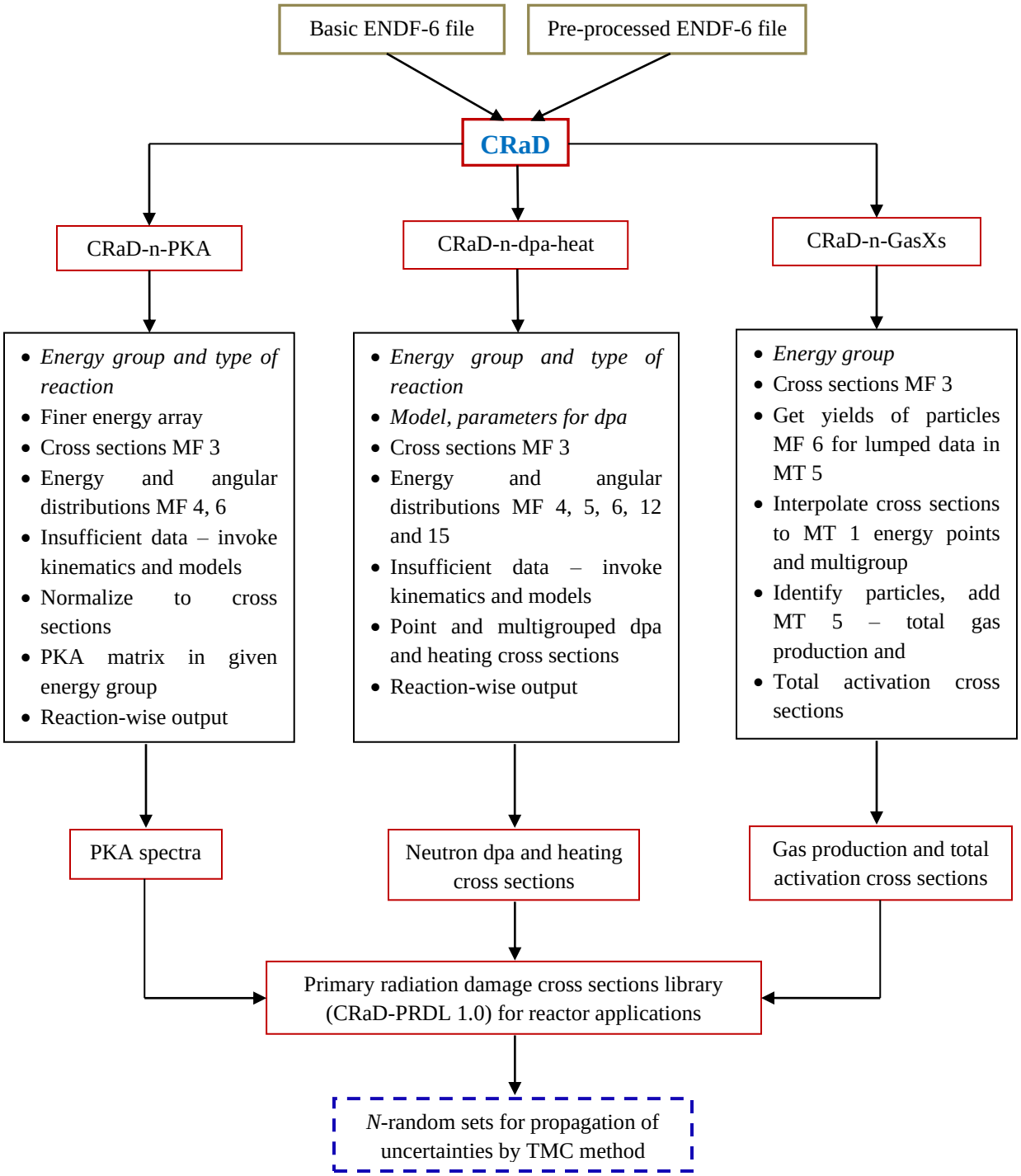

Fig. 2.1: Block diagram of CRaD code describing the salient features (the main user inputs in each calculation are shown in italics)

CRaD-n-PKA – In the computation of PKA spectra, the CRaD code takes the type of energy group structure as input. It makes this energy group finer by introducing more points equally in each group and then calculates the PKA spectrum by considering these points for both the incident and recoil energies. So, the same energy group structure is followed for both incident neutrons and recoil atoms. The PKA spectrum is integrated over the full energy range of recoils and it is normalized to the basic cross section corresponding to the original incident neutron energy group structure. The PKA spectra matrix finally obtained is of the order ($N \times N$), where N is the number of energy groups given as input.

CRaD-n-dpa-heat – The atom-displacements functions that can be optionally implemented while using the CRaD code are the NRT model and the arc-dpa model. The parameters E_d, b_{ad} and c_{ad} has to be given as inputs, which, if not provided the code uses the in-built values specific to the target material in order to find the number of defects. In order to compute neutron heating, the general approach followed is that by the direct method which uses the particle, recoil data from the unprocessed file and also applies the kinematic equations whenever required. For the given types of reactions (it can also be total dpa / heating), the code gives both dpa and heating cross sections in point energy-cross sections form and in the multigrouped data form (the energy group structure option is given as input).

CRaD-n-GasXs – The calculation of the gas production cross sections is performed in the required multigrouped forms which will be suitable for the estimations of the concentrations of gases for a given neutron spectrum in the subsequent steps. The MT numbers (in File 3) for the required CPO reactions are identified and the corresponding cross sections are multi-grouped and added in a sequence to get the total production cross sections of a particular type of particle.

The neutron energy range in all the above calculations is limited from 10^{-5} eV to 20 MeV. The point and multigrouped primary radiation damage cross sections and their neutron spectra-integrated quantities for some important structural materials thus computed by using the basic evaluated nuclear data files are compiled into a library called CRaD-PRDL 1.0. In a similar way, a large number (N) of random databases of these cross sections are generated in order to study the propagation of nuclear data uncertainties in the metrics according to the TMC [62] methodology.

2.5 Summary

The ENDF-6 basic evaluated nuclear data necessary in the estimations of the metrics of primary radiation damage and the methodologies to compute the metrics as developed in the CRaD code are discussed. The salient working structures of the CRaD code are described. The neutron spectra-integrated quantities corresponding to each of these metrics such as PKA rates, average energies of PKAs, dpa, concentrations of gases and heating rates are determined from the corresponding cross sections which are obtained by following the standard ENDF-6 procedures and methodologies as discussed in this chapter.

Chapter 3

The Effects of Nuclear Data and Neutron Spectra on the Primary Radiation Damage Metrics

3.1 Introduction

The metrics of primary radiation damage are estimated using the CRaD code by applying the methodologies developed in the previous chapter. As these estimations are performed, the results are compared with the NJOY-2016 [29], NJOY21 [85] codes and other available data from the literature. The dependence of these metrics on the incident neutron spectra are investigated and the neutron spectra-integrated primary radiation damage parameters such as the PKA rates, dpa, concentrations of produced gases, neutron heating rate, etc are estimated in this chapter. This chapter is organized into four parts based on the investigations on the four metrics. The investigations on PKA spectra and related quantities are presented in Section 3.2, dpa cross sections and integrated dpa are presented in Section 3.3, gas production due to transmutation reactions and related quantities are presented in Section 3.4 and neutron heating cross sections and integrated neutron heating rates are presented in Section 3.5.

3.2 PKA spectra metric of atom-displacement damage

The displacement damage of the atoms in a lattice structure is most often quantified by estimating the displacements per atom (dpa) in the material due to irradiation of neutrons. Both dpa and PKA spectra, combined together, give a more complete picture of the primary radiation damage that occurs in different irradiation conditions. The PKA spectra in different reactions are computed according to the methods discussed in Chapter 2 and are compared with the data obtained from the NJOY codes. The contributions of various neutron reactions to the energy

distribution of PKAs, rate of formation of PKAs and their cumulative fractions for given neutron fields are studied.

3.2.1 Comparison of PKA spectra between CRaD and NJOY-2016 codes

The PKA spectra for different isotopes at various incident neutron energies computed using CRaD code have been compared with the results from the NJOY-2016 code. A few of these comparisons are presented here. The PKA spectra due to elastic scattering of a 17.1 MeV neutron in ^{58}Ni obtained using CRaD code and the GROUPR module of NJOY-2016 are shown in Fig. 3.1. It can be observed here that the probability to form the PKAs per unit energy of the recoiling nucleus is nearly constant at low energies (up to about 1 keV) and then decreases at higher energies. The oscillatory behavior around 100 keV recoil energy region is a manifestation of the anisotropic elastic scattering of higher energy neutrons.

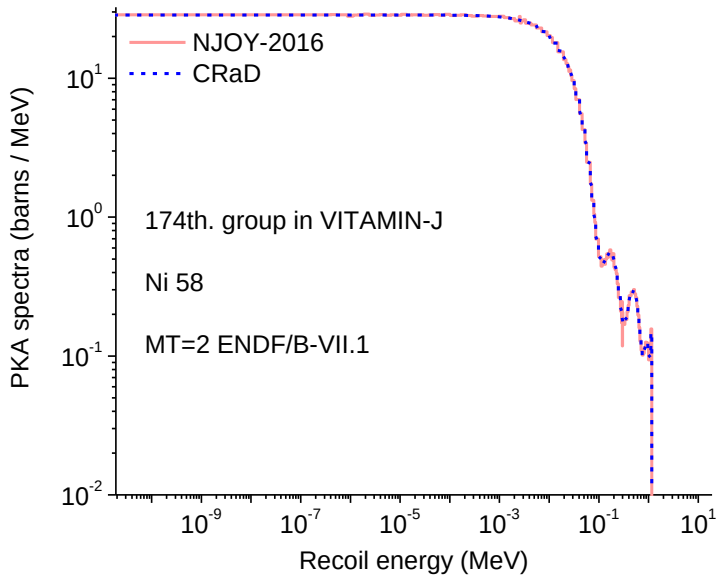

Fig. 3.1: Comparison of PKA spectrum resulting from elastic scattering of a 17.1 MeV neutron in ^{58}Ni, between CRaD and data obtained from GROUPR module of NJOY-2016.

The PKA spectrum due to inelastic scattering of a 10.25 MeV neutron from the 6th resolved level of the compound ^{58}Ni nucleus, as calculated using the CRaD code is shown in Fig.

3.2 (a). The PKA spectrum from the continuum and total inelastic scattering are shown in Fig. 3.2 (b) and (c). These results show good agreement with the data from NJOY-2016 code. Note that, unlike the resolved level inelastic scattering, the PKA spectrum from continuum inelastic scattering has non-zero contribution in the low energy region.

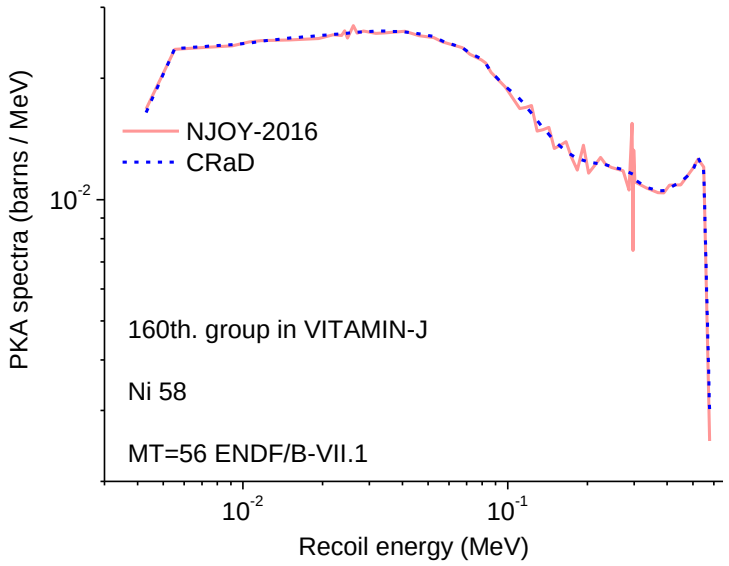

Fig. 3.2 (a)

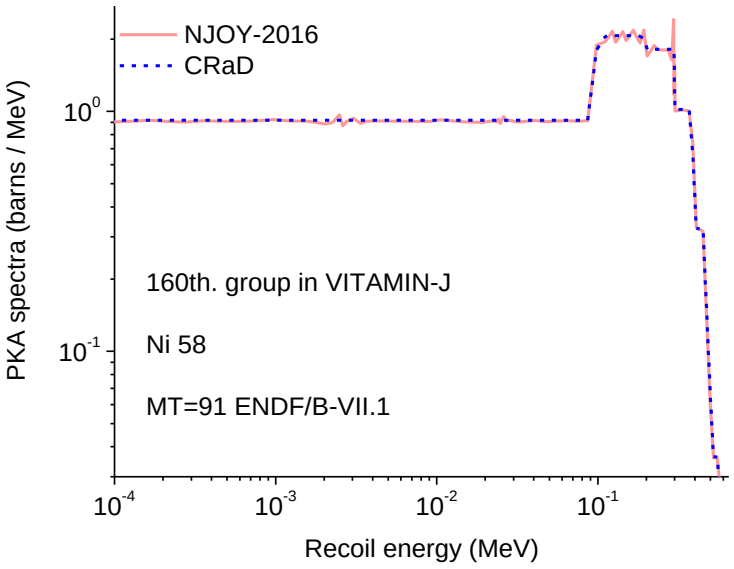

Fig. 3.2 (b)

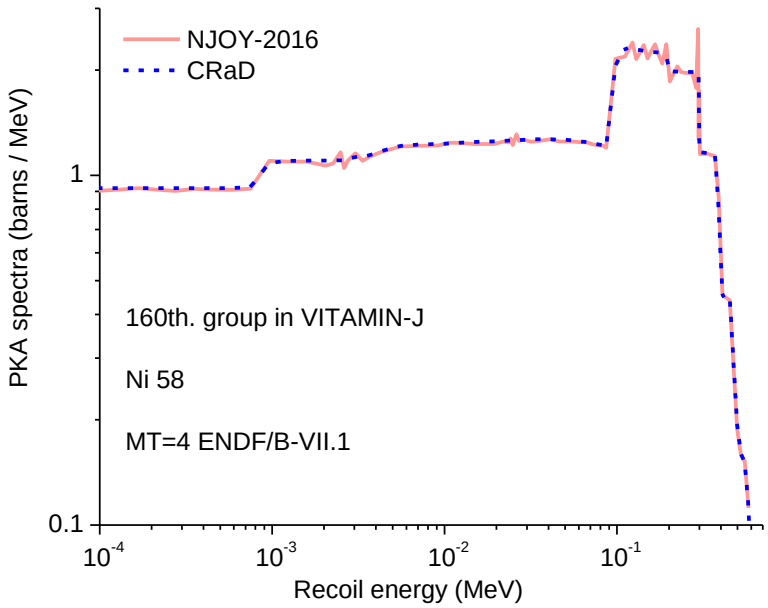

Fig. 3.2 (c)

Fig. 3.2: Comparison of the PKA spectrum due to inelastic scattering of a 10.25 MeV neutron as obtained by using CRaD and GROUPR module of NJOY-2016; (a): from the 6th resolved level of the compound nucleus; (b): from the continuum; (c): total.

The PKA spectrum calculated for the 6th excited level in (n, p) reaction and the continuum (n, p) reaction in ^{28}Si by a 14 MeV neutron are shown in Fig. 3.3, for illustration. The agreement with the result from NJOY-2016 is found to be good.

In a similar manner as described above, the PKA spectra at other incident energies are also compared with the outputs of GROUPR module and good agreements are observed. Similar exercises are also performed with different target isotopes and basic evaluated nuclear data libraries, and the computation methodologies of PKA spectra in the CRaD code are successfully validated. The PKA spectra resulting from many possible partial reactions of a 14.5 MeV neutron with ^{58}Ni, calculated by CRaD code are presented in Fig. 3.4. The 'sum' PKA spectra is obtained by adding all the partial contributions shown here. Note that the major contributions in this case come from (n, n), (n, n′), (n, n p), (n, p) and (n, α) reactions. The (n, α) reaction gives a large share of higher energy PKAs.

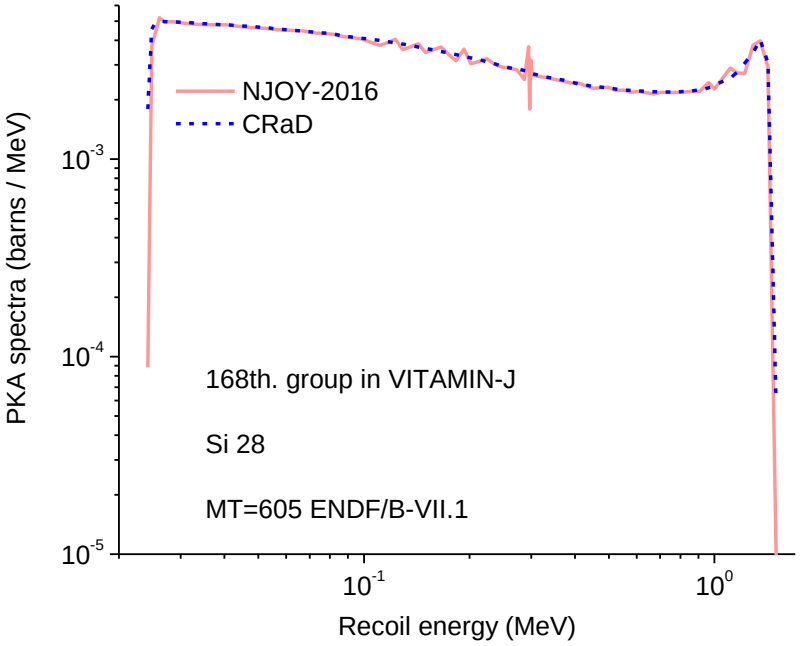

Fig. 3.3 (a)

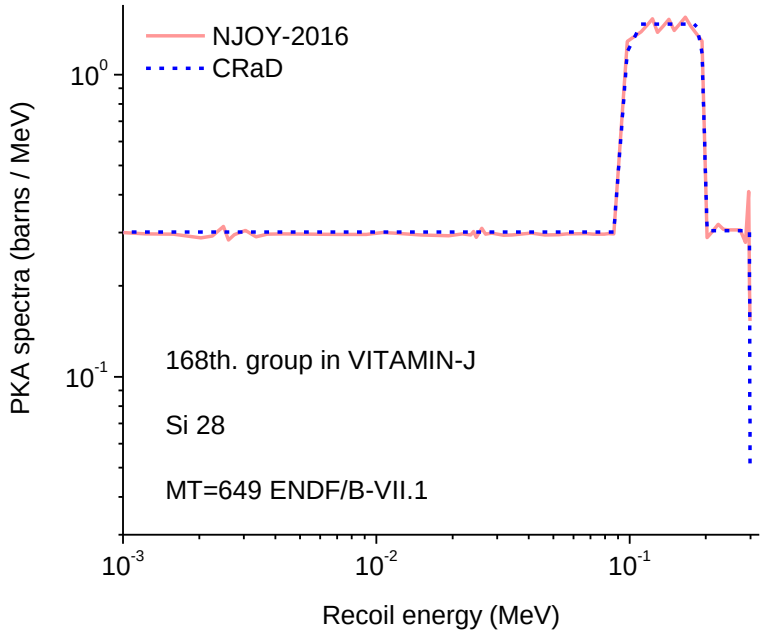

Fig. 3.3 (b)

Fig. 3.3: Comparison of PKA spectrum in (n, p) reaction of a 14 MeV neutron in ^{28}Si as obtained by using CRaD and GROUPR module of NJOY-2016; (a): 6th discrete level of the compound nucleus; (b): continuum.

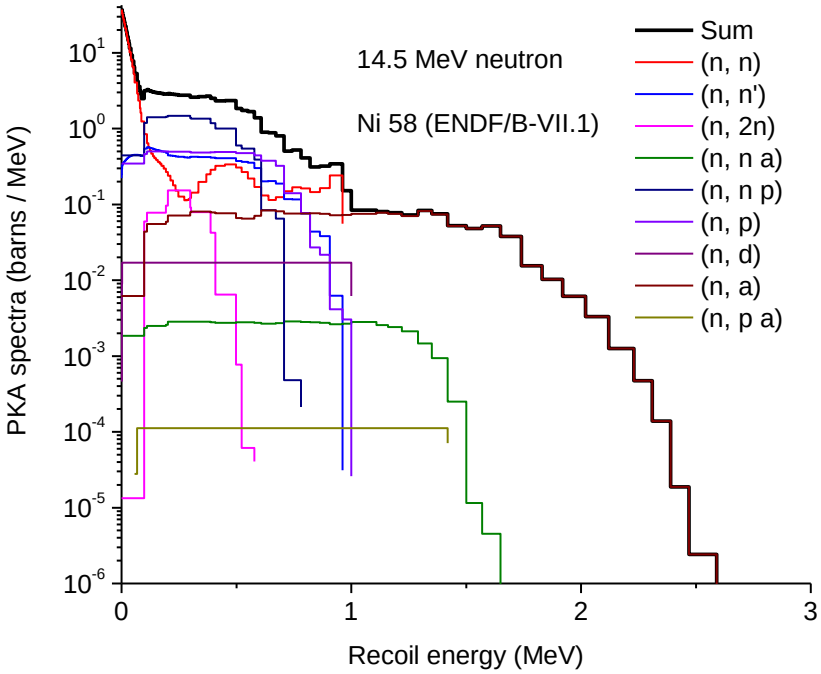

Fig. 3.4: The spectra of the PKAs resulting from various partial reactions of a 14.5 MeV neutron in ^{58}Ni isotope calculated by the CRaD code using the nuclear data in ENDF/B-VII.1 library. The 'Sum' PKA spectra is obtained by adding the partial contributions shown here.

3.2.2 Rate of formation of PKAs and cumulative PKA spectra

As observed in [102-105], the PKA spectrum is of foremost importance to influence the micro structural evolution of damage in the radiation induced material. Since the formation of PKAs is the first event in the primary damage production phenomena, the spectra of these atoms directly connect to the morphology of radiation damage. When combined with the incident neutron field, the PKA spectra characterize the primary radiation damage that is specific to the radiation environment. The PKA spectra thus computed are applied here to estimate the rate of formation of energetic PKAs and the cumulative PKA spectra, which are useful to differentiate between the effects of different incident neutron spectra. Often in these estimates, it is required to specify the physical quantities in the target element, rather than in individual isotopes. Hence, we calculate the PKA spectra and other quantities in the element, from their isotopic values by

weighting with the isotopic abundances (A_{iso}). The PKA spectrum in the target element is calculated as follows:

$$\left(\frac{d\sigma(E,E_R)}{dE_R}\right)_{element} = \sum_{iso} A_{iso}\left(\frac{d\sigma(E,E_R)}{dE_R}\right)_{iso} . \quad (3.1)$$

The rate of PKAs per unit volume is calculated by multiplying the PKA rate with the atom density of the target element. For the neutron spectrum φ and atom density of target ρ, it is defined for a recoil energy group as follows:

$$\left(PKA\,rate\right)_{g_R} = 10^{-24}\rho\sum_{g_n=1}^{G}\left(\frac{d\sigma(E,E_R)}{dE_R}\right)_{g_n}(E_{g_R+1}-E_{g_R})\varphi_{g_n} . \quad (3.2)$$

When the units of σ, ρ and φ are barns, cm^{-3} and $neutrons.cm^{-2}.s^{-1}$ respectively, the units of PKA rate are $PKAs.cm^{-3}.s^{-1}$. In Eq. (3.2), the PKA spectrum value obtained from CRaD code is multiplied with the width of the particular recoil energy group (g_R) to find the cross section for forming a PKA in the interaction where energy transfer from E to E_R takes place. The product of this cross section and neutron flux in an incident energy group (g_n) gives the PKA rate in the particular neutron group. On summing over the full neutron energy spectrum and multiplying with ρ and 10^{-24}, we obtain the rate of PKAs produced per unit volume in the material for a given recoil energy. Following this procedure for all the recoil energy groups, the PKA spectra can be converted to the spectra giving the rate of PKAs formed per unit volume of the target subjected to a neutron spectrum. Fig. 3.5 shows a few neutron spectra for which we estimate the PKAs. Here, representative cases of fast neutron fission (PFBR [106] core centre), thermal neutron fission (PWR-RPV and BWR-RPV [107]) and fusion neutron (ITER-DT and JAEA-FNS [107])

spectra are shown. Also, the neutron spectra at the radial blanket, grid plate top and lattice plate locations of PFBR [106] are considered for illustrations. The PWR-PRV and BWR-RPV neutron spectra are plotted in 198-energy groups [107] and all the other spectra are plotted in the VITAMIN-J 175-energy groups [107].

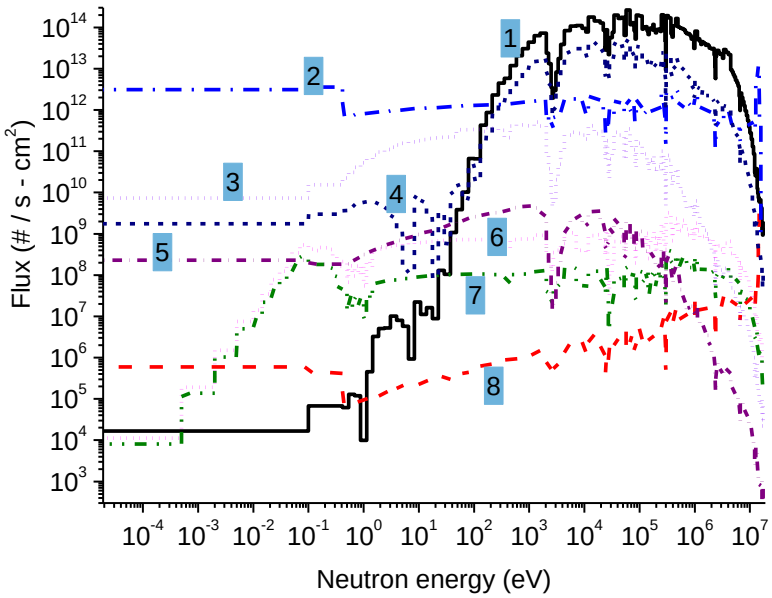

(1) PFBR core centre (2) ITER-DT (3) PFBR grid plate top (4) PFBR radial blanket
(5) PFBR lattice plate (6) PWR-RPV (7) BWR-RPV (8) JAEA-FNS

Fig. 3.5: Neutron energy-flux spectra of different sources

The PKA rates in Fe corresponding to these neutron spectra are calculated for illustration. These are presented in Fig. 3.6. The variation of the formation of PKAs with recoil energy depends on the incident neutron spectrum. In all the neutron spectra, the rate of forming PKAs with energy greater than 1 MeV is very less (about 10^3) compared to that with energy in the range of a few keV. It is should be noted that the absolute magnitudes of the formation of PKAs differs due to the differences in the absolute magnitudes of the neutron spectra. Compared to the neutron spectrum at the core centre location of PFBR, all other neutron spectra considered here are softer and have significant proportion of neutrons in the low energies. Hence, in PFBR core

centre the PKA rates are proportionately higher in the 1 to 100 keV recoil energy range, whereas in other neutron spectra these are mostly uniform from very low to the keV recoil energy range. The rate of formation of higher energy PKAs will be more for lighter target elements like C, Si, etc.

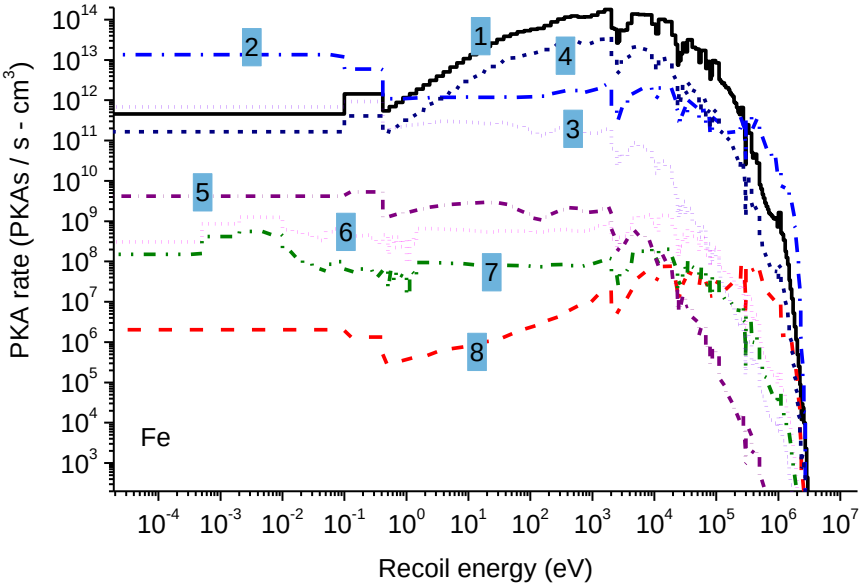

(1) PFBR core centre (2) ITER-DT (3) PFBR grid plate top (4) PFBR radial blanket
(5) PFBR lattice plate (6) PWR-RPV (7) BWR-RPV (8) JAEA-FNS

Fig. 3.6: The rate of formation of PKAs in Fe as target material in different neutron fields.

The rate of formation of the PKAs is integrated over the recoil energy to obtain the cumulative distribution of the PKAs. For some representative incident neutron spectra, the cumulative distributions of the PKAs in Fe are presented in Fig. 3.7. Again, this cumulative distribution bears the signature of the incident neutron spectrum. For a given neutron spectrum, the corresponding cumulative distribution of the PKAs quantify the fraction of PKAs that are below a particular recoil energy. The cumulative distribution shows a steep or a moderate slope depending on the relative number of neutrons in different energy regions. Consider for example, the cumulative distributions of the PKAs in the fusion neutron spectra ITER-DT and JAEA-FNS and all the other neutron spectra. The PKA distributions corresponding to the fusion spectra have

steeper slopes compared to the other cases shown in Fig. 3.7. In the medium mass structural nuclei, like Fe, the fission neutron spectrum produces PKAs predominantly within the energy range of 1 to a few tens of keV. However, in lighter target nuclei, like C, a small number of PKAs can also be formed with 2 – 6 MeV energies under the fission neutron spectrum. The average energy of Fe PKAs in fusion neutron spectrum is about a few hundred keV. It can be observed from Fig. 3.7 that 60% of Fe PKAs in PFBR core centre are formed with energy less than about 30 keV, while in case of PWR-RPV and BWR-RPV spectra this energy is slightly higher, about 50 keV. In the ITER-DT and JAEA-FNS spectra, this fraction of Fe PKAs lies approximately below 300 keV. Also note that, in the radial blanket, grid plate top and lattice plate locations of PFBR, 50% of the Fe PKAs are formed much below 10 keV. Overall, the shape of the neutron spectrum plays an important role in ascertaining the neutron spectrum-averaged PKA energy.

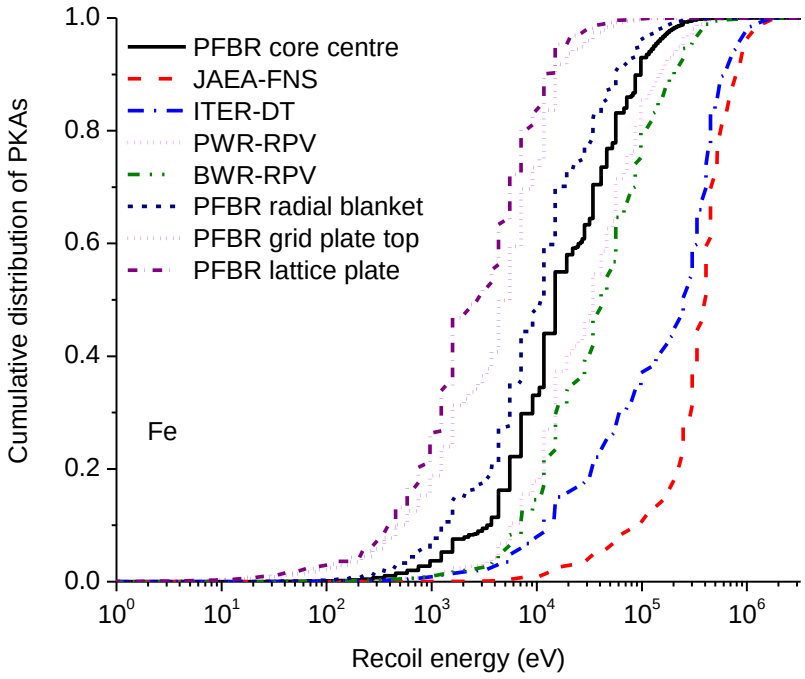

Fig. 3.7: Fraction of Fe PKAs that are formed below particular recoil energy when irradiated in different neutron fields.

3.3 The dpa metric of atom-displacement damage

The evaluation of the reaction kernels is the most important aspect in the computation of the dpa cross sections. A few general features observed in the energy-wise variations of dpa cross sections are discussed in Section 3.3.1. The dpa cross sections and dpa rates computed using the CRaD code are compared with the ASTM data [19] and the results that are obtained from NJOY-2016 and other codes [98]. These are discussed in Section 3.3.2. The results obtained by applying the arc-dpa model in the CRaD code [108] are discussed in Section 3.3.3.

3.3.1 Energy variations of dpa cross sections

The anisotropy of neutron scattering must be considered accurately and its effect is to reduce the dpa cross sections because of reduction in the transfer of energy and momentum to the recoil nucleus with increasingly forward-peaked elastic angular distribution. It is illustrated in Fig. 3.8 for the elastic scattering of neutrons in ^{56}Fe, where the neutron cross sections and angular distributions of secondary neutrons from ENDF/B-VII.1 are used. The effect becomes significant beyond about 100 keV. At 2 MeV, for instance, the dpa cross sections are found to be lower by about 62% compared to the situation when isotropic scattering is assumed. The anisotropy in case of inelastic scattering and other higher energy reactions must also be considered accurately, but their effects are comparatively smaller.

The total dpa cross sections along with the contributions from various partial interactions of neutrons in ^{56}Fe target, computed with CRaD code by using the data in ENDF/B-VII.1 nuclear data library are presented in Fig. 3.9 (a), for illustration. The fractional contributions of the partial reactions to the total dpa cross sections are presented in Fig. 3.9 (b). Note that, the main contribution in the low energy region is due to the recoil of the nucleus following radiative

capture of neutrons. The contribution from elastic scattering is substantial over the full energy range 0 – 20 MeV. In the MeV region, contributions from inelastic scattering and other non-elastic reactions become significant. The total dpa cross sections in an element are calculated by adding the isotopic contributions with their abundances. The dpa cross sections in Fe obtained from 5.845% of ^{54}Fe, 91.754% of ^{56}Fe, 2.119% of ^{57}Fe and 0.282% of ^{58}Fe isotopes are shown in Fig. 3.10.

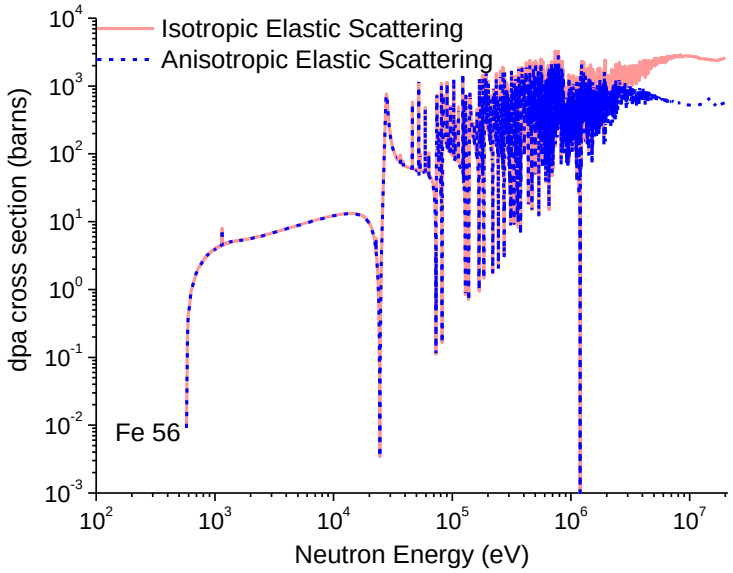

Fig. 3.8: The effect of anisotropic elastic scattering of neutrons on dpa cross section in ^{56}Fe.

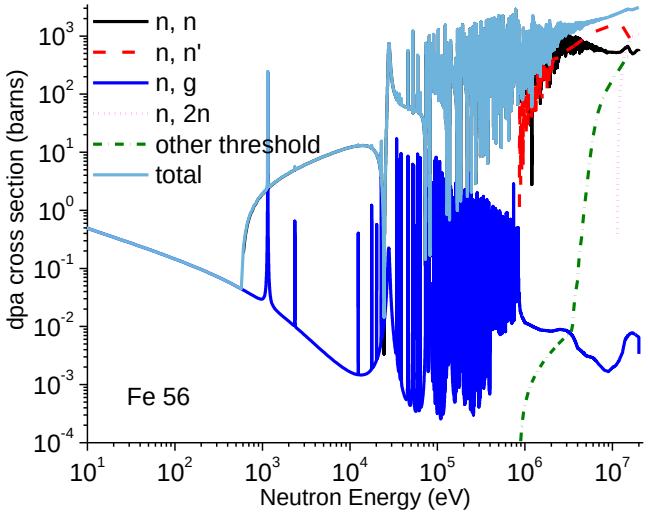

Fig. 3.9 (a)

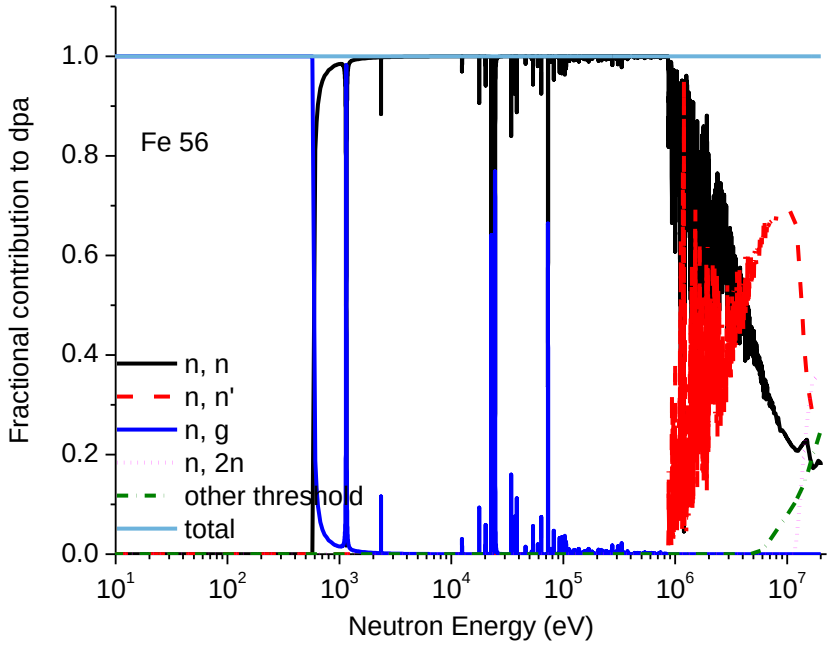

Fig. 3.9 (b)

Fig. 3.9: dpa cross sections in ^{56}Fe; (a): contributions from partial neutron interactions to dpa cross sections; (b): relative contributions of partials to total.

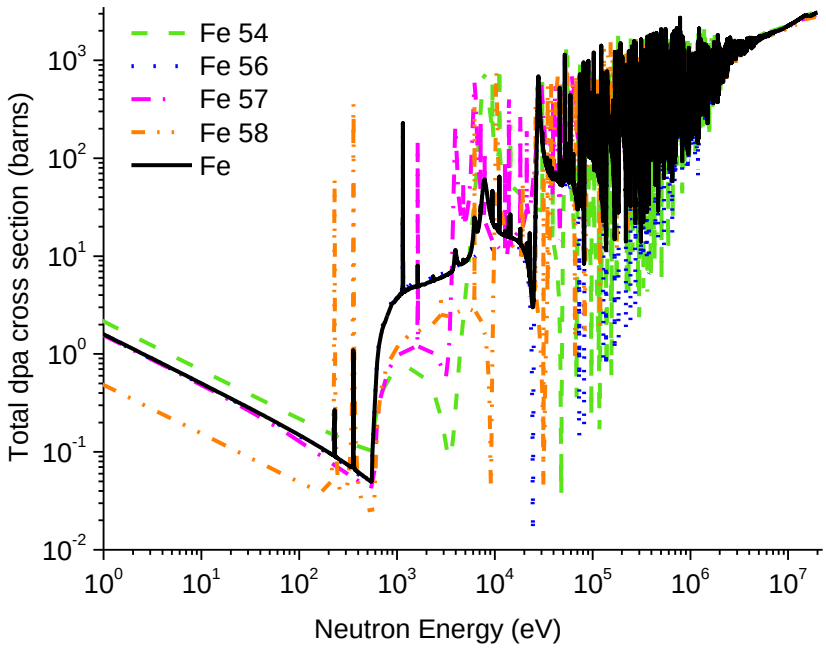

Fig. 3.10: Total dpa cross sections in Fe and its isotopes calculated with the CRaD code by using the data in ENDF/B-VII.1.

3.3.2 Comparison of NRT-dpa cross sections between CRaD and other available standards

The dpa cross sections computed using CRaD code are compared with NJOY-2016 and ASTM E693-12 data [98]. The comparison of total dpa cross sections with NJOY-2016 data are presented in Fig. 3.11. The overall agreement is found to be within 1%. The large difference around 1 keV can be explained by looking at the NRT model in Eq. (2.17) as follows. The second condition in NRT function says that there can be a displacement of only one atom if the damage energy lies between E_d and $2E_d/0.8$. This condition is exactly followed while computing the number of displacements by using the CRaD code. The dpa cross sections are obtained from HEATR/NJOY-2016 by multiplying a factor $0.8/2E_d$ with the damage energy cross sections which are its natural output. While this procedure is all right for damage energies above $2E_d/0.8$, it deviates from following the second condition in the NRT model and under predicts the number of displacements when damage energies are between 40 and 100 eV (corresponding to incident neutrons of energy between ~ 500 to 1500 eV).

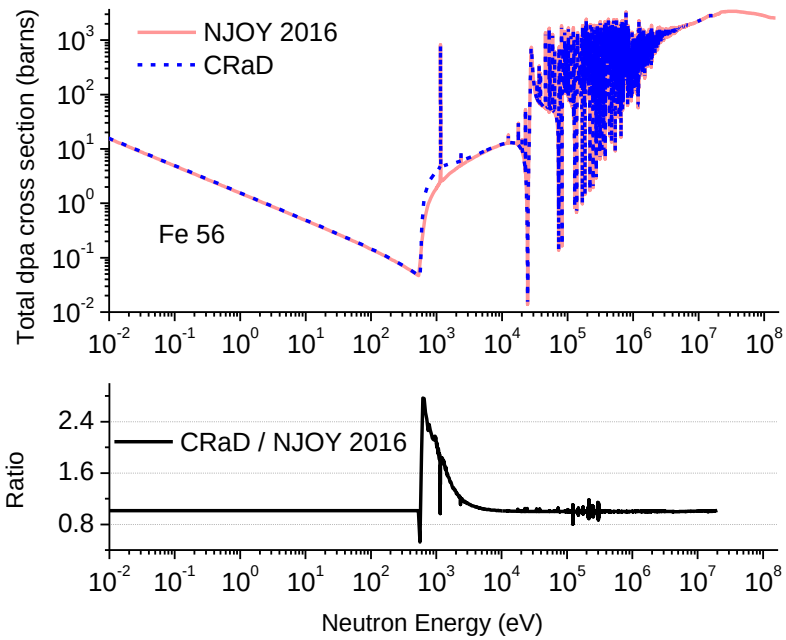

Fig. 3.11: Total dpa cross section in ^{56}Fe: comparison between CRaD and NJOY-2016.

The ASTM NRT-dpa cross sections were processed from ENDF/B-VI library in the 640 extended SAND-II group structure [98]. There is not much difference in the cross sections of iron between the ENDF/B-VI and VII.1 libraries. The references for the temperature of the material, self-shielding effects and the weighting function are not provided with this data. In order to compare with the ASTM NRT-dpa cross sections, we assumed a constant weighting flux in Eq. (2.20) for averaging dpa cross sections of Fe at room temperature. The comparison of these dpa cross sections are presented in Fig. 3.12. The agreement is found to be good and some differences (spikes in ratio plot) are observed in predicting too small values of dpa cross sections, where the differences are in the range of 0.02 to 0.1 barns only.

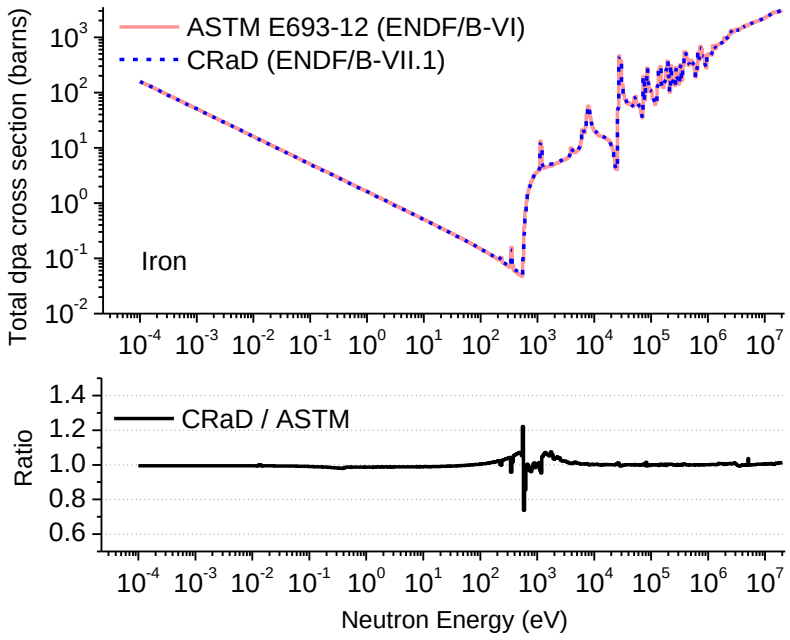

Fig. 3.12: dpa cross section of Fe in 640 energy groups: CRaD vs. ASTM E693-12.

3.3.3 Comparison of NRT dpa in structural materials from different codes

The elements Fe, Ni and Cr are the most important and dominant constituents in different types of structural stainless steels. The total dpa for irradiation time t is calculated from the dpa cross sections and flux spectrum φ of neutrons as follows:

$$dpa = t\sum_{g=1}^{N}\sigma_{D,g}^{t}\varphi_{g} \quad . \tag{3.3}$$

Here, *N* is the total number of energy groups. The dpa rates in Fe, Cr and Ni at some selected core locations of PFBR is compared in Table 3.1 by using the NRT-dpa cross sections from NJOY-2016 and CRaD codes. For Fe, the comparison is also made with ASTM E693-12 standard dpa cross sections [98]. At all the locations, because of its higher dpa cross sections, Ni is found to have higher dpa rates than the other two elements. The agreement between the dpa rates in Fe obtained from CRaD and ASTM E693-12 is about 4% and that from CRaD and NJOY-2016 codes is about 1.2%. For Ni and Cr, the agreement between the dpa rates obtained from CRaD and NJOY-2016 codes are about 1.2% and 1% respectively [98].

Table 3.1: Comparison of dpa rates (s^{-1}) in Fe, Cr and Ni at selected core locations of PFBR

Element	Code	Core Centre	Grid Plate Top	Lattice Plate	Radial Blanket
Fe	ASTM	2.095E-06	5.753E-10	3.864E-12	2.109E-07
	CRaD	2.081E-06	5.525E-10	3.815E-12	2.085E-07
	NJOY-2016	2.077E-06	5.478E-10	3.773E-12	2.080E-07
Ni	CRaD	2.587E-06	1.012E-09	6.750E-12	2.855E-07
	NJOY-2016	2.586E-06	1.003E-09	6.668E-12	2.850E-07
Cr	CRaD	2.279E-06	6.349E-10	3.766E-12	2.262E-07
	NJOY-2016	2.280E-06	6.312E-10	3.735E-12	2.260E-07

In PFBR [106], the clad and wrapper materials of fuel and blanket assemblies are made of D-9 steel, which contains 66.1% of Fe, 14% of Cr, 15% of Ni and remaining of the elements C, Si, B, Mn and Mo. The composition of D-9 steel used in the study is presented in Table 3.2. The grid plate and control plug of PFBR use SS-316-LN type steel. It is mainly the cumulative radiation damage on the structural materials of the above core components that decides the life of the reactor. The primary sodium pumps and the fuel and blanket assemblies rest on the grid plate at the bottom of the core. The control plug is positioned above the core sub-assemblies. It

contains very critical components like thermo-couples, neutron detectors and control rod drive mechanisms. The fuel and blanket assemblies in PFBR are replaced after 540 effective full power days (efpd) of operation.

Table 3.2: Elemental Composition in D9 Steel

Element	Fe	Cr	Ni	Mo	Mn	C	Si	B
wt%	66.080	14.0	15.0	2.250	2.0	0.043	0.625	0.002

The dpa cross sections of D-9 steel are computed by weighting the dpa cross sections of its constituent elements with their elemental compositions. Since 26 group (ABBN-93) 3-D diffusion theory calculations are performed for estimating core neutronics parameters in PFBR, the dpa cross sections are also computed in this group structure for estimation of dpa in core structural elements. The core-1 flux is used in Eq. (2.20) to collapse the point dpa cross sections into multi-group form. The total dpa in D-9 steel for 540 efpd at various core locations are presented in Table 3.3. Note that the total dpa in D-9 steel at core centre is the lowest (79 dpa for 3 cycles of operation) with dpa cross sections from the ENDF/B-IV based RECOIL [26] code. However, the predictions made by SPECTER [27], NJOY-2016 [29] and CRaD codes for this location are consistently higher than that made by the RECOIL code. Similar trends can also be observed for other locations.

Table 3.3: Estimation of dpa in D9 Steel in PFBR for 3 Cycles (cycle length 180 efpd)

Neutron Flux	Total dpa for 540 efpd of operation			
	RECOIL (ENDF/B-IV)	SPECTER (ENDF/B-V)	NJOY-2016 (ENDF/B-VII.1)	CRaD (ENDF/B-VII.1)
Averaged over inner core	51.1	68.6	69.8	70.8
Inner core maximum*	78.9	106.2	107.9	109.5
Outer core maximum	54.2	72.9	74.1	75.3
Radial blanket maximum	12.5	16.7	16.9	17.2

** Peak flux is 8E+15 neutrons $cm^{-2}s^{-1}$*

3.3.4 Application of arc-dpa model to predict primary radiation damage

The NRT and arc-dpa models are implemented in the CRaD code to assess primary radiation damage. The differences between these two models that give rise to significantly different estimates of dpa are investigated in case of a few important structural materials.

3.3.4.1 The efficiency of damage production in NRT and arc-dpa models

The number of Frenkel pairs in NRT model follows a linear relationship with the damage energy, third condition in Eq. (2.17). The damage efficiency is unity here. But the damage efficiency term in arc-dpa model is energy-dependent and gives a non-linear relation between the number of formed defects and the damage energy. Based on these two models, the variations of damage energy and number of defects formed with the PKA energy in Fe are shown in Fig. 3.13. The parameters [25] of the atom-displacement damage models used in this study are given in Table 3.4. Note, for damage energies above 100 eV, the number of NRT defects is simply 0.01 times the damage energy, whereas the arc-dpa number of defects follows different relations depending on the increasing damage energy. For Fe, both NRT and arc-dpa models predict the formation of only one defect within an energy range 40 to 100 eV in Fig. 3.13. As the energy increases, the results from these two models differ. For Fe, the number of defects predicted by the arc-dpa model saturates to about one-third of the NRT value.

The fractions of the remaining defects to the NRT predicted values for Fe, Ni, Cr, Si and C, calculated using the model parameters (Table 3.4), are shown in Fig. 3.14. Note, the function ξ follows the boundary condition $\xi(2E_d/0.8) = 1$. Although the damage efficiency is greater than one near the threshold [20, 109], this is done to maintain similarity with the NRT model. The damage efficiencies in different materials approach to different constant values. For materials

like Ni, Fe and Cr with higher densities the saturation value is approximately between 0.24 and 0.4, whereas for less dense materials like Si and C it can vary from 0.5 to 0.8 and above. This is because, in the latter materials the interstitials move efficiently towards the periphery of the displacement cascades, thereby reducing the chances for their recombination. This happens due to absence of (or not well localized) heat spikes during the primary radiation damage event in the low density, high melting point and open structure materials, especially in case of Si [89].

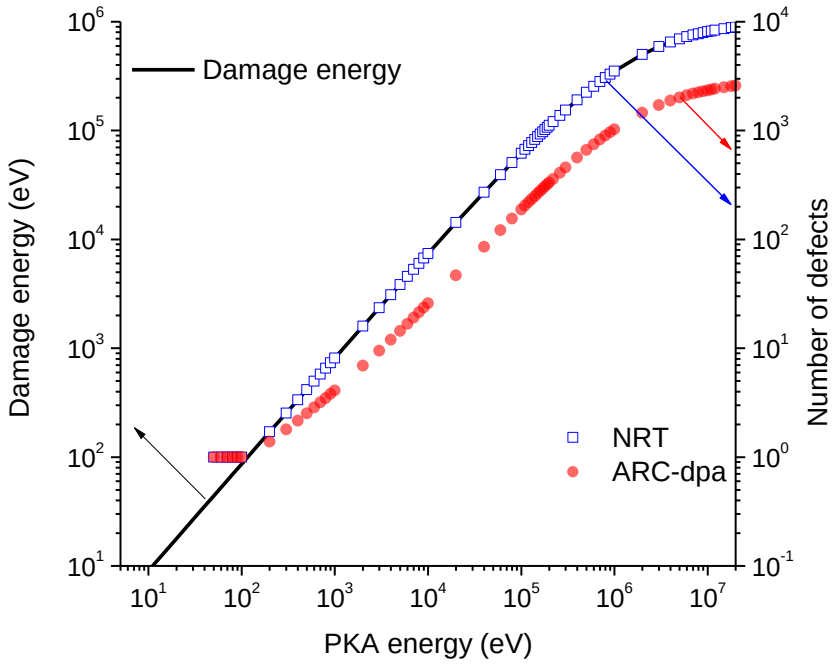

Fig. 3.13: The damage energy as a function of PKA energy in Fe; and the variations of number of defects with damage energy, calculated from the NRT and arc-dpa models. Note that number of defects follows linear relation with damage energy in NRT model, but not in arc-dpa model.

Table 3.4: Model parameters adapted in CRaD for calculation of dpa cross sections

Elements	E_d (eV)	b_{ad}	c_{ad}	Elements	E_d (eV)	b_{ad}	c_{ad}
B	40	-1.0	0.58	Fe	40	-0.568	0.286
C	31	-1.0	0.71	Ni	40	-1.007	0.227
N	40	-1.0	0.5	Cu	40	-0.68	0.16
Si	25	-1.0	0.5	Y	36	-1.0	0.5
Ti	40	-1.0	0.83	Zr	40	-1.0	0.7
V	40	-1.0	0.51	Mo	60	-1.0	0.46
Cr	40	-1.0	0.37	Ta	90	-1.0	0.72
Mn	40	-1.0	0.33	W	70	-0.564	0.119

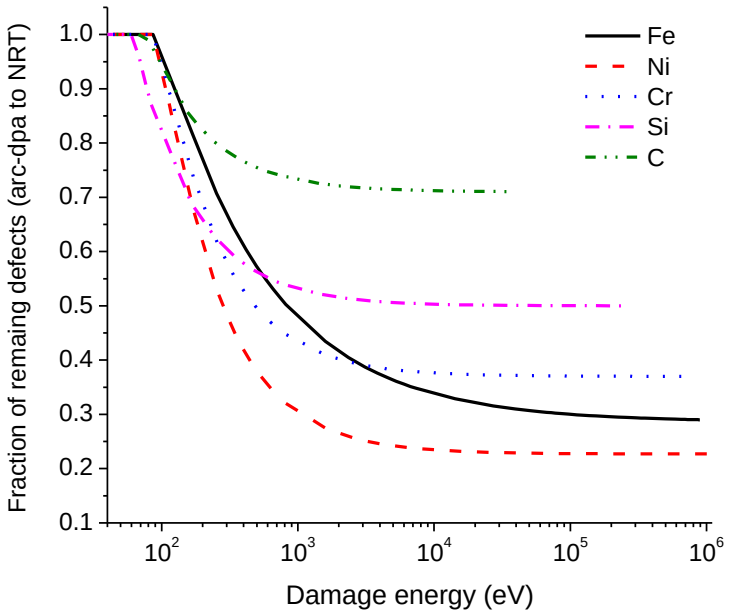

Fig. 3.14: The ratio of the number of actually remaining defects to that predicted by the NRT model in case of a few structural elements.

3.3.4.2 Neutron spectrum averaged damage efficiency

The spectra and the average energies of PKAs calculated by CRaD code using the ENDF/B-VII.1 data are used to find the average damage efficiencies in various materials subjected to neutron irradiations specific to different spectra, viz. PFBR core centre [106], JAEA-FNS, DEMO-HCPB-FW, ITER-DD, and ITER-DT [107]. The neutron spectrum-averaged damage efficiencies for Fe, Ni, Cr, Si and C are presented in Table 3.5. The minimum energy of PKAs in these elements is around 0.5 keV, which result due to radiative capture of low energy neutrons. The PKA energies are higher than 1 keV for high energy neutrons. Hence, the damage efficiencies of the materials are found to be approximately around their respective saturation values for the whole neutron spectrum. Note that the damage efficiency depends moderately on the neutron spectrum. The lowest damage efficiency occurs for the spectrum where the fraction of neutrons above 1 MeV is highest. In JAEA-FNS spectrum, the number of neutrons above 1 MeV has a large increasing trend (see Fig. 3.5) and the average damage

efficiency is lowest here. The variation of the damage efficiency with the neutron spectrum is found to be more for elements like Fe (~ 11%), Ni (~ 3%), etc. compared to that for Si (~ 0.4%) and C (~ nil). This is in accordance with experiments and MD simulations, because the effects of damage recombination are more prominent in metals like Fe, Ni, Cu, etc., whereas Si and C are rather insensitive to these effects (following closely the NRT predictions).

Table 3.5: Neutron spectrum averaged damage efficiency, $\bar{\xi}$

Material	Spectrum				
	PFBR core centre	JAEA - FNS	DEMO-HCPB-FW	ITER-DD	ITER-DT
Fe	0.331	0.299	0.305	0.318	0.304
Ni	0.235	0.228	0.229	0.231	0.229
Cr	0.376	0.371	0.372	0.373	0.371
Si	0.502	0.5	0.501	0.501	0.5
C	0.711	0.711	0.711	0.711	0.711

3.3.4.3 Comparison of dpa cross sections from NRT and arc-dpa models

The neutron dpa cross sections in structural materials based on ENDF/B-VII.1 data are calculated using the CRaD code by applying both the NRT and arc-dpa models. These cross sections are compared here. A few candidate elements and alloys important for applications as structural materials in fusion blanket and core of fission reactors are considered [108]. For illustrations, only the estimated values for D-9 steel and Eurofer97 ferritic steel (see compositions in Table 3.2 and 3.6) are presented here.

Table 3.6: Percentage composition of elements in Eurofer97 ferritic steel

Elements	B	C	N	Si	V	Cr	Mn	Fe	Ta	W
wt %	0.001	0.12	0.029	0.05	0.2	8.5	0.4	89.5	0.1	1.1

The total neutron dpa cross sections in these materials are calculated by adding the fractional contributions from individual elemental dpa cross sections. These are presented in Fig. 3.15. Note, the dpa cross sections from both the models are similar around the neutron energy range which results into the damage energies of the PKAs in the region of threshold lattice displacement energy. For the steel kind of alloys, this threshold energy is considered to be around 40 eV, and with iron as the dominant element, this energy can be transferred via elastic scattering of the neutrons having energies around 500 – 1000 eV. This similarity in this energy range is because both these models give same number of defects around the threshold lattice displacement energy. In all other energy regions, the dpa cross sections from arc-dpa model are smaller than that from NRT model. In the low neutron energy regions, the displacement damage is mainly from the 0.5 – 1.5 keV PKAs produced due to the (n, γ) reaction. At higher energies (~1 MeV neutrons), arc-dpa model yields dpa cross sections which are less than about one-third of those from NRT model. In order to compare the computed dpa cross sections from both models, the dpa cross sections available in JEFF-3.3 dpa database [74] are also shown here.

The total dpa for 1 efpy due to irradiations in various neutron spectra are estimated using CRaD code and from the JEFF-3.3 dpa database. These results are compared in Table 3.7. Note that, the order of magnitude of primary radiation damage in these materials under a given neutron spectrum is similar. The displacement damage (dpa) based on arc-dpa model is lower (about one-third) compared to NRT dpa in both the materials. In case of a vanadium alloy, the predictions from arc-dpa model is found to be about half that of the NRT value [108]. In general, the agreement between the present calculations and the JEFF-3.3 data are found to be good. The differences observed between the values of dpa from CRaD code and JEFF-3.3 data can be attributed to any of the following facts. For some elements, the value of E_d used in CRaD is

different from that used in the evaluation of the JEFF-3.3 database. For example, in case of Si, the E_d value used in CRaD is 25 eV [110], whereas in JEFF-3.3 database it is 36.93 eV; also note that, for C it is 31 eV [111] as used in CRaD, while a value of 69.28 eV is used in JEFF-3.3; etc. The advanced dpa cross sections in JEFF-3.3 are estimated based on following either the arc-dpa model or a combined MD-BCA approach. The uncertainty in dpa due to the uncertainties in the parameters of material physics models is about 5 – 20% [72]. Since the basic neutron interaction data used in the evaluation of JEFF-3.3 dpa database can be different from ENDF/B-VII.1, an additional nuclear data uncertainty of around 6% in the prediction of total dpa is possible [99]. Hence, from the general agreement of the results, the databases generated by the CRaD code are expected to be reliable.

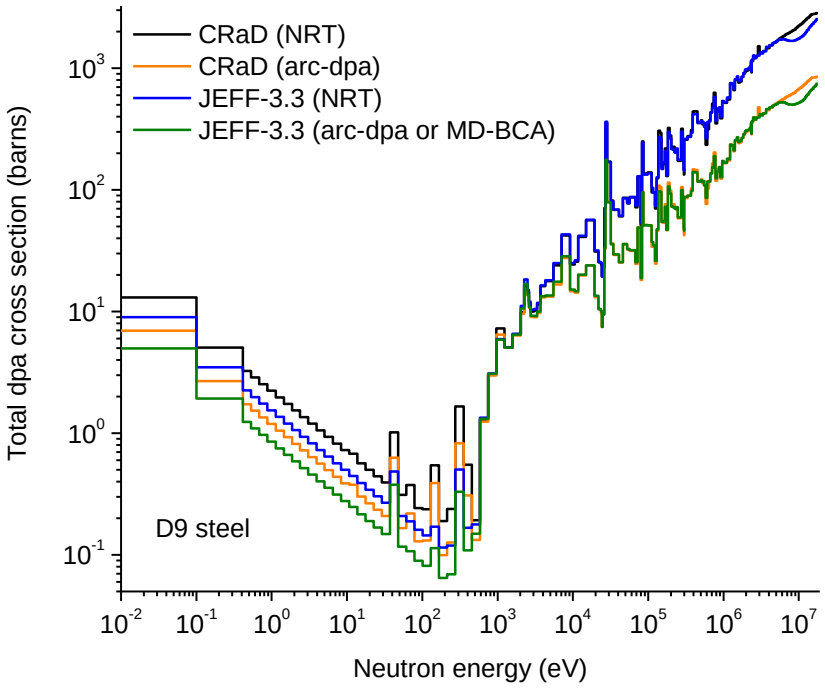

Fig. 3.15 (a)

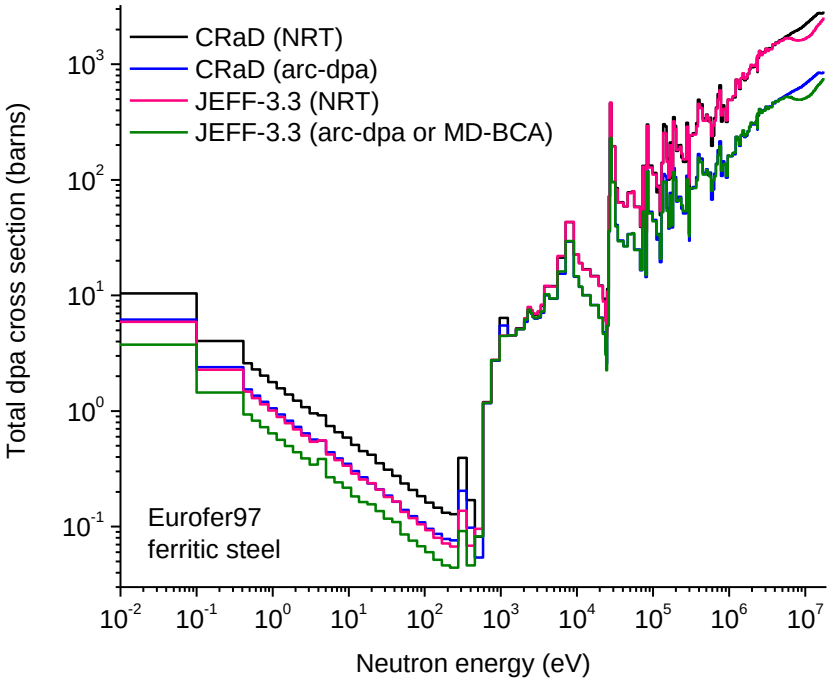

Fig. 3.15 (b)

Fig. 3.15: Total neutron dpa cross sections from JEFF-3.3 database and CRaD code (using ENDF/B-VII.1 data); (a): D-9 steel; (b): Eurofer97 ferritic steel

Table 3.7: Model dependence of total neutron dpa in candidate structural alloys due to 1 efpy of irradiation in different neutron spectra

Structural alloys	Source	Neutron spectrum				
		PFBR core centre	JAEA - FNS	DEMO-HCPB-FW	ITER-DD	ITER-DT
NRT model						
D9 steel	CRaD	68.87	9.10e-4	12.84	1.80e-2	5.19
	JEFF-3.3	68.63	7.48e-4	11.24	1.82e-2	4.48
Eurofer97 Ferritic	CRaD	65.28	9.08e-4	12.64	1.75e-2	5.13
	JEFF-3.3	64.39	7.21e-4	10.69	1.77e-2	4.28
Arc-dpa model						
D9 steel	CRaD	22.97	2.73e-4	3.98	5.73e-3	1.60
	JEFF-3.3	22.87	2.20e-4	3.44	5.79e-3	0.71
Eurofer97 Ferritic	CRaD	22.46	2.76e-4	3.97	5.66e-3	1.61
	JEFF-3.3	22.14	2.18e-4	3.4	5.70e-3	0.46

3.3.5 Necessity to rescale measurements of radiation damage with improved dpa

The use of different basic evaluated nuclear data libraries and computer codes lead to differences in the dpa cross sections and hence, in the predicted values dpa, because of the differences in the evaluation of nuclear data (this part shall be discussed in more detail in Chapter 5) and differences in the methodology of computing dpa cross sections in various codes. Also, different atom-displacement damage models give varying estimates of the dpa cross sections and dpa. Hence, it becomes important to realize how these variations in the predicted primary radiation damage should be dealt with and whether these affects, in any way, the practical designing of the materials for nuclear reactor systems [108].

The observed quantities for radiation damage are the physical and mechanical states of a sample irradiated to a certain fluence of radiation. It is only in the subsequent step, where the measured changes in the properties of the material are correlated to the dpa unit. For example, let's say that a material, after being irradiated to a particular fluence has undergone detrimental changes in its mechanical behavior to an extent that limits its usage for the remaining period, and the standard displacement damage model predicts the dpa accumulated in this material to be 100. So, 100 dpa forms the standard (maximum tolerable dose by the material). The design of any application with this material should be such that the maximum dose achieved is within this highest limit for safety.

Now, with the use of improved nuclear databases, different computer codes and advanced modeling the prediction of the limits of dpa for various irradiation spectra can differ from the previously prescribed standards. However, it can be appreciated that all these predictions aim to determine and compare the *same* real state of the primary radiation damage of the material.

Whatever its value in dpa may be (before or after improvement), it is the same material damage which is being correlated. Neither the material nor the irradiation fluence has changed, only the limit of the predicted dpa can be different now. For example, this implies that, if the improved prediction gives 30 dpa instead of 100 dpa for the same material and fluence as above, then the designer has to simply re-adjust the scale which correlates a material property with dpa. This should not have any impact on the in-reactor operation time for the particular material. Because, in the same irradiation conditions, it is the same time (say t) after which the material will undergo that particular prohibitive damage state, only the accumulated radiation dose responsible for this is 30 dpa (an improved value) instead of 100 dpa. One should not misinterpret the revised or improved predictions of dpa to increase or decrease the operation time of the materials in the reactor. The material, its irradiation conditions and its damage are all remaining the same as before; only the dpa parameter to quantify primary radiation damage is re-assessed with improved data and models, which may necessitate a rescaling of the existing correlations.

3.4 The gas production metric of primary radiation damage

The charged particles responsible for accumulating as gases in materials are generally produced in higher energy threshold type of reactions, but there are exceptions like the overwhelming production of helium in ^{10}B, ^{59}Ni, etc. which can occur even with the low energy neutrons in non-threshold (n, α) reaction. The gas production cross sections and concentrations of gases produced in various structural materials due to irradiations in neutron spectra are computed using the CRaD code [100]. The comparison of gas production cross sections are presented in Section 3.4.1. The single-step and two-step processes of gas production considered in the study are discussed in Section 3.4.2. The concentrations of gases estimated in structural materials for different neutron spectra are presented in Section 3.4.3.

3.4.1 Comparison of particle production cross sections between CRaD and NJOY codes

The GASPR and GROUPR modules of the NJOY-2016.31 are executed after the BROADR module to obtain the multi-grouped gas production cross sections. These data are compared with the gas production cross sections obtained using the CRaD code. The comparisons of the gas production cross sections in ^{58}Ni using ENDF/B-VII.1 data are presented in Fig. 3.16, for illustrations. The maximum deviation between the results from these two codes is found to be about 8% (at threshold energies). The neutron spectrum averaged gas production cross sections in a few structural isotopes for the PFBR core centre spectrum, calculated by using the two codes, are presented in Table 3.8. The overall agreement between the two sets of results is found to be good. The maximum deviation observed is about 1.5%, in case of (n, x d) cross section in ^{59}Ni.

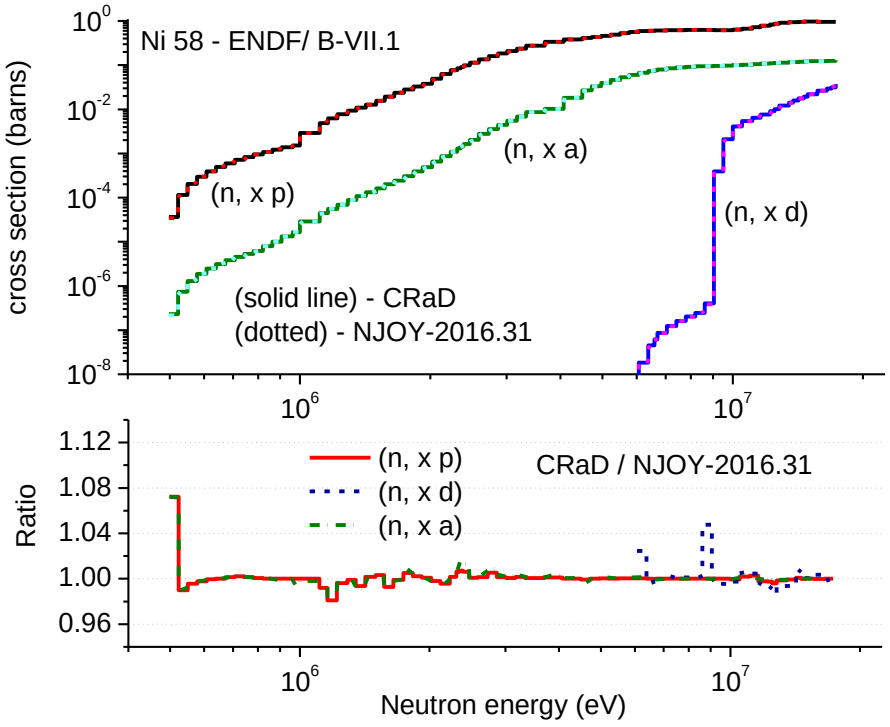

Fig. 3.16: Comparison of gas production cross sections in ^{58}Ni obtained from ENDF/B-VII.1 data by using CRaD and NJOY-2016.31 codes.

Table 3.8: Neutron spectrum averaged one-group gas production cross sections from ENDF/B-VII.1 for PFBR core centre spectrum

Isotope	Code	Cross section (barns)				
		(n, x p)	(n, x d)	(n, x t)	(n, x ^{3}He)	(n, x α)
^{58}Ni	CRaD	1.21e-2	8.39e-7	-	-	6.02e-4
	NJOY-2016.31	1.21e-2	8.39e-7	-	-	6.03e-4
^{59}Ni	CRaD	4.42e-2	5.46e-7	4.79e-8	1.10e-10	1.41e-2
	NJOY-2016.31	4.42e-2	5.38e-7	4.79e-8	1.11e-10	1.42e-2
^{56}Fe	CRaD	8.98e-5	1.31e-7	4.88e-10	5.24e-11	3.78e-5
	NJOY-2016.31	8.97e-5	1.31e-7	4.88e-10	5.21e-11	3.78e-5
^{28}Si	CRaD	6.21e-4	4.53e-7	-	-	2.75e-4
	NJOY-2016.31	6.21e-4	4.54e-7	-	-	2.76e-4

3.4.1.1 Some observations with processing of particle production cross sections using NJOY

In the process of validating the results from CRaD code, a few discrepancies have been noted in processing the gas production cross sections in the isotopes of Fe from ENDF/B-VIII.0 by using the NJOY-2016.31 code system [112]. It is observed that NJOY-2016.31 adds the discrete level (n, p) and (n, α) reaction cross sections two times while computing the (n, x p) and (n, x α) cross sections. However, this issue with NJOY-2016.31 has been corrected in the revised and latest version of NJOY, i.e. NJOY21 code system [85, 112]. It is to be noted that these two versions of the NJOY code sometimes generate the (n, p) and (n, α) cross sections (i.e. MT = 103 and 107) [100] even though they are not explicitly disentangled in the original evaluation. In such cases, these cross sections are incomplete and must be verified before use.

3.4.2 Role of single and two-step processes in transmutation gas production

The gas production cross sections are computed in VITAMIN-J 175 and 198 group structures to estimate the concentrations of gases produced due to the irradiations of various structural materials in thermal and fast fission and fusion neutron spectra. The two main processes considered in this estimation are single-step and two-step processes of gas production.

3.4.2.1 Single-step process of gas production

The number of atoms of gas species (accumulated due to the production of a particle, represented by β) produced per unit volume from nuclide of mass number A because of neutron irradiation with flux, Φ, is calculated as follows:

$$N_{\beta}^{A}(t) = N_{0}^{A}\,\sigma_{\beta}^{A}\,\phi \int_{0}^{t} e^{(-\sigma_{act}^{A}\phi)t'}\,dt' \quad . \tag{3.4}$$

Here, N_0^A is the number of atoms of nuclide A at time $t = 0$. The cross sections in this expression are the neutron spectrum averaged one-group cross sections of nuclide A, σ_{act}^{A} and σ_{β}^{A} are respectively the cross sections for total activation and total production of the particular charged particle. It is assumed that the flux is independent of time. The number of charged particles produced increases with time as the nuclide A gets activated through various reaction channels. The maximum limit to which the number density of β reaches after long period of irradiation depends on the total production cross section of β and cross sections for various other competing reactions. This maximum limit (corresponding to infinite time of irradiation) is given by

$$N_{\beta}^{A} = N_{0}^{A}\,\frac{\sigma_{\beta}^{A}}{\sigma_{act}^{A}} \quad . \tag{3.5}$$

It is generally observed that among all the gases, hydrogen and helium are produced in predominant quantities in the material. Other species of gases, such as deuterium, tritium and helium-3 are generally produced in lesser quantities [100].

3.4.2.2 Two-step processes of gas production

It is important to consider the two-step processes of gas production from ^{59}Ni when stainless steels are used as structural materials, which contain about 15% of Nickel. The ^{59}Ni is not a natural isotope and forms only during irradiation, predominantly by activation through radiative capture of neutrons in ^{58}Ni. These transient ^{59}Ni atoms, produced in-situ, contribute to significant production of hydrogen and helium through (n, p) and (n, α) activation channels even with very low energy neutrons. The total particle production and activation cross sections in ^{59}Ni calculated by CRaD code using ENDF/B-VIII.0 data are presented in Fig. 3.17. The total activation cross section here is the sum of the all the reaction cross sections given in Eq. (2.21).

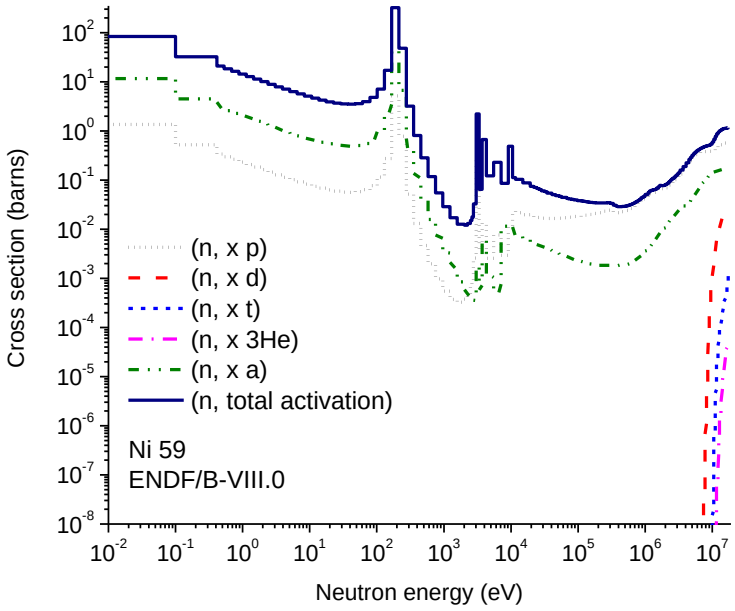

Fig. 3.17: The cross sections for partial activation reaction channels and total activation in ^{59}Ni calculated by CRaD in VITAMIN-J 175 energy group structure using ENDF/B-VIII.0 data.

The two-step reaction processes by which gas production takes place from ^{59}Ni are represented as ^{58}Ni (n, γ) ^{59}Ni (n, *x* β) ^{A}X. The exit particles β from this reaction in ^{59}Ni can be one of the charged particles responsible for gas production and X is the corresponding heavy

recoil nucleus. The number density of particle β produced in this way from ^{59}Ni is calculated as follows [49, 50]:

$$N_{\beta}^{59}(t) = N_0^{58} \frac{\sigma_{\gamma}^{58}\sigma_{\beta}^{59}\phi}{\sigma_{act}^{59} - \sigma_{act}^{58}} \int_0^t e^{(-\sigma_{act}^{58}\phi)t'} - e^{(-\sigma_{act}^{59}\phi)t'} dt' \quad . \tag{3.6}$$

Here, N_0^{58} is the initial number of ^{58}Ni nucleus and the formation of ^{59}Ni depends on the radiative capture cross section of ^{58}Ni (σ_{γ}^{58}). Both the nuclides ^{58}Ni and ^{59}Ni get simultaneously activated by all their respective activation reaction channels; the particle production cross section σ_{β}^{59} of ^{59}Ni contributes to the increasing concentration of the gas corresponding to particle β. The maximum concentration of these gas particles after long time of irradiation is given by

$$N_{\beta}^{59} = N_0^{58} \frac{\sigma_{\gamma}^{58}\,\sigma_{\beta}^{59}}{\sigma_{act}^{59}\,\sigma_{act}^{58}} \quad . \tag{3.7}$$

The neutron spectrum averaged cross sections, needed to estimate the production of helium from ^{58}Ni and ^{59}Ni at PFBR core centre, are calculated from different basic evaluated nuclear data libraries (see Table 3.9). The helium production in these isotopes in PFBR core centre is shown in Fig. 3.18 (a). The concentrations of helium produced from ^{59}Ni at short times (fluences less than 10^{20} n/cm^2) fluctuate and can become negative for some selected combinations of the fluences and the activation cross sections of ^{58}Ni and ^{59}Ni. This behavior is physically unexpected, as no processes are considered here that would lead to reduce the concentration of helium that has been produced once. The time-variation of the concentrations of gases has only one minimum at zero fluence and one maximum at a fluence given by $\frac{2}{\sigma_{act}^{59}+\sigma_{act}^{58}}$ [100]. In the present study, only the absolute values of the concentrations of gases are used. Such

unphysical trends in the prediction of the concentrations of gases at low fluences can be avoided by maintaining the previous value, if the present value is found to have decreased or become negative.

Table 3.9: One-group activation cross sections at PFBR core centre

Isotope	Cross section (barns)			
	ENDF/B-VII.1	JENDL-4.0	TENDL-2017	ENDF/B-VIII.0
	(n, γ)			
^{58}Ni	0.0198	0.0238	0.0237	0.0199
^{59}Ni	-	-	-	-
	(n, x α)			
^{58}Ni	6.02e-4*	7.09e-4	6.89e-4	7.36e-4
^{59}Ni	1.41e-2	1.47e-2	7.22e-3	1.15e-2
	(n, activation)			
^{58}Ni	0.0325	0.0366	0.0365	0.0325
^{59}Ni	0.147	0.126	0.136	0.118

3.4.2.3 Comparison of transmutation of ^{58}Ni to ^{59}Ni using different nuclear data libraries

The transmutation process of ^{58}Ni and ^{59}Ni in the case of irradiation in PFBR core centre spectrum is illustrated in Fig. 3.18 (b). The activation of ^{58}Ni shown is only through the radiative capture of neutrons and forming ^{59}Ni, whereas the activation shown for the latter nuclide is through all the possible activation reaction channels such as (n, γ), (n, p), (n,α) etc. The concentration of ^{59}Ni starts growing steadily with time only after about 10^7 seconds (fluence ~8×10^{22} n/cm^2). Then onwards, the concentration of the helium produced from ^{59}Ni increases steadily with time (see Fig. 3.18 (a)). The concentration of ^{59}Ni reaches to maximum after 10^9 seconds (fluence ~ 8×10^{24} n/cm^2) and its absolute value depends on the neutron spectrum-averaged cross sections. From Fig. 3.18 (b), it is observed that the maximum fraction to which ^{59}Ni is produced via transmutation of ^{58}Ni differs by about 31% among different libraries, estimate from JENDL-4.0 giving the highest value and that from ENDF/B-VII.1 giving the lowest.

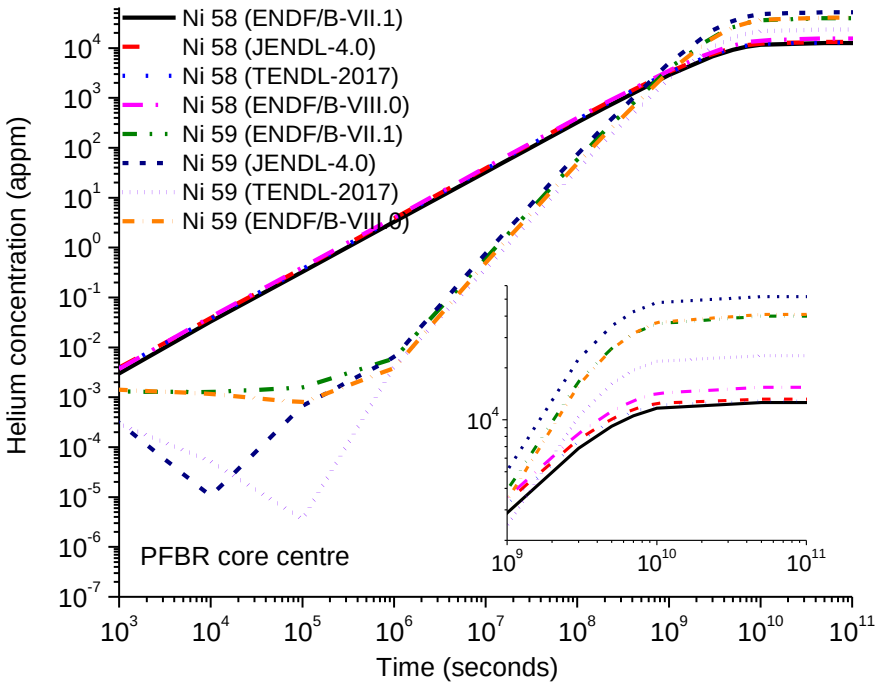

Fig. 3.18 (a)

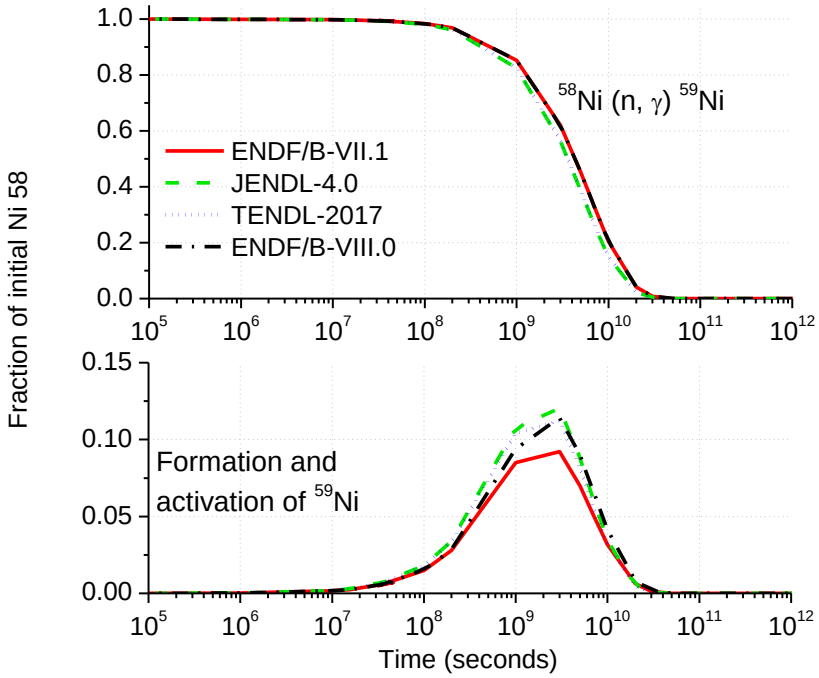

Fig. 3.18 (b)

Fig. 3.18: The effect of differences in the neutron cross sections from different basic evaluated nuclear data libraries on the prediction of gas production in ^{58}Ni and ^{59}Ni; (a): Differences in helium produced from ^{58}Ni and ^{59}Ni during irradiation in PFBR core centre; (b): Differences in the transmutation behaviour between ^{58}Ni and ^{59}Ni.

3.4.2.4 Effect of various neutron flux spectra on transmutation of ^{58}Ni to ^{59}Ni

In order to compare the transmutation process in different incident neutron spectra, similar calculations are carried out using the cross sections data from TENDL-2017. The neutron spectrum-averaged cross sections (in PFBR core centre, ITER-DT and PWR-RPV) of (n, γ) reaction in^{58}Ni and the activation reactions in ^{59}Ni from TENDL-2017 obtained here are presented in Table 3.10. The transmutation processes of ^{58}Ni and ^{59}Ni in these neutron spectra are presented in Fig. 3.19. Total neutron flux in PFBR core centre, ITER-DT and PWR-RPV are 8.0×10^{15}, 2.1×10^{14} and 1.12×10^{11} neutrons.cm^{-2}.s^{-1}, respectively. Note that, it requires a fluence of about 10^{24} neutrons/cm^2 at which the ^{58}Ni fraction steadily decreases as a result of activation due to (n, γ) reaction, and correspondingly, the fractional concentration of ^{59}Ni reaches its maximum value. The maximum fractional concentration of ^{59}Ni in PFBR core centre is about 4 times larger as compared to those in ITER-DT and PWR-RPV spectra. This is due to the large difference between the neutron spectra averaged total activation cross sections (see Table 3.10) of ^{59}Ni in case of PFBR core centre and the other two spectra. These estimates also indicate that there are larger contributions from (n, p) and (n, α) reaction channels towards the activation of ^{59}Niin ITER-DT and PWR-RPV spectra as compared to those in PFBR core centre spectrum.

Table 3.10: TENDL-2017 based one-group cross sections of^{58}Ni and ^{59}Ni for different neutron spectra

Isotope	Cross section (barns)					
	(n, γ)			(n, activation)		
	PFBR core centre	ITER-DT	PWR-RPV	PFBR core centre	ITER-DT	PWR-RPV
^{58}Ni	0.0237	0.142	0.126	-	-	-
^{59}Ni	-	-	-	0.136	5.12	4.6

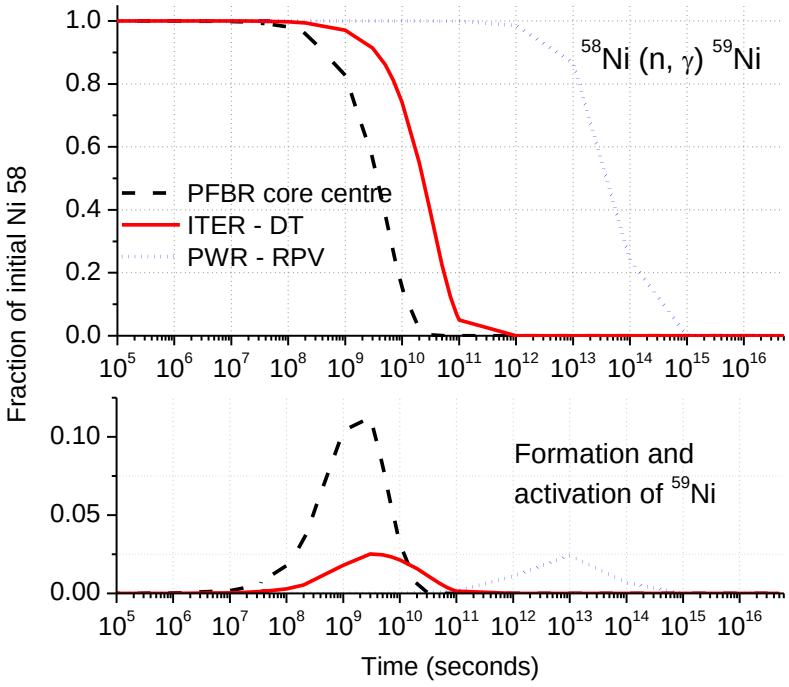

Fig. 3.19: The characteristic transmutation behaviour between ^{58}Ni and ^{59}Ni in various neutron spectra, calculated using neutron interaction cross sections from TENDL-2017.

3.4.2.5 Comparison of concentrations of gases between CRaD code and published data

The concentrations of hydrogen and helium produced in ^{56}Fe in ITER/FW spectrum have been calculated by Simakov et al. [72] from the data in TENDL-2013 as respectively 410 ± 72 appm/efpy and 92 ± 21 appm/efpy. In the present calculations using CRaD code [100] from the TENDL-2017 data, the concentrations of hydrogen and helium gases produced in ^{56}Fe in the ITER-DT spectrum (with same fluence), are found to be 400.6 appm/efpy and 111.9 appm/efpy.

The estimated helium concentration from ^{59}Ni due to neutron irradiation of a nickel sample at the location of a nuclear facility HFIR-CTR31 corresponding to a fluence of 5.44×10^{22} n/cm^2 reported by Greenwood et al. [49] is 3990 appm. Similar methodology of the two-step reaction processes was applied by Greenwood et al. to calculate the helium concentrations from ^{59}Ni. Their estimated results were found to be within 10% of the measured data. The numerical values of neutron flux spectrum at the location of measurement were not reported. So, in the

present study, the "HFIR-high res" neutron spectrum [107] is used, which is very close to the one used in the reference study, in order to obtain the one-group cross sections. The estimated helium concentration from ENDF/B-VII.1 nuclear data is found to be about 23.5% higher. However, if σ_{α}^{59} and σ_{act}^{59} are considered to be 4.30 b and 34.10 b respectively from Ref. [49], then the present estimation is only 1.6% higher. The observed differences with respect to the reference values are due to the differences in the basic neutron cross sections from different libraries and neutron spectra used to calculate the one-group cross sections. Hence, the calculated concentrations of gases are reliable.

3.4.3 Concentrations of gases produced in different neutron flux spectra

3.4.3.1 Structural elements

The production of hydrogen and helium gases in structural elements Fe, Ni, Cr, C and Si are estimated by the CRaD code using the data from ENDF/B-VII.1. The contributions from individual isotopes are added with the abundances to obtain the estimates in elements. The appm concentrations of these gases in these elements for an irradiation time of 6.3 years (considered for illustration) in PFBR core centre, ITER-DT and PWR-RPV neutron spectra are presented in Table 3.11for a comparative study [100]. The production of these gases in all these elements, except Ni, is higher in ITER-DT than in PFBR core centre. In Ni, the concentrations of hydrogen and helium gases become higher in the ITER-DT spectrum after longer time periods. The total flux in ITER-DT is less (about 40 times) compared to that in PFBR core centre. The energy variations of hydrogen and helium production cross sections in ^{58}Ni and ^{59}Ni, relative contributions from ^{58}Ni and ^{59}Ni to the production of these gases with time and basic neutron spectra averaged reaction cross sections in these two spectra are other factors that affect the

overall production of these gases in Ni. There are also significant productions of helium gas in C in PFBR core centre and ITER-DT neutron spectra. However, in PWR-RPV spectra these gases are found to build up in C only after longer time periods (in about 30 years). Note that, significant quantities of these gases are also produced due to irradiation of Si in the PFBR core centre and ITER-DT spectra.

Table 3.11: Production of hydrogen and helium gases due to neutron interactions in structural elements using ENDF/B-VII.1 nuclear data

Element	Gas produced in ~ 6.3 years (appm)					
	Hydrogen			Helium		
	PFBR core centre	ITER-DT	PWR-RPV	PFBR core centre	ITER-DT	PWR-RPV
Fe	934	1680	4.3e-2	65.4	408	6.5e-3
Ni	13600	6630	0.46	927	954	4e-2
Cr	468	1240	2.74e-2	48.1	270	3.98e-3
C	2.71e-2	0.741	0	146	667	0
Si	940	2940	7.91e-2	448	1700	4.03e-2

3.4.3.2 D-9 steel used in PFBR

The D-9 steel is considered to be irradiated with neutrons corresponding to the spectra at four locations of PFBR. The actual grid plate and lattice plate structural materials are different from D-9 steel. The productions of hydrogen and helium gases in D-9 alloy for irradiations up to various time durations estimated by using the isotopic neutron reaction cross sections from ENDF/B-VII.1 are presented in Fig. 3.20. The gas production values beyond the maximum residence times for fuel and blanket sub-assemblies in PFBR (~ 1.5and 6 years respectively) are also given as a theoretical study. The relative contributions of elemental Ni to the production of these gases are found to be large (70 – 90%). The non-linear behavior before reaching the maximum values is due to the transmutation behavior between ^{58}Ni and ^{59}Ni. The estimated production of hydrogen is relatively larger than that of helium at core centre and radial blanket, whereas it is opposite in grid plate top and lattice plate locations. This is due to the energy

dependent behavior of (n, p) and (n, α) cross sections in ^{59}Ni and differences in the neutron spectra at these locations [100]. The neutron energy spectra at the grid plate top and lattice plate locations are softer and the fluxes for the low energy neutrons are larger compared to that at the radial blanket and core centre locations.

The productions of five different species of gases in D-9 steel for irradiations at core centre and radial blanket locations of PFBR are estimated by using ENDF/B-VII.1 nuclear data library and presented in Table 3.12. At the core centre location of PFBR, the estimates of hydrogen and helium in D-9 steel are respectively 5.7 H appm/dpa and 0.4 He appm/dpa [100].

It is to be noted that the methodology applied in the present study to compute the concentrations of gas species does not take into account the contributions coming from all possible transient isotopes that can be produced during irradiations and the time-dependent changes in the isotopic compositions that occur due to transmutations. These effects can be taken into account in full scale estimations by developing a more detailed methodology.

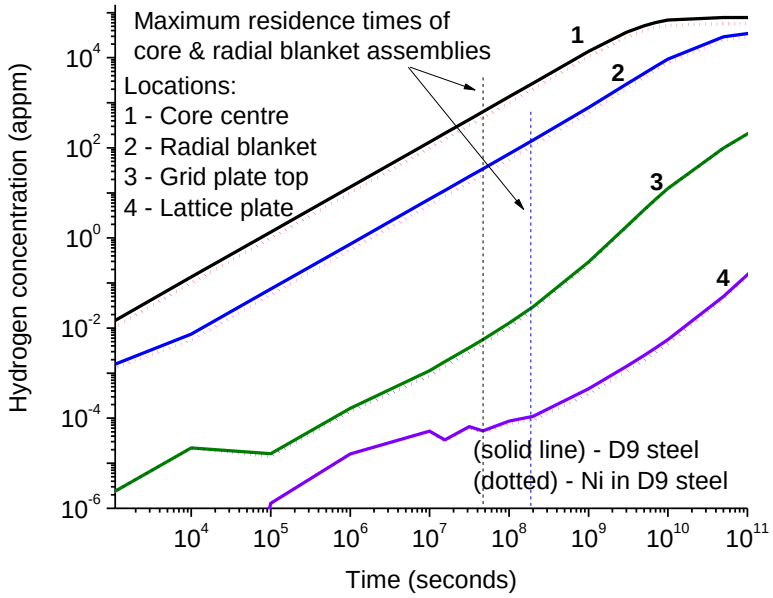

Fig. 3.20 (a)

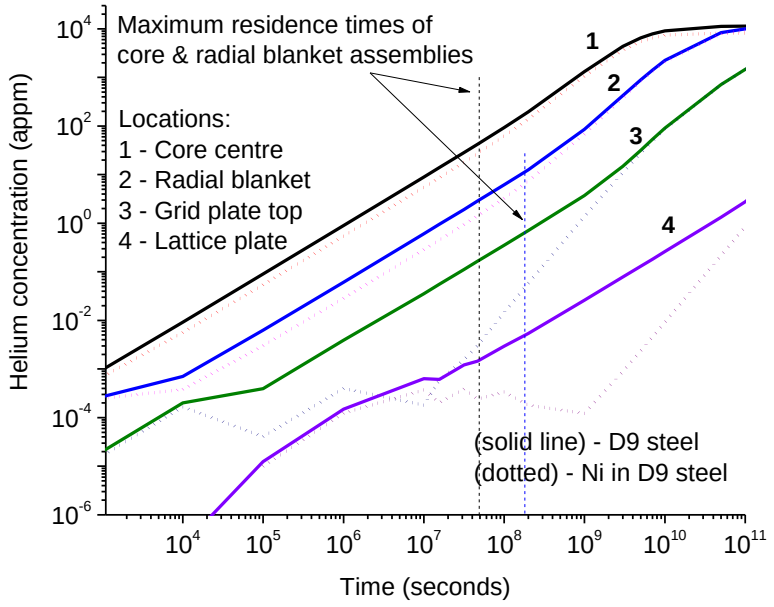

Fig. 3.20 (b)

Fig. 3.20: Accumulation of gases in D-9 steel and Ni present in the alloy for irradiations up to various time durations at different locations of PFBR, calculated by CRaD using the data from ENDF/B-VII.1; (a): Hydrogen; (b): Helium. The dotted vertical lines indicate the maximum residence times for fuel and radial blanket assemblies at their locations.

Table 3.12: Gases produced (in appm) in D-9 steel due to irradiation at core centre and radial blanket locations of PFBR, calculated by using ENDF/B-VII.1

Time (y)	fluence (n/cm^2)	Hydrogen	Deuterium	Tritium	^{3}He	Helium
Core centre						
1	2.5e+23	426	5.79e-2	3.95e-3	7.72e-6	28.4
1.5	3.7e+23	631	8.55e-2	5.11e-3	1.14e-5	42.2
Radial blanket						
1	4.03e+22	23.1	2.86e-3	2.8e-4	4.06e-7	1.92
6.3	2.54e+23	148	1.81e-2	1.24e-3	2.57e-6	12.6

3.5 The neutron heating metric of primary radiation damage

The general trends of energy-wise variations of neutron heating cross sections are discussed in Section 3.5.1. The comparison of the results between CRaD and NJOY-2016.31

codes and neutron spectrum dependence of heating rates in various structural elements are presented in Section 3.5.2.The neutron heating rates in D-9 steel are estimated in Section 3.5.3.

3.5.1 Energy variations of neutron heating cross sections

The total neutron kerma coefficient (heating) is the sum of all the kerma coefficients due to partial reactions of neutron. It is illustrated for ^{56}Fe in Fig.3.21, by using the data from ENDF/B-VII.1 nuclear data library. The main contributions to total kerma come from elastic scattering, (n, n´), (n, 2n), (n, γ) and the (n, particle) types of neutron reactions, see Fig.3.21 (a). In ^{56}Fe, the predominant contribution below ~ 100 eV comes from (n, γ) reaction and above that, there is significant contribution from elastic scattering. Above ~ 1 MeV, the threshold reactions are major contributors. This observation is also generally true for the structural isotopes. In (n, remaining threshold) reactions the heating of the material is due to the deposition of kinetic energies of the charged particle as well as the recoil nucleus. The contributions from different CPO reactions to the total (n, remaining threshold) kerma coefficient are shown in Fig. 3.21 (b).

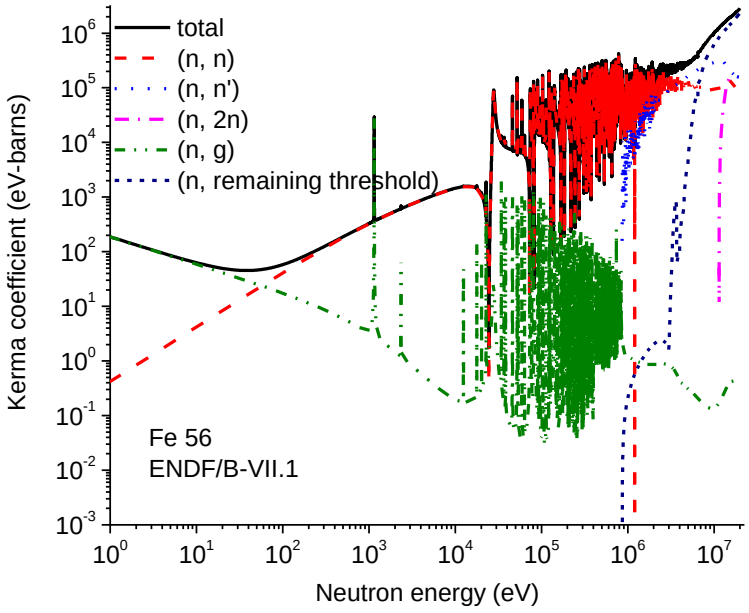

Fig.3.21 (a)

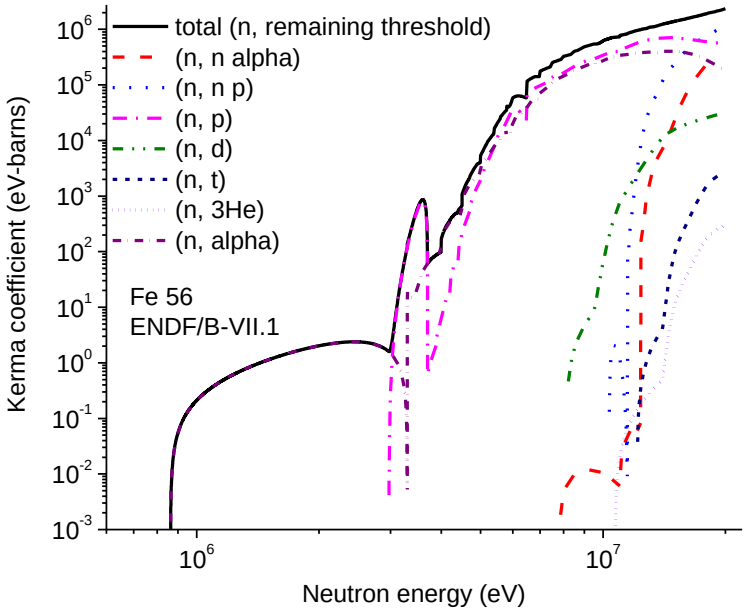

Fig.3.21 (b)

Fig. 3.21: The kerma coefficients due to partial interactions of neutrons calculated by CRaD code, illustrated in case of ^{56}Fe; (a): major category of reactions; (b): contributions from (n, remaining threshold) reactions.

3.5.2 Comparison of neutron kerma coefficients between CRaD and NJOY-2016.31 codes

The kerma coefficients calculated using CRaD code are compared with the results obtained from NJOY-2016.31 code system. Extensive validation exercises have been carried out by comparing the point kerma cross sections data of important structural isotopes [101]. The point-wise energy versus kerma coefficient data are multi-grouped in required energy group structures using Eq. (2.20). These isotopic kerma cross sections are added with their abundances to find the total kerma in an elemental target. The comparison of multi-grouped (in VITAMIN-J 175 energy group structure) total neutron kerma cross section in elemental Fe between CRaD and NJOY-2016.31, using the data from ENDF/B-VII.1, is presented in Fig. 3.22. It can be seen here that the ratios of CRaD to NJOY-2016.31 kerma cross sections are nearly 1 up to about 2 MeV. The spike near 1 keV is assessed to be due to processing of emitted photon data from Files 12 and 15. At higher energies, the differences are more, about 10%, where contributions to the

total kerma are primarily from the (n, remaining threshold) reactions. These differences arise from the portion of energy that is deposited by the recoil nucleus and light charged particles produced in different neutron-induced CPO reactions at higher energies [101, 113]. It is observed that, at higher incident energies, often the total energy deposited by these products is not sufficient enough to give the neutron heating values equal to those obtained by the energy balance method [101]. However, if these differences are small, then the prediction of spectra-integrated total neutron kerma from both energy balance (NJOY-2016) and direct (CRaD) methods will be similar.

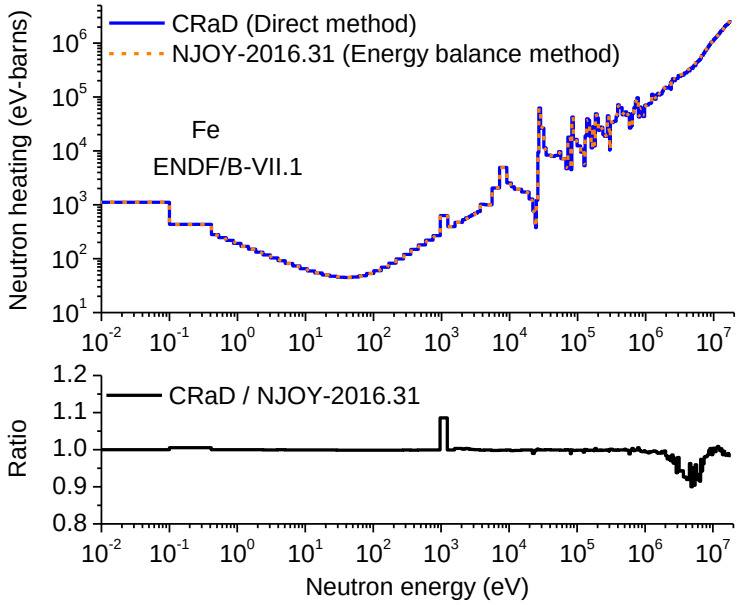

Fig. 3.22: Comparison of total neutron kerma (heating) cross sections in Fe between CRaD and NJOY-2016.31 code systems.

The total neutron heating rate in material *p* for a given spectrum is calculated in the units of (watt / kg) as follows:

$$heating\ rate = \frac{1.6\times10^{-16} N_A}{M} \sum_{g=1}^{N} k_{p,g}\varphi_g \quad . \tag{3.8}$$

Here, N_A is Avogadro number, M is atomic mass of one mole of target in grams and $k_{p,g}$ and φ_g are respectively the multi-grouped kerma cross section and neutron flux in energy group g. The total neutron kerma coefficients in a few structural elements, such as Fe, Ni, Cr, C and Si for irradiations in PFBR core centre and ITER-DT spectra, as computed by CRaD and NJOY-2016.31 codes using ENDF/B-VII.1 nuclear data, are compared in Table 3.13. Note the differences in the heating rates due to the differences in neutron spectra. The contributions to neutron heating from elastic scattering, inelastic scattering and other threshold reactions in the energy range of few keV to 10 MeV are higher in PFBR core centre than in ITER-DT neutron spectra. This results into higher spectrum averaged neutron heating rates in PFBR core centre compared to those in ITER-DT. The maximum difference between the results from NJOY-2016.31 and CRaD codes is observed to be about 14.3%, in case of irradiation of C in ITER-DT spectrum.

Table 3.13: Comparison of total neutron kerma coefficients calculated by CRaD and NJOY-2016.31 codes using ENDF/B-VII.1 nuclear data

Element	Neutron Heating (W / kg)			
	PFBR core centre		ITER-DT	
	CRaD	NJOY-2016.31	CRaD	NJOY-2016.31
Fe	5.48e+2	5.57e+2	1.51e+2	1.52e+2
Ni	8.98e+2	1.04e+3	3.71e+2	4.03e+2
Cr	6.49e+2	6.50e+2	1.28e+2	1.27e+2
C	1.02e+4	1.02e+4	9.34e+2	1.09e+3
Si	2.12e+3	2.12e+3	5.53e+2	5.85e+2

The advantages of using the direct method are: neutron heating cross sections are always positive; and the damage energy and dpa cross sections can also be calculated in a straightforward way (after correcting for electronic energy losses) from the energy of the recoil nucleus that is used in neutron heating. On the other hand, the use of energy balance method is

advantages because: it can give more accurate heating cross sections in case of inadequate recoil and charged particle data, as emitted neutron and photon data are always given for transport calculations; and the evaluation of these neutron and photon data can be checked for inconsistencies, if any (giving rise to negative neutron heating cross sections).

3.5.3 Total neutron kerma coefficient (heating rate) in D-9 steel

It is assumed that the D-9 alloy is irradiated with neutron spectra corresponding to various locations of PFBR, viz. core centre, radial blanket, grid plate top and lattice plate. The total neutron heating rates in D-9 alloy for these irradiation spectra, based on the data from ENDF/B-VII.1, as calculated by CRaD code, are presented in Table 3.14. The contributions from individual elements are added with their corresponding fractional compositions in the alloy. The values obtained by using the NJOY-2016.31 code are also compared here. It is to be noted that the energy balance kerma for $^{92, 94, 96, 97, 98, 100}$Mo isotopes obtained from NJOY-2016.31 (and NJOY21) code are found to be negative, so the corresponding kinematic kerma (MT = 443) [29] for these isotopes and ^{95}Mo are used in this calculation. Maximum neutron heating in the material (around 614 W/kg) will occur at the core centre. Due to the differences in neutron spectra, the neutron heating from low energy neutrons will be more in grid plate top and lattice plate compared to that in core centre and radial blanket locations. In D-9 steel, the low energy neutron heating mainly comes from ^{10}B due to its high non-threshold (n, α) cross sections. The differences between neutron heating rates in D-9 steel calculated by the direct method (CRaD code) and by the energy balance method (NJOY-2016.31 code) are found to be within 7%.

The total neutron heating rate in ^{59}Ni in PFBR core centre has been estimated to be about 1930 W/kg using the CRaD code and nuclear data from TENDL-2017. The contributions from partial reactions are found to be mainly from (n, n), (n, n′), (n, p) and (n, α) reactions, which are

respectively around 29.4%, 6.49%, 45.9% and 18.1%. The neutron heating from ^{59}Ni has to be additionally considered with the value presented in Table 3.14, by noting the time of irradiation and taking 68.08% of the corresponding amount (which is shown in Fig. 3.19) of this isotope that is produced from ^{58}Ni.

Table 3.14: Neutron heating rates in D-9 steel irradiated at various locations of PFBR calculated using ENDF/B-VII.1 nuclear data library

PFBR location	Neutron Heating (W / kg)	
	CRaD	NJOY-2016.31
Core centre	6.14e+2	6.42e+2
Radial blanket	5.71e+1	5.88e+1
Grid plate top	1.67e-1	1.59e-1
Lattice plate	1.12e-3	1.05e-3

3.6 Summary

The metrics of primary radiation damage estimated using the CRaD code are compared with the results obtained from other available standard codes such as RECOIL, SPECTER, NJOY-2016 and NJOY21 and literature data. The agreements of the results from CRaD code with these standards are found to be satisfactory. The value of dpa in D-9 steel used in PFBR obtained with the RECOIL code is found to be lower compared to the values obtained using the other standard codes. A discrepancy in the NJOY-2016 code is noted with respect to the complete application of the NRT model to compute dpa cross sections. In some cases, it is observed that NJOY-2016.31 and NJOY21 codes generate incomplete MT = 103 and 107 cross sections, when it is not directly permitted in the original evaluation.

The effects of different neutron spectra on the PKA rates, total dpa, concentrations of gases and heating rates are discussed. The maximum fraction to which the transmutation isotope ^{59}Ni (produced from ^{58}Ni) reaches is highest in PFBR core centre compared to those in ITER-DT

and PWR-RPV spectra, depending on their total neutron flux and activation cross sections in ^{59}Ni. The differences in basic evaluated nuclear data from different libraries give rise to differences in the predicted values of the primary damage metrics, as for instance, the maximum fraction to which ^{59}Ni reaches as a result of transmutation from ^{58}Ni in PFBR core centre is found to differ by 31% when the basic cross sections from ENDF/B-VII.1 and JENDL-4.0 are used in the calculation.

The arc-dpa model along with its parameterization is found to reproduce the observations of the primary damage phenomena in structural elements that are made in realistic MD simulations and irradiation experiments. Hence, it is established that this model can be adapted to estimate the realistic dpa in materials quite easily, without having to perform extensive MD simulations. This will facilitate the regular design applications for fast reactors. The measured values of radiation damage in materials can be rescaled to the dpa values obtained by using the improved nuclear data and atom-displacement models without affecting the design time limits of their operation. This is essential in order to maintain consistency with the improvements in evaluated nuclear data and modeling of primary radiation damage.

The neutron heating obtained by applying the direct and energy balance methods differ mainly in the higher energy region due to the (generally observed) lower values of energy deposition by the recoil nucleus and light charged particles in the direct method. However, the direct method is advantageous because heating values are always positive and the displacement damage (which is due to damage energy corresponding to the energy of the recoil nucleus only) can be estimated in a more straightforward way.

Chapter 4

Self-ion Simulations in Elemental and Polyatomic Target Materials using SRIM-2013

4.1 Introduction

In Chapter 3, the CRaD code has been used to calculate the dpa cross sections in materials due to neutron interactions by directly reading the data from ENDF-6 basic evaluated nuclear data libraries and applying the atom-displacements models on the estimated damage energies. In this chapter, the displacement damage due to neutrons is investigated through self-ion simulations method by applying the information on PKA spectra and average energies of PKAs calculated by CRaD code in the SRIM-2013 [40] software. In this approach, it is intended to find an additional way to predict atom-displacements damage in elemental and polyatomic target materials in both neutron and ion irradiation environments by using the CRaD code [114]. This chapter is organized as follows. The procedure to simulate the formation of primary radiation damage using SRIM-2013 is discussed in Section 4.2. The methodology adapted to compute dpa cross sections by applying the self-ion simulations is described in Section 4.3 and the results obtained are presented in Section 4.4. The chapter is summarized in Section 4.5.

4.2 Simulation of primary radiation damage formation using SRIM-2013 software

The primary displacements damage production due to heavy ion irradiation can be simulated by using the SRIM/TRIM Monte Carlo code developed by Biersack, Ziegler, Littmark and others [40]. The SRIM software is routinely used for varied research purposes by the ion irradiation experimentalists. It is reliable and provides the much required scientific simulation

platform for quick first-hand assessments that are required to plan and carry out these experiments. SRIM is based on the binary collision approximation (BCA) method, where it randomly samples the impact parameters of succeeding collisions based on the interaction cross section, atomic density and composition of the target. It requires the inputs like types of ion and target and the energy of incident ion in the range ~ (1eV to 2 GeV). It keeps the track of the displacement cascades initiated in the radiation-material interaction process and calculates several parameters related to an ion-target combination, viz. the ion penetration depth, straggle of the ion beam, electronic and nuclear energy losses, energy deposition in the target medium, phonon production, sputtering rate, vacancy concentration, etc.

SRIM code can also be used to calculate the source term of primary radiation damage in the units of dpa. However, it should be used with caution, because there are different working modes in SRIM, which give different results for the computed dpa. The two mostly used modes in SRIM to determine dpa are “Ion Distribution and Quick Calculation of Damage” and “Detailed Calculation with full Damage Cascades”. The type of damage calculations in these two working modes are respectively given the nomenclatures as “Quick: Kinchin-Pease” and “Full Cascades”. In the following discussions, we shall refer to them by abbreviations Q: K-P and F-C respectively. There are some inconsistencies between the results obtained from these two modes of SRIM [40-41]. In particular, the number of vacancies that results from an F-C simulation is found to be higher by a factor of 2 or more when compared to the Q: K-P values. It is probably due to computing the number of vacancies from a more detailed simulation of the subsequent cascades in the F-C mode. However, the damage energies calculated in both these modes of SRIM are very similar and are close to what is obtained by applying the Robinson partition function [17] for a particular PKA energy [114, 41].

The SRIM code has been recommended to be used in the Kinchin-Pease mode for primary damage cascade simulations [41]. The lattice binding energies must be set equal to 0 eV while simulating primary damage in an elemental target, in order to be fully consistent with the theory of Norgett et al. [18, 41]. The damage energy deposited by an incident ion is the sum of the energies shared to the lattice phonons by the incident ion and the recoiling ions in the target material. This is calculated from the SRIM results by using Eq. (4.1).

$$T_{dam} = E_i^0 - E_i^I - E_T^I = E_i^P + E_T^P , \tag{4.1}$$

where

$$E_i^0 = E_i^P + E_T^P + E_i^I + E_T^I$$

and

E_i^0 = incident ion energy;

E_i^I = incident ion energy lost to ionization;

E_T^I = recoil energy lost to ionization;

E_i^P = incident ion energy lost to phonons;

E_T^P = recoil energy lost to phonons.

Once the damage energy is obtained, the number of defects is subsequently estimated by putting this damage energy in the NRT model in Eq. (2.20). It has been observed by Stoller, et al. [41] that the primary damage predicted in this way is very similar to that predicted directly by the application of NRT model. Hence, the SRIM code must be employed according to the procedure as described above in order to estimate the primary radiation damage by irradiations of ions. Note that the SRIM code gives the number of vacancies formed as outputs in the two modes of its simulation. These values are also used in the study in order to compare the results with the prescribed procedure.

4.3 Method of computation

The dpa cross sections of neutrons covering the entire fast reactor energy spectrum are derived by performing simulations with the self-ions as projectiles on elemental and polyatomic target materials. The important steps in this computation are given as follows:

(a) Compute PKA spectra in the isotopes of structural elements by using the basic evaluated nuclear data from ENDF-6 library. Then combine the isotopic PKA spectra with respective isotopic abundances to determine PKA spectra in the corresponding elements.

(b) Estimate the energies of elemental PKAs by averaging over the PKA spectra in each incident neutron energy group to get the average PKA energies according to the incident neutron group structure used in the calculation. The VITAMIN-J 175, ABBN-93 (26 groups), 100 and 198 energy group structures are used to multi-group the point energy-cross sections. An energy group structure is shown in Appendix A, as a typical example.

(c) The average energies of PKAs in each neutron group are then considered as energies of the projectile ions and BCA based simulations are performed with SRIM-2013 software.

(d) Estimate the damage energy (using Eq. (4.1)) and number of displacements per ion (using Eq. (2.17)) from the outputs of SRIM code.

(e) Compute dpa cross sections by combining the numbers of displacements with the multi-grouped basic neutron interaction cross sections obtained by using CRaD from the pre-processed basic point interaction cross sections.

Note that, in case of elemental targets, the damage energies and numbers of stable displacements can also be computed from the PKA energies by using the analytical energy-partition expressions (Eq. (2.16)) and arc-dpa model (Eq. (2.18)), instead of using the SRIM

software and the NRT model. Since, the purpose of self-ion simulation is to emulate the neutron irradiation, the simulated self-ion dpa cross sections and the integrated primary radiation damage source term (i.e. dpa) must correspond to those obtained in the direct method of computation using incident neutrons. For this, the self-ion dpa cross sections and integrated dpa shall be compared with the direct results from CRaD code; standard data obtained by using NJOY-2016 code and other published data.

4.3.1 Calculation of average energy of PKAs

Another very useful quantity in the modeling of primary radiation damage (in addition to those discussed in Chapter 3) that can be derived from PKA spectra is, the average energy of the PKAs. The average energy of the PKAs corresponding to the incident neutron of energy E is calculated from the PKA spectrum that results after the interaction of the energetic neutron. This is done as follows:

$$\overline{E}_R(E) = \frac{\sum_{g_R=1}^{G} E_R \frac{d\sigma(E,E_R)}{dE_R}(E_{g_R+1} - E_{g_R})}{\sum_{g_R=1}^{G} \frac{d\sigma(E,E_R)}{dE_R}(E_{g_R+1} - E_{g_R})}. \quad (4.2)$$

The summation is carried over the entire energy range of the recoil energy group structure; however, it is non-zero only within the range where PKAs can be formed by an incident neutron of energy E limited by the reaction cross sections and conservation of energy in reaction kinematics. The recoil energy E_R in the numerator of the equation is taken as the middle point of the group. The average energy of the elemental PKAs can be similarly calculated from the PKA spectrum in the element. This is done as follows:

$$\overline{E}_R(E) = \frac{\sum_{g_R=1}^{G} E_R \left[\sum_{iso} A_{iso} \left(\frac{d\sigma(E, E_R)}{dE_R} \right)_{iso} \right] (E_{g_R+1} - E_{g_R})}{\sum_{g_R=1}^{G} \left[\sum_{iso} A_{iso} \left(\frac{d\sigma(E, E_R)}{dE_R} \right)_{iso} \right] (E_{g_R+1} - E_{g_R})}. \quad (4.3)$$

The average energy of PKA in each neutron group computed using the data in ENDF/B-VII.1 library is plotted in Fig. 4.1. For neutrons at low energies (< 10 keV), the average energies of PKAs is about 500 eV. It is contributed mainly by the recoils from (n,γ) reaction, see Fig. 4.2. The average energies of these recoils are computed as follows:

$$(\overline{E}_R)_{n,\gamma} = \frac{\overline{E_\gamma^2}}{2(A+1)mc^2}. \quad (4.4)$$

Here E_γ is the energy of emitted photon; A is mass of target nucleus with respect to mass of neutron and the value of mc^2 is taken as 939.5 MeV.

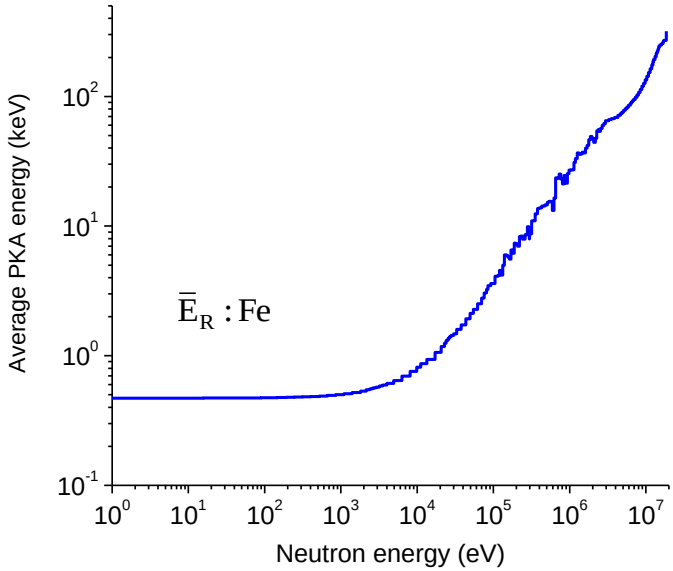

Fig. 4.1: Average energy of PKAs due to interaction of neutrons from each group in Fe (175 energy groups are considered). The average recoil energy below 10 keV neutrons is about 500 eV, coming from the recoil of the nucleus following the emission of capture gammas.

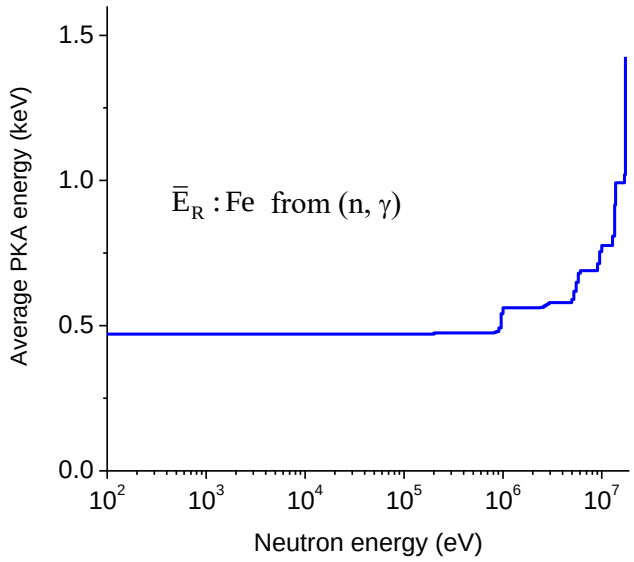

Fig. 4.2: Average energy of PKAs produced by (n,γ) reaction (from each neutron group) in Fe.

4.3.2 Calculation of displacement damage cross sections for incident neutrons

The displacement cross section for incident neutrons in each neutron energy group is calculated from the SRIM simulation results by multiplying the number of displaced atoms, $\nu_g(T_{dam}(\bar{E}_R))$ with the total neutron cross section,$\sigma_{n,t}^g$, according to Eq. (4.5). The SRIM simulation by using incident ions with energy, $\bar{E}_R$, gives rise to the secondary knock-on atoms in the target, having the overall damage energy, T_{dam}. This results into the defects (vacancy-interstitial pairs), given by the parameter ν_g. Thus, the neutron displacement cross section in the neutron energy group g becomes

$$\sigma_d^g = \sigma_{n,t}^g \times \nu_g(T_{dam}(\bar{E}_R)). \tag{4.5}$$

Total dpa in the material is calculated from Eq. (3.3). Similarly, the damage energy cross section in a neutron group g can be obtained by simply multiplying the damage energy with the basic neutron cross section, as follows:

$$\sigma_{DE}^{g} = \sigma_{n,t}^{g} \times T_{dam}(\overline{E}_R). \tag{4.6}$$

This methodology is continued for all neutron groups covering the energy range of the entire neutron flux spectrum.

The total dpa cross section of the polyatomic target material of type $A_{q1}B_{q2}$is calculated by adding the displacement damage produced due to each of the species of PKAs with the corresponding probabilities for their generation after neutron interaction. Consider the example of a polyatomic target $A_{q1}B_{q2}$, comprising of the elements A and B with stoichiometries q_1 and q_2. After neutron interaction in the polyatomic target, the PKA formed can be of either A or B type element. Each of these two species in the polyatomic material has different neutron interaction cross sections, varying with the neutron energy. The probability that a neutron in energy group *g* (with energy mid-value *E*) will form a PKA of *j* type of element is given by

$$p_{g,j} = \frac{\sigma_{gt,j}(E)}{\sum_i \sigma_{gt,i}(E)}. \tag{4.7}$$

Here, σ_{gt} is the total microscopic cross section in neutron energy group *g*. Then the total dpa cross section of $A_{q1}B_{q2}$for each incident neutron energy group is computed as follows:

$$\begin{aligned}\sigma_{d,A_{q1}B_{q2}}^{g}(E) = &\frac{q_1}{q_1+q_2} p_{g,A}(E)\sigma_{g,A}(E)\nu_{g,A}(T_{dam}(\overline{E}_R)) \\ &+ \frac{q_2}{q_1+q_2} p_{g,B}(E)\sigma_{g,B}(E)\nu_{g,B}(T_{dam}(\overline{E}_R))\end{aligned}, \tag{4.8}$$

where $\nu_{g,A}$ and $\nu_{g,B}$ are the number of displacements produced in the polyatomic target by an incident A and B ion respectively. Here, $q_1/(q_1+q_2)$ and $q_2/(q_1+q_2)$ are the weights assigned from

stoichiometries of the elements, to denote the chances of 'seeing' the respective element in the polyatomic material. In the present study, the elements A and B are Si and C respectively and the polyatomic target considered is silicon carbide (SiC). The generalized expression for Eq. (4.8) can be easily adapted for applications in polyatomic targets with more number of elements.

4.4 Results and discussions

The target width in case of elements like Fe, Ni and Cr is set to 1μm and the factor ν_g in each neutron group is calculated using Eq. (4.1) and Eq. (2.17), with E_d= 40 eV. For the polyatomic target, SiC, the built–in compound dictionary in SRIM-2013 is selected. It contains silicon carbide (ICRU 590) as one of the target materials. The material specific parameters are given as follows: density = 3.21 g/cc; lattice binding energy of C = 3 eV, Si = 2 eV; surface binding energy of C = 7.4 eV, Si = 4.7 eV. The atom stoichiometries are taken as 1 for both C and Si. Two cases are simulated: one with Si and another with C as the incident ions (Table 4.1). The E_d values are set to 35 eV for Si, 24 eV for C when the incident ion is silicon; and 20 eV for C, 42 eV for Si when the incident ion is carbon [43]. The target width is set to 1000 μm. The target width in this case is set larger to ensure that the high energy projectile ions (which are in the order of MeV for lighter elements) do not get transmitted through it, but deposit the full energy within the target material. In each simulation, 5000 ions are projected on the target. In case of the polyatomic target, it is necessary to know a single effective value of lattice displacement energy for the compound. As suggested in Ref. [115], average threshold displacement energy of 25 eV is used as the value of E_d to find the number of defects in SiC target. The SRIM-2013 code is set up with the inputs as given in Table 4.1.

Table 4.1: Inputs to SRIM-2013 software

Ion Data				Target Data				
Symbol	Atomic number	Energy (keV)	Angle of incidence	Layer	Symbol	Displacement energy (eV)	Lattice binding energy (eV)	Surface binding energy (eV)
Fe	26	Computed PKA energies	0	1	Fe	40	0	0
Si[a]	14	”	0	1	C	24	3	7.4
					Si	35	2	4.7
C[b]	6	”	0	1	C	20	3	7.4
					Si	42	2	4.7

[a]Si ion on SiC target

[b]C ion on SiC target

4.4.1 Comparison between K-P and F-C models

The simulations are performed with SRIM-2013 by using both the Q: K-P and the F-C options. There is a significant difference (~by a factor 2 for higher PKA energy) between the numbers of vacancies predicted by F-C and Q: K-P models; the values from F-C model are higher, see Fig. 4.3. At lower energies, the deviation is larger than 2. Similar observations were also made by R.E. Stoller et al. [41] with SRIM-2008. The number of defects estimated using the Robinson’s energy partition function and NRT model are also presented here. The Q: K-P mode is more suitable because it yields closer values when compared to the complete application of the NRT model (from PKA to Robinson partition function, then NRT model) and it works faster compared to the detailed simulations in F-C mode.

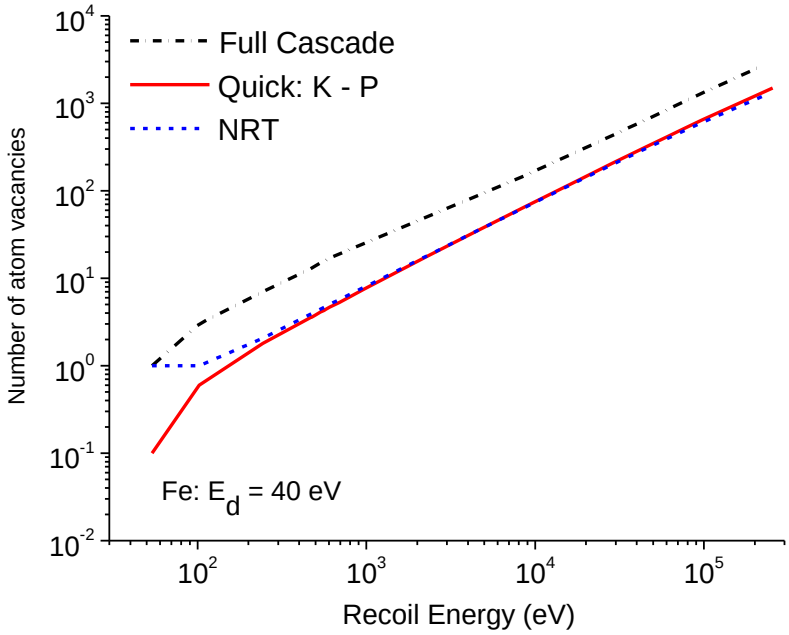

Fig. 4.3: Numbers of vacancies from F-C and Q: K-P models of SRIM-2013 simulations and NRT analytical model with Robinson's energy partition function.

The numerical results obtained for a few incident ion energies are given in Table 4.2 and 4.3. When the Q: K-P mode is selected, the number of vacancies computed from combined damage energy plus NRT model (from Eq. (4.1)) are very close to that given in the SRIM-2013 output file "vacancy.txt". It means that the number of vacancies from Q: K-P model is in agreement with the standard NRT model. The maximum deviation between the numbers of vacancies produced with Q: K-P and F-C option is about 10%, if only the damage energies combined with NRT model are used for their estimations, see Table 4.3.The damage energy cross sections of iron, calculated using Eq. (4.6), from both modes of SRIM are shown in Fig. 4.4. A maximum deviation of about 12% is observed between the two modes. These observations imply that the damage energies simulated by SRIM-2013 in both the working modes are nearly equivalent. It is hence justified that, for computing primary radiation damage by using SRIM-2013, the simulated damage energy (preferably from Q: K-P mode) plus NRT model approach should be followed.

Table 4.2: Number of vacancies for 3 self-ion simulations in Fe with SRIM-2013

PKA energy (keV)	Number of displaced atoms from SRIM file "vacancy.txt"*		
	K – P	F-C	F-C / K-P
0.47	3.6	13	3.61
28.82	207.2	432	2.08
97.58	644.6	1307.3	2.03

to illustrate the discrepancy between F-C and K-P outputs

Table 4.3: Number of vacancies with NRT model in Fe using damage energies from SRIM-2013

PKA energy (keV)	Damage energy (eV) from SRIM simulation		Number of vacancies with NRT model		
	K – P	F-C	K – P	F-C	F-C / K-P
0.47	368.7	402.9	3.69	4.03	1.09
28.82	20984	21963	209.8	219.6	1.05
97.58	64994	69264	649.9	692.6	1.07

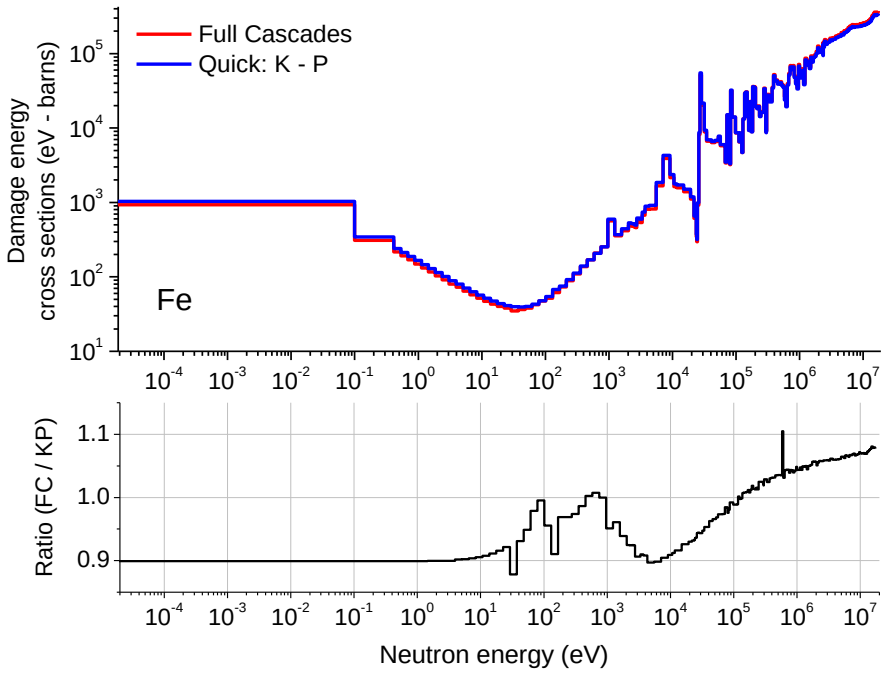

Fig. 4.4: Damage energy cross sections in iron from Q: K-P and F-C models of SRIM-2013.

4.4.2 Comparison of dpa cross sections

4.4.2.1 Elemental targets (Fe)

Based on the observations noted above, the dpa cross sections of iron are calculated using the NRT model with damage energies estimated from SRIM simulations. These dpa cross sections are compared with those obtained using NJOY-2016 [29]. The HEATR module of this code calculates damage energy only when the recoil energy is greater or equal 25 eV. Below 25 eV, it assumes the damage energy to be zero. So the dpa cross sections are calculated here in the following way. The damage energies corresponding to PKA energies greater than 25 eV are multiplied with the factor $0.8/2E_d$, where E_d = 40 eV for iron, nickel and chromium, to get the number of defects produced. The numbers of defects for PKA energies below 25 eV are set to zero. The comparisons between the values obtained from NJOY-2016 and the two modes of SRIM-2013 are presented in Fig. 4.5.

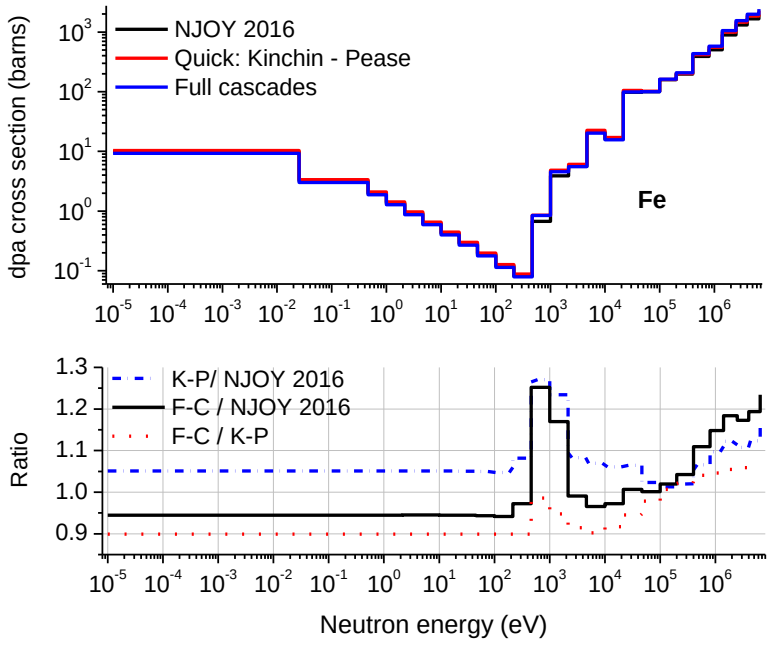

Fig. 4.5: Comparison of NRT-dpa cross sections of Fe from SRIM-2013 (using Eq. (4.1) and (2.20)) and NJOY-2016.

The differences in these results, as observed in Fig. 4.5, are primarily due to three reasons. There is a difference in the procedure adapted here and that followed in NJOY-2016 to arrive at the dpa cross sections. Firstly, in the present study, the damage energies and vacancies are simulated from the energies averaged over the total spectrum of the PKAs resulting from the neutron interactions. In the HEATR module of NJOY-2016, the primary recoil spectrum is not calculated separately, but it is implicit in its way of computation. In this module, the damage energy contribution from each reaction is calculated separately at each energy point and they are added to get the total damage energy cross sections. Secondly, there is inexactness involved in the computation of average PKA energies used as basic inputs here, which is partly due to the averaging procedures and partly due to the inexactness in the calculation of PKA spectra from nuclear reaction kinematics and basic evaluated nuclear data. However, these differences are expected to be reduced with more accurate estimations of PKA spectra using the CRaD code. The third reason for the observed differences could be due to the difference between the damage energy calculated using the analytic expressions of Robinson in NJOY-2016 and that simulated by SRIM-2013.

4.4.2.2 Polyatomic targets (SiC)

The dpa cross sections of SiC in the hundred energy group structure have been computed by Heinisch et al. [43] with the SPECOMP code [28] (developed by L.R. Greenwood). These data are considered as the standard in order to compare the present estimates. The average PKA energies of Si and C for the hundred incident neutron energies, calculated from their respective PKA spectra are used in SRIM (Q: K-P mode) to compute the damage energies in SiC. Then the total NRT-dpa cross sections of SiC are calculated using Eq. (4.8). These are compared with the

data given by Heinisch et al in Fig. 4.6. The maximum deviation is about 40%. However, from the overall agreement, the predictions of dpa are expected to be comparable.

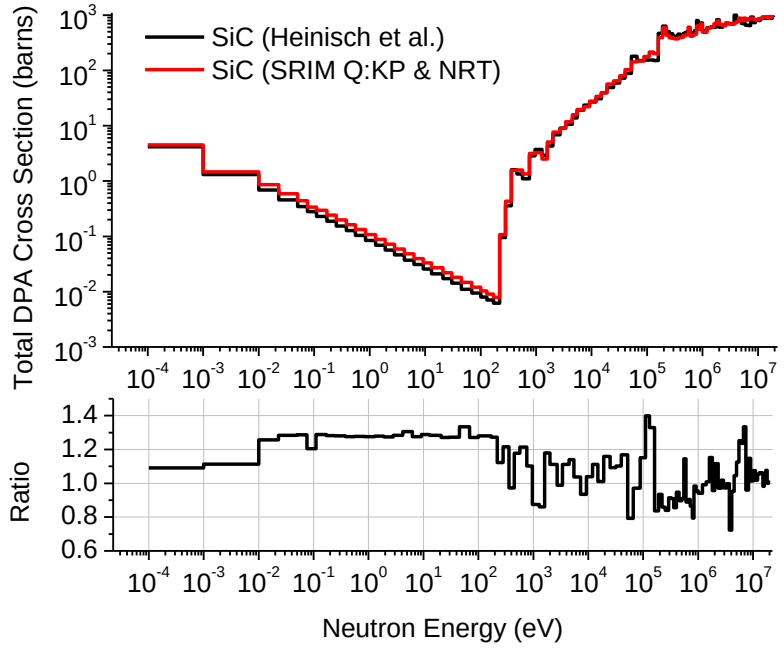

Fig. 4.6: Comparison of dpa cross sections of SiC obtained by using CRaD and SRIM-2013 (coupled Q: K-P mode and NRT model) and the results of Heinisch et al. [43].

4.4.3 Comparison of neutron dpa with ion induced dpa from SRIM-2013

Neutron spectra for different sources [106, 107] are shown in Fig. 4.7. Fast reactor neutron spectra (PFBR, Phenix, Super Phenix, EBR 2), typical thermal spectra (PWR-RPV, BWR-RPV, HFIR low res) and experimental fusion spectra (DEMO HCPB FW, HCLL FW, HCPB FW, ITER D-T) are chosen for the present study. The spatial distribution of neutron flux in PFBR [106] is obtained from the neutronics calculations. The neutron transport theory calculations in 175 groups are performed by using the DORT code [116] and the FARCOB system [117] is used to solve the 3-D diffusion equation in order to obtain the neutron flux in 26 groups.

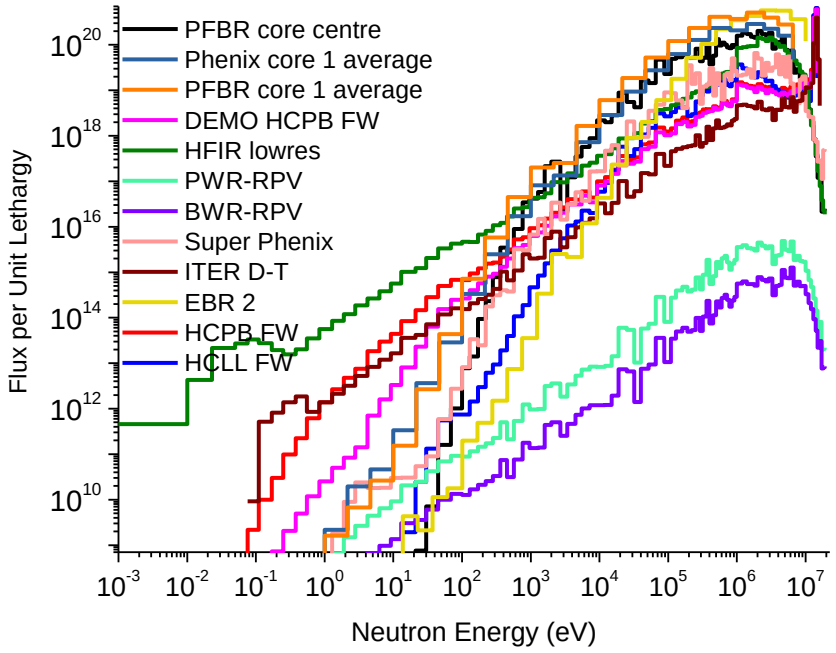

Fig. 4.7: Neutron flux spectra in different reactors.

4.4.3.1 Elemental targets (Fe, Cr and Ni)

The total dpa in Fe, Cr and Ni for 1 efpy of irradiation in some of these neutron spectra are estimated from the respective dpa cross sections obtained using SRIM-2013. These are compared with the total dpa obtained by using the standard dpa cross sections, see Table 4.4. The reference dpa cross sections considered here include ENDF/B-VII.1 based data from NJOY-2016 and CRaD codes. The recommended dpa data for Fe, Cr and Ni given by Fischer et al. (IAEA-CRP) [118] and the ASTM E693-12 [19] standard dpa cross sections of Fe are also considered for comparative study. The deviations between total dpa estimated with SRIM-2013 (Q: K-P option) and all the standard procedures are found to be within 10%. The maximum deviation in total dpa with respect to the reference values is found to be about 23%, with F-C option of SRIM-2013, in case of Ni. From these observations, it can be inferred that the approach of Q: K-P mode plus NRT model gives reasonable estimates of dpa in elemental targets. The total dpa in Fe per efpy due to various incident neutron spectra are also presented in Fig. 4.8.

Table 4.4: Comparison of total dpa in Fe, Cr and Ni using NRT-dpa cross sections from SRIM-2013 simulations and from the standard methods

Spectra	Element	Total dpa/efpy estimated with NRT-dpa cross sections					
		Standard procedure: neutron irradiation				Self-ion irradiation	
		Evaluations by Fischer et al.	ASTM E693-12	ENDF/B-VII.1		ENDF/B-VII.1SRIM2013+NRT model	
		IAEA-CRP: DXS	ENDF/B-VI	NJOY-2016	CRaD	Q: K-P	F-C
PFBR: core centre	Fe	66.9	66.2	65.5	65.5	70.3	73.0
	Ni	83.1	-	81.8	81.8	89.9	100.7
	Cr	77.7	-	71.6	71.6	79.1	80.4
PFBR: core1 averaged	Fe	42.5	45.1	45.1	44.3	46.4	48.0
Superphenix	Fe	9.8	9.9	9.6	9.8	10.3	10.6
Phenix: core 1 averaged	Fe	23.5	24.9	24.8	24.4	25.6	26.5
DEMO-HCPB-FW	Fe	13.0	13.1	12.9	13.0	14.1	15.0
BWR-RPV	Fe	2.1E-04	2.2E-04	2.2E-04	2.2E-04	2.3E-04	2.4E-04

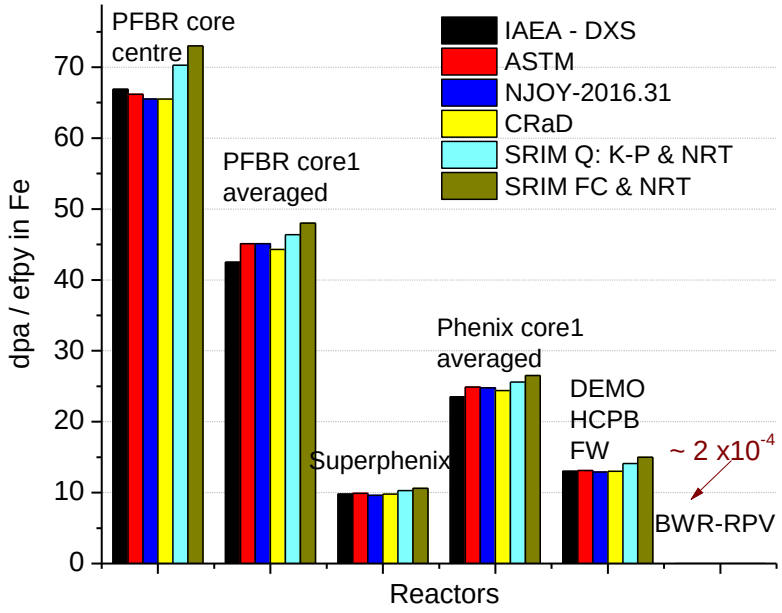

Fig. 4.8: Total accumulated dpa/efpy in Fe for various neutron flux spectra.

4.4.3.2 Polyatomic targets (SiC)

The total dpa per efpy in SiC in various neutron spectra are estimated from the dpa cross sections given by Heinisch et al. and that obtained in the present study using CRaD and SRIM-2013 codes. These are given in Table 4.5. In addition to the procedure described above, the dpa cross sections of SiC are also computed by taking the number of vacancies/ion directly from SRIM output in both F-C and Q: K-P modes, without using the corresponding estimates of damage energies and the NRT equation. The dpa and neutron spectrum-averaged one-group cross section values in the columns marked Q: K-P and F-C in Table 4.5 correspond to these simulations. The different levels of primary damage (dpa) accumulated in SiC for various spectra are presented in Fig. 4.9.The Q: K-P mode simulation gives only the total number of vacancies per ion. But, the merit of F-C mode simulation is that it gives the total number of vacancies of each atom species (which is here C and Si) separately. However, the predictions from F-C mode are always higher compared to the standard data. Among all the different methods attempted in this study, the best agreement with the results of Heinisch et al. is observed with the use of the combined Q: K-P and NRT model approach.

The total dpa in a material depends on the incident neutron spectrum. Due to higher contributions to dpa cross sections from elastic and inelastic scattering in fast reactors (with higher fast flux), the total dpa in iron in fast reactors is higher compared to that in thermal or fusion reactors. In silicon carbide, the total dpa in fusion reactors is lower than that in fast or thermal reactors. However, in fast reactors total dpa in SiC is higher (for e.g., by about 23% in PFBR core centre) than that in Fe. It is due to greater contribution from elastic scattering in case Si and C compared to that in Fe, in the fast neutron energy region.

Table 4.5: Comparison of dpa and neutron spectrum-averaged displacement cross section in SiC

Reactor spectra	dpa cross sections (barns)				dpa/efpy			
	Neutron irradiation	Self-ion irradiation			Neutron irradiation	Self-ion irradiation		
	Heinisch et al.	Q: K-P	F-C	Q: K-P & NRT	Heinisch et al.	Q: K-P	F-C	Q: K-P & NRT
EBR – 2	458	374	496	442	47.8	39	51.8	46.1
PFBR Core Centre	316	257	343	303	81.6	66.5	88.8	78.4
HFIR-low res	158	129	169	154	25.4	20.8	27.3	24.8
DEMO-HCPB-FW	391	328	417	391	6.22	5.21	6.63	6.21
HCLL-FW	440	362	469	430	12.1	9.95	12.9	11.8
HCPB-FW	338	283	361	337	7.04	5.9	7.52	7.03
ITER D–T	380	321	402	383	2.71	2.28	2.86	2.73
BWR – RPV	331	272	356	323	1.9E-04	1.5E-04	2.0E-04	1.8E-04
PWR – RPV	331	269	354	319	1.2E-03	9.8E-04	1.3E-03	1.2E-03

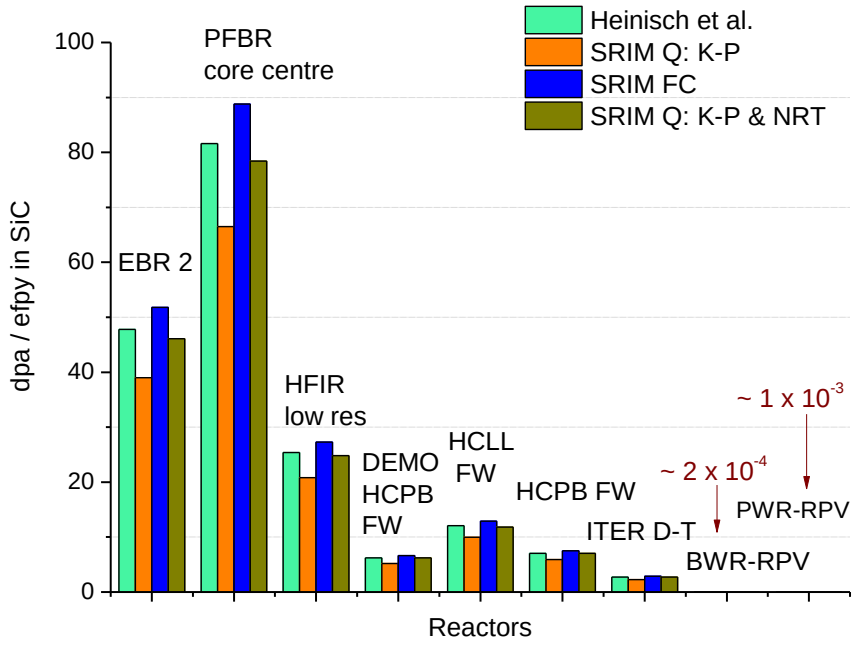

Fig.4.9: Accumulated dpa/efpy in SiC for various neutron flux spectra.

4.4.4 Self-ion plus arc-dpa modeling in elements using analytical expressions

As noted in Section 4.3, the damage energy and number of defects in elements can be calculated using the analytical energy-partition expressions (Eq. (2.16)) and arc-dpa model (Eq. (2.18)). This approach of estimating damage energy is suitable in case of elemental targets, where time consuming simulations using the SRIM code is an alternative method. In case of polyatomic targets, however, the analytical expressions cannot be used, except in few cases [78] where too many possibilities of different sub-lattice interactions have to be considered by changing the values of Z and A in Eq. (2.16) and E_d in the atom-displacement model. Hence, it is preferable to use the SRIM code for simulating the damage energy in polyatomic materials.

The dpa cross sections in Fe, Ni, Cr and Si are estimated using Eq. (4.5), where T_{dam} and ν_g are calculated from Eq. (2.16) and arc-dpa model in Eq. (2.18) respectively. The total dpa per efpy obtained in this way for various neutron spectra [106, 107] are compared with the dpa values estimated using the direct method in CRaD code as discussed in Chapters 2 and 3 [108]. These are presented in Fig. 4.10. In all the materials, the dpa predicted using both the methods compare reasonably well. However, there is a maximum difference of about 39% (prediction using the self-ion plus arc-dpa method is higher compared to that from the incident neutron method) in case of Si subjected to JAEA-FNS spectrum. The absolute magnitude of dpa in this neutron spectrum is very small, about 5×10^{-4} dpa/efpy. The observed differences are due to the aforementioned differences in the procedures of computation that are followed in these two methods. Note that, the predictions of dpa using the present self-ion plus arc-dpa approach can also be performed for polyatomic target materials like SiC, if the corresponding parameters b_{ad} and c_{ad} are known to estimate the damage efficiency in these kinds of materials.

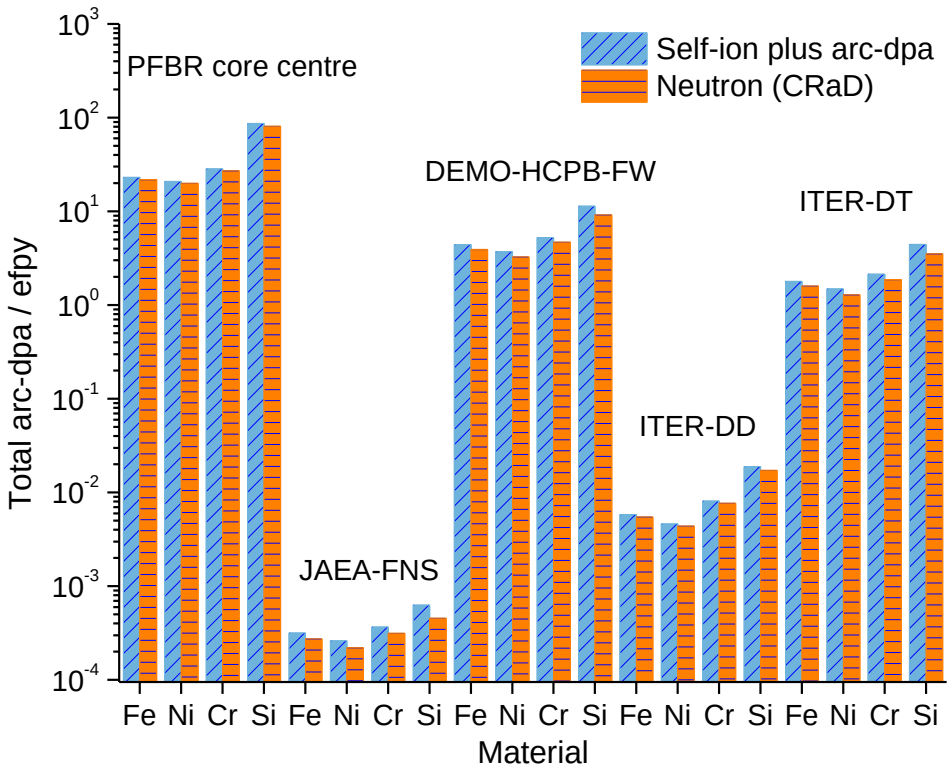

Fig. 4.10: Total dpa for 1 efpy obtained using the arc-dpa model in different elements for various neutron flux spectra.

4.5 Summary

An alternative method to compute the dpa cross sections in elemental and polyatomic materials through self-ion simulations using the SRIM-2013 software is described. The average energies of PKAs calculated by the CRaD code are used as the input energies of projectile ions in the simulations of damage energies with the SRIM-2013 software. The self-ion based dpa cross sections and total integrated dpa in various neutron spectra for both the elemental and polyatomic materials have shown good agreement on comparison with the standard data. Hence, it is established that the source term of primary radiation damage (in the units of dpa) can be equivalently determined by performing simulations with self-ions [114]. The present self-ion simulations method can be useful in another way, i.e. one would be able to map and correlate

various primary and secondary damage effects more realistically by performing self-ions simulations with PKA energies exactly as formed in reactor locations.

This method is envisaged to be a useful way to compute dpa cross sections and integrated dpa in the target materials which are polyatomic in nature. The method of self-ion simulations with the use of PKA energies calculated by CRaD code also has the potential to yield realistic dpa cross sections based on the molecular dynamics (MD) theory. In order to obtain the dpa cross sections from MD simulations the PKA energies have to be corrected for the energy losses due to electronic interactions and the corresponding damage energies have to provided as the inputs.

Chapter 5

Propagation of Nuclear Data Uncertainties to the Metrics of Primary Radiation Damage by Total Monte Carlo Methodology

5.1 Introduction

The information about the reactions of continuous energy neutrons are obtained from the evaluated nuclear data libraries, such as the very recently released ENDF/B-VIII.0 [58]. At present, there exists a number of basic evaluated nuclear data libraries, such as ENDF/B-VII.1, JENDL-4.0, JEFF-3.3, CENDL-3.1, TENDL-2017 [75] etc. Because of varying treatment of nuclear reactions in terms of models, parameter values and their uncertainties [63], etc., varying subjective assessments and interpretation of the experimental results and their uncertainties compiled in the IAEA-EXFOR database [64] and using of different statistical inference tools in the process of evaluation, the neutron reaction data in these libraries differ from each other. As a consequence, each of the parameters of primary radiation damage due to neutrons derived from these libraries differ among themselves; and the nuclear data uncertainties in these parameters need to be quantified to meet the design objectives of structural materials for nuclear reactors.

The traditional method to propagate the uncertainties in neutron reaction data is to follow the perturbation theory [70] and the more recent approach follows the Total Monte Carlo (TMC) methodology [61-62]. In the present study, the TMC methodology has been employed to determine the nuclear data uncertainties in the parameters of primary radiation damage. The applications of this methodology to determine the uncertainties in these derived parameters have been demonstrated in several works presented at the recently concluded CRP of the IAEA [71-

73, 119-120]. The applications of TMC methodology to study the effects of uncertainty in nuclear data on various other reactor physics parameters have been demonstrated previously in several works [59, 62, 65-68, 121-124].

The TMC methodology employs a large number of random evaluated nuclear data files to propagate the uncertainties in nuclear data to the derived quantities. These random files are generated using random sampling of the nuclear model parameters from their respective distributions. It is an alternative to the traditional first-order sensitivity analysis (also called sandwich formula for error propagation) or higher order approximations that follows the perturbation theory. It can be applied to propagate uncertainties for quantities where the perturbation methodology could not be applied because of non-applicability of approximations involved in sandwich formula, non-availability of covariance information and specific computational tools. However, consistency between the applications of both perturbation and TMC methodologies can be maintained and they can be compared only if both methods use the equivalent nuclear data. This implies that both the average and the probability distributions of the nuclear interaction cross sections, resonance parameters, ν-bar and other single and double differential data from all the randomly generated files must correspond to the respective quantities and their covariance information in the unique ENDF file that is used in the perturbation method [121]. This is fulfilled, provided normal probability distributions of nuclear model parameters are assumed while generating the random data by TMC methodology. The TMC calculations use random evaluated nuclear data files which are generated based on the covariance of TALYS [60] model parameters. These random evaluated data files do not follow the normal probability distribution for each of the evaluated nuclear data quantities, by default. The TMC methodology has the advantage, that, it is not limited by the restricted convention so

far being followed in the storage of ENDF covariance data, that the first and second multivariate moments would be sufficient for any probability distribution, which is compatible with the application of sandwich formula for error propagation. The integral parameters for large scale nuclear systems may sometimes follow non-normal probability distributions and the derived integral quantity can, in some cases show strongly skewed probability distribution and the uncertainty from nuclear data can be actually higher than what is predicted from the assumption of a normal distribution [62, 122].

The TENDL-2015 and TENDL-2017 [59] nuclear data libraries contain a large number of random files (say *N*, ~300 to 700) which are generated by the nuclear reaction code system TALYS by randomly sampling the basic input model parameters of nuclear reactions, viz. level density, transmission coefficients, optical model parameters, compound nucleus model parameters, any other input of nuclear reaction models [63] etc., within their pre-estimated uncertainties. The number of such random nuclear data files *N* required for a nuclide to carry out physically meaningful calculations is determined by the evaluators of nuclear data based on the study of the relative sensitivities of calculated cross sections on the variation of various nuclear model parameters [59]. The nuclear data evaluated from the default parameter values (unperturbed set of model parameters which is used for a global nuclear model calculation) corresponds to the unperturbed data. The derived quantity estimated from the unperturbed data file forms the reference value [59]. It is denoted by giving a suffix *0* to the respective quantity. In an ideal case, the mean of results from random data files should be very close to this reference value. This happens when uncertainties in the parameters and consequently the spread in derived results are both relatively small, i.e. non-linearity is not too high [59, 61]. More detailed

discussions on the applications of TMC methodology to propagate the uncertainties of nuclear data to various derived parameters can be found in Ref. [59, 62, 65-68, 71, 72, 119-124].

The present chapter is organized as follows. An overall outline of the methodology to quantify the uncertainties in the parameters of primary radiation damage by TMC approach using the CRaD code is given in Section 5.2. In Section 5.3, a discussion is made on various statistical parameters that are estimated from the results obtained by computation using the data in random ENDF-6 files. In Section 5.4, the nuclear data uncertainties in dpa cross sections and integrated dpa are quantified. The nuclear data uncertainties in PKA spectra and average energy of PKAs are quantified in Section 5.5. The uncertainties in nuclear data are propagated to the uncertainties in damage energy and production of primary defects in target materials by using the average PKA energies from CRaD code in the SRIM-2013 [40] software. This is discussed in Section 5.6. Sections 5.7 and 5.8 are devoted to the estimations of nuclear data uncertainties in gas production and neutron kerma coefficients respectively, where, correspondingly, uncertainties in gas production cross sections, concentrations of gases, neutron kerma cross sections and integrated neutron kerma coefficients are estimated. The chapter is summarized in Section 5.9.

5.2 Outline of the calculation methodology

The generalized calculation methodology adapted to propagate the uncertainties from nuclear data to the metrics of primary radiation damage according to the TMC approach is briefly outlined in Fig.5.1. The random ENDF-6 nuclear data files in TENDL-2015 and TENDL-2017 libraries [59] are used for this study. It is to be noted that, apart from many other important isotopes, TENDL-2017 library has provided random data files for all the four important isotopes of iron, whereas such data for ^{56}Fe, ^{58}Ni, ^{28}Si and ^{48}Ti are available in TENDL-2015. The

parameters of primary damage are also computed from other basic evaluated nuclear data libraries, such as ENDF/B-VII.1 [125], ENDF/B-VIII.0 [58], JENDL-4.0 [76] and TENDL 2014 [59] so that they can be compared with the mean values of the respective parameters that are obtained using the random ENDF-6 files. A summary of the list of evaluated nuclear data files available and used in this study is presented in Table 5.1. A special routine has been implemented in the CRaD code to compute various statistical quantities like mean, standard deviation, covariance and correlation matrices and skewness of the parameters of primary radiation damage. The important steps followed in this procedure are given below [99-100, 113]:

a) Pre-process neutron cross sections for important structural isotopes at 300K from the random ENDF-6 files [79] (N ~ 300 to 500) of TENDL-2015 and TENDL-2017, in addition to other basic evaluated nuclear data libraries (ENDF/B-VII.1, JENDL-4 and TENDL-14) by using the RECONR and BROADR modules of NJOY-2016 code system [29].
b) Compute the parameters of primary radiation damage in point-wise and multigroup formats from all the above files (random and other basic evaluated files) for each nuclide using CRaD code. Then, estimate the neutron spectra-averaged quantities, such as integrated dpa, average PKA energy, one-group gas production cross sections and concentrations of gases and the integrated neutron kerma coefficients.
c) Compute various statistical parameters like mean, standard deviation, skewness and energy-energy covariance and correlation matrices of the damage parameters obtained from random files and compare the mean values of these parameters obtained using the TMC methodology with that obtained using the reference / unperturbed evaluated nuclear data files.
d) Estimate nuclear data uncertainties in damage energy and number of vacancies produced in the material by using SRIM-2013 self-ion simulations. Here, the average PKA energies and

their uncertainties obtained from steps (b) and (c) and the concept discussed in Chapter 4 are applied.

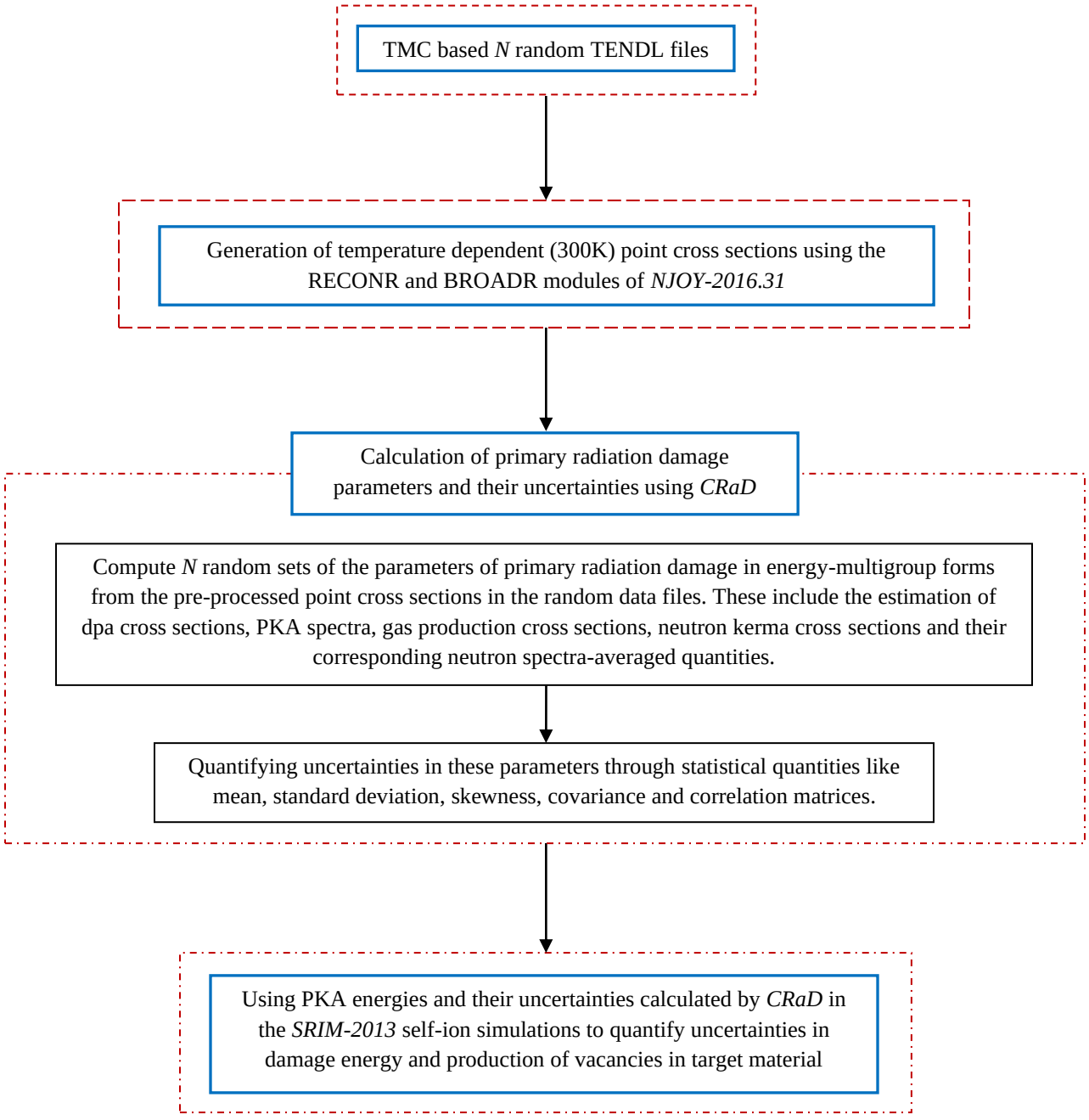

Fig. 5.1: Block diagram of the working methodology to propagate uncertainties in nuclear data to the uncertainties in the parameters of primary radiation damage by applying TMC approach. Blue boxes signify the important stages in the methodology of uncertainty propagation which are performed by different codes / software, linking one to the other.

Table 5.1: The unperturbed and random neutron reaction data files from different libraries that are available and used to estimate and compare primary radiation damage parameters

Isotopes	ENDF/B-VII.1	ENDF/B-VIII.0	JENDL-4.0	TENDL-2014	TENDL-2015	TENDL-2017
^{54}Fe	1	1	1	-	1	1 + (500)*
^{56}Fe	1	1	1	-	1 + (300)	1 + (613)
^{57}Fe	1	1	1	-	1	1 + (732)
^{58}Fe	1	1	1	-	1	1 + (500)
^{58}Ni	1	1	1	1	1 + (300)	-
^{28}Si	1	1	1	1	1 + (300)	-
^{48}Ti	1	-	1	1	1 + (300)	-
^{59}Ni	1	1	1	-	-	1
^{60}Ni	1	1	1	-	-	1
^{61}Ni	1	1	1	-	-	1
^{62}Ni	1	1	1	-	-	1
^{64}Ni	1	1	1	-	-	1
^{50}Cr	1	1	1	-	-	1
^{52}Cr	1	1	1	-	-	1
^{53}Cr	1	1	1	-	-	1
^{54}Cr	1	1	1	-	-	1
^{55}Mn	1	1	1	-	-	1
^{12}C	-	1	-	-	-	1
^{13}C	-	1	-	-	-	1
nat. C	1	-	1	-	-	-
^{29}Si	1	1	1	-	-	1
^{30}Si	1	1	1	-	-	1
^{10}B	1	1	1	-	-	1
^{11}B	1	1	1	-	-	1
^{92}Mo	1	1	1	-	-	1
^{94}Mo	1	1	1	-	-	1
^{95}Mo	1	1	1	-	-	1
^{96}Mo	1	1	1	-	-	1
^{97}Mo	1	1	1	-	-	1
^{98}Mo	1	1	1	-	-	1
^{99}Mo	1	1	1	-	-	1
^{100}Mo	1	1	1	-	-	1

*number of random files is mentioned within parentheses

5.3 Calculation of statistical parameters

As mentioned in Section 5.2, the statistical quantities are calculated after computing the parameters (denoted by the symbol *x*)dpa cross sections, integrated dpa, PKA spectra, average PKA energies, gas production cross sections, concentrations of gases, neutron kerma cross sections and integrated neutron kerma coefficients, from the random evaluated nuclear data files. The elements of covariance matrix are calculated as

$$V_{ij} = \frac{1}{N}\sum_{n=1}^{N}(x_i^{(n)} - \bar{x}_i)(x_j^{(n)} - \bar{x}_j);\ \ i, j = 1\,\text{to}\,G \quad . \tag{5.1}$$

Here, N is the number of random data sets and G denotes the number of energy groups. The mean of the quantity in each energy group 'i' is given by

$$\bar{x}_i = \frac{1}{N}\sum_{n=1}^{N} x_i^{(n)}, \quad \text{i} = 1\,\text{to}\,\text{G} \quad . \tag{5.2}$$

The correlation matrix is calculated from the covariance matrix as

$$C_{ij} = \frac{V_{ij}}{\sqrt{V_{ii}V_{jj}}} \quad . \tag{5.3}$$

The standard deviation (uncertainty) in the quantity in i^{th} energy group is calculated as

$$SD_{i(nucl.data)} = \sqrt{\frac{1}{N}\sum_{n=1}^{N}(x_i - \bar{x}_i)^2} \quad . \tag{5.4}$$

The calculated random parameters of primary radiation damage may or may not follow normal distribution. The skewness (which gives the extent to which they are asymmetric) in the set of N data is calculated from the third moment as follows:

$$\gamma_{1i} = \frac{\sum_{n=1}^{N}(x_i^{(n)} - \bar{x}_i)^3}{N(SD)_i^3};\ i = 1\,\text{to}\,G \quad . \tag{5.5}$$

The sample sizes of random files vary from 300 to 732 (see Table 5.1), where, 300 files from TENDL-2015 and 500 files from TENDL-2017 are used in this study. Thus, the statistical parameters like skewness, correlation coefficients, etc. are uncertain due to sampling error which arises because of the limited sample sizes. Therefore, the confidence intervals of these parameters are quantified in a few cases (for illustrative purposes) where proper convergence of the statistical parameter seems to become more apparent by considering even larger sample sizes. Since the true distributions of these parameters are not known, the 95% bootstrap confidence intervals [126] are quantified.

The above statistical quantities can be helpful while refining nuclear data to achieve the desired target accuracies in the derived quantities. In such pursuits, the (energy-wise, reaction-wise, isotope-wise, etc.) correlations observed in these quantities can guide in tailoring the differential nuclear data more accurately. To illustrate the concept of propagation of nuclear data uncertainties using random files, the results are discussed here in detail for a few important structural targets, such as ^{58}Ni, ^{28}Si, ^{48}Ti, Fe and its isotopes.

5.4 Uncertainty in dpa cross sections and integrated dpa due to nuclear data

5.4.1 Contributions of partial neutron reactions to dpa uncertainty

The dpa cross sections due to each of the contributing neutron induced reactions in Fe and its isotopes and their uncertainties are calculated from the random files (N = 500) in TENDL-2017 in VITAMIN-J 175 group structure using the CRaD code [99]. The total dpa cross sections of ^{56}Fe and their uncertainties are presented in Fig. 5.2. The top part in this figure contains the mean dpa cross sections obtained from random data along with the calculated uncertainties. The part below shows the relative variation of mean dpa cross sections with

respect to the dpa cross sections calculated from the unperturbed data set. The ratios of mean of random files to unperturbed values of dpa cross sections are found to be very close to unity in most of the energy ranges, except at the energies where uncertainties in dpa cross sections are large. The extents to which the distributions of random dpa cross sections deviate from symmetric behavior (i.e. skewness at each energy point) are shown in the right-hand axis of the plot below. In general, the distributions are found to be asymmetric and uncertainties in cross sections and the deviations of their distributions from normal behavior (skewness) are found to be closely related to the ratios of mean to unperturbed.

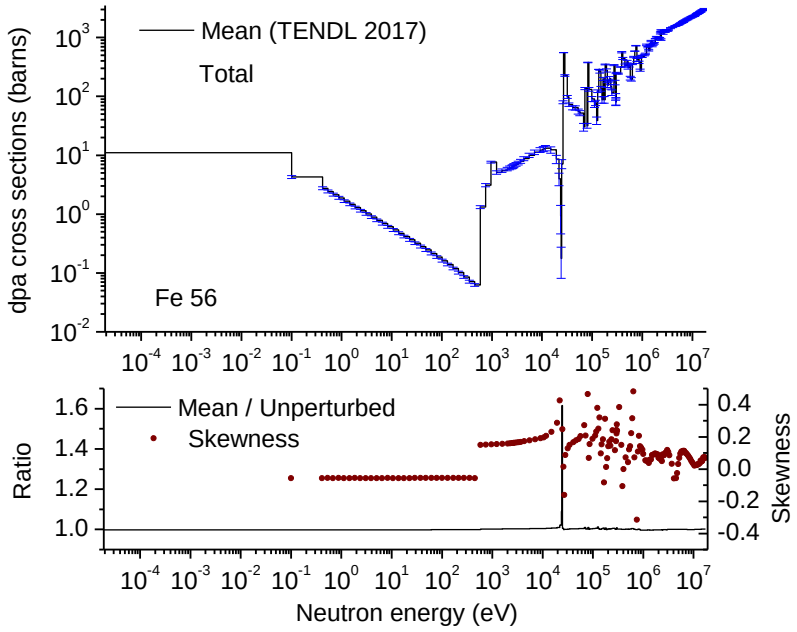

Fig. 5.2: The total neutron dpa cross sectionsin^{56}Fe. Mean dpa cross sections along with nuclear data uncertainties calculated by CRaD code using TENDL-2017 data (plot at the top); Ratio of mean to unperturbed dpa cross sections and energy-wise skewness of distributions of the random dpa cross sections (plot at the bottom).

The extents of variations of neutron dpa cross sections due to randomly sampled nuclear data files is illustrated in Fig. 5.3 with the total neutron dpa cross sections in ^{56}Fe as an example [99]. The ratios of the random to mean and the mean to the unperturbed dpa cross sections are

plotted in this figure. Fig. 5.4 (a) illustrates how the statistical parameters, viz. energy group to group correlation coefficients and the skewness of total dpa in ^{56}Fe converge to their final values with the increasing number of random files. The convergences of parameters viz. total dpa cross section (the value at 100th energy group is shown as an example) and total dpa to their respective unperturbed values are presented in Fig. 5.4 (b). The dpa calculated here is for one efpy at the core centre location of PFBR [106].

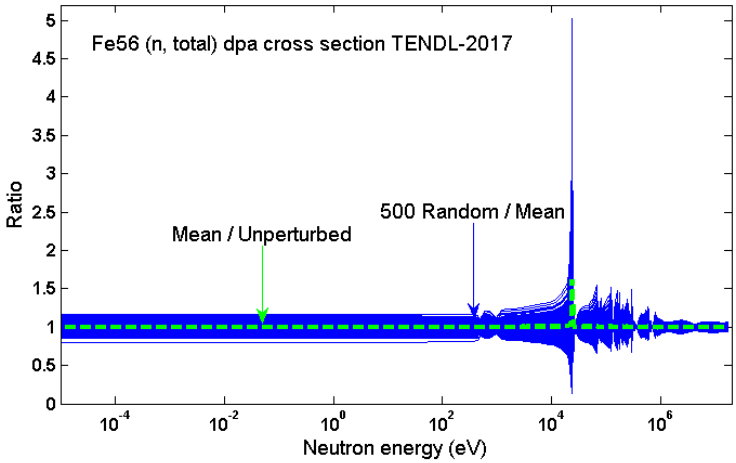

Fig. 5.3: Ratios of the random values to the mean value of the dpa cross section and the mean value to the unperturbed value of the dpa cross section in ^{56}Fe isotope.

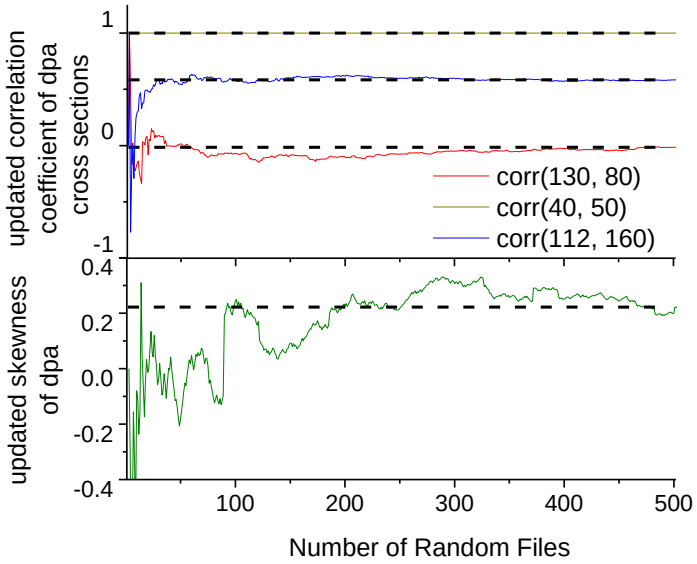

Fig. 5.4 (a)

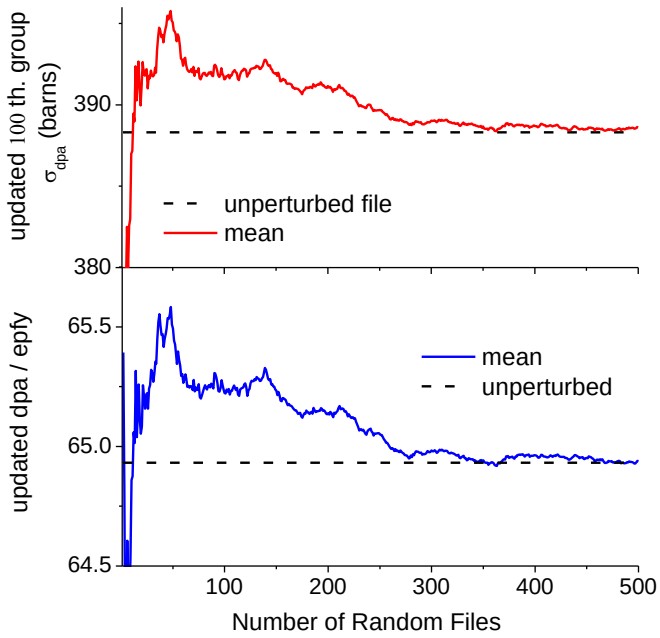

Fig. 5.4 (b)

Fig. 5.4: (a): The convergence of group-to-group energy correlations in total dpa cross sections and that of skewness in the total dpa/efpy to their respective final values represented by black dot-lines; (b): The convergence of dpa cross sections (as an e.g. in 100th energy group) and that of the total dpa/efpy to their respective unperturbed values represented by black dot-lines. The plots are shown for the ^{56}Fe isotope. The neutron energy groups are in the VITAMIN-J 175 group structure.

The energy–energy correlations of total dpa cross sections in ^{56}Fe are shown in Fig. 5.5 (a). It can be observed here that the dpa cross sections at different neutron energies are not all uncorrelated, but show some correlations among them. There are three main blocks of high correlations, with the remaining ones having negligible or zero correlations. The energy-energy (or group to group) cross-correlations between various partial dpa cross sections in ^{56}Fe are shown in Fig. 5.5 (b). These cross-channel correlations indicate how the individual partial dpa cross sections correlate with the others, the correlations between different nuclear reaction kinematic models to calculate them and the combination of all these quantities.

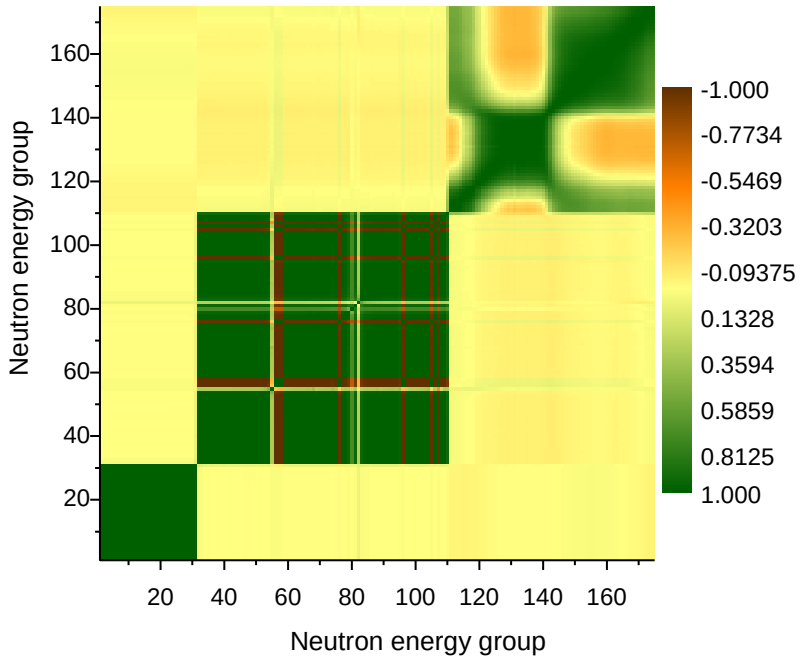

Fig. 5.5 (a)

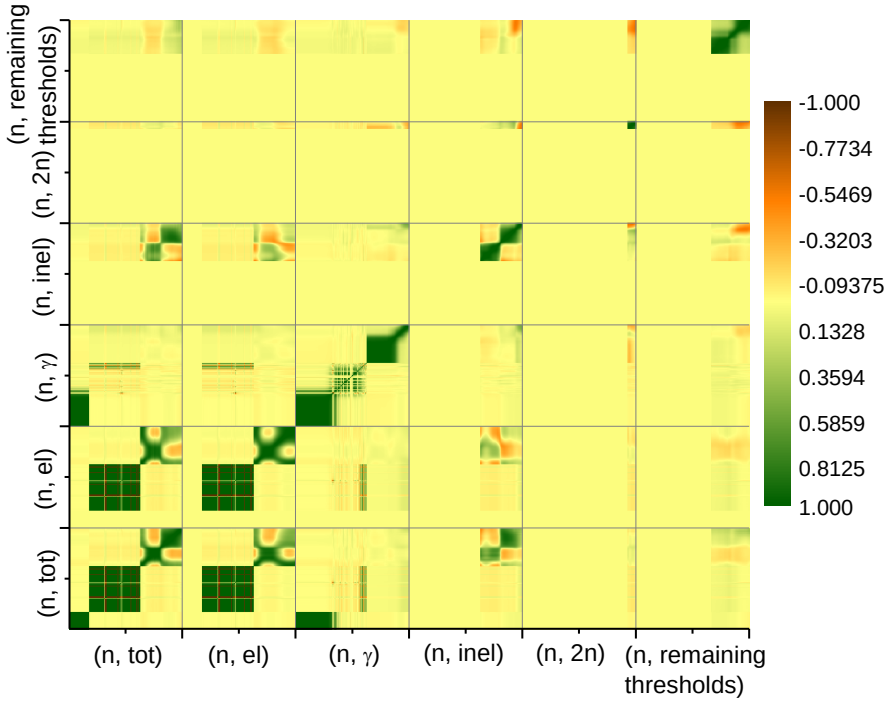

Fig. 5.5 (b)

Fig. 5.5: (a): Energy-energy correlations in total dpa cross sections; (b): Correlations of neutron dpa cross sections in various partial reactions. These are illustrated here in case of ^{56}Fe isotope. The x- and y-axes are neutron energy groups in the VITAMIN-J 175 group structure.

The unperturbed neutron dpa/efpy in Fe and its isotopes, their mean values and uncertainties due to irradiation at the core centre location of PFBR from various contributing reactions, as calculated from TENDL-2017 data using the CRaD code, are presented in Table 5.2. The overall uncertainty in total dpa in an isotope (and in the element) is found to be within 3%. The fact that (n, 2n) and other threshold reactions contribute very less to total dpa in this case, negates the effect of their large uncertainties (~ 35%). High correlations among the contributing reactions also affect the overall uncertainty. The random dpa cross sections are found to be distributed non-symmetrically [99] and the skewness in dpa values (see Table 5.2) are non-zero. Compared to that simply envisaged from the estimated standard uncertainties in cases of normal distribution, the skewed distributions of dpa add to the chances of rare events. As discussed in Section 5.3, there can be uncertainties in the estimated statistical parameters and their proper convergence may not be ensured due to the limited sample sizes. Hence, the confidence intervals for the skewness of dpa are calculated in a few cases, for illustrative purposes. For the skewness in total dpa/efpy (Table 5.2) in ^{54}Fe, ^{56}Fe, ^{57}Fe and ^{58}Fe, the confidence intervals are respectively [0.0013, 0.3362], [0.0385, 0.4772], [-0.2335, 0.1161] and [-0.0278, 0.3476]. In general, the convergence of these parameters is observed for 300 or more number of random files [66, 121]. However, the minimum number of random files required for the convergence of important parameters may also depend on the physical quantity that is estimated and its sensitivity on the randomness of basic evaluated nuclear data.

The derived parameters estimated from different basic evaluated nuclear data libraries sometimes show significant spread. The variations of dpa cross sections and total integrated dpa calculated from different nuclear data libraries for some important structural isotopes are investigated in the next two sections.

Table 5.2: The reaction-wise and total dpa/efpy at core centre location of PFBR in Fe and its isotopes using TENDL-2017

Reactions	Unperturbed value (dpa)	Mean of random data (dpa)	Nuclear data uncertainty (dpa)	Skewness
		^{54}Fe		
Elastic	79.4	79.3	1.4 (1.8%)	0.22
Inelastic	7.3	7.2	0.18 (2.5%)	0.05
(n, γ)	3.3e-2[#]	3.3e-2	6.7e-4 (2%)	0.81
(n, 2n)	4.1e-5	4.2e-5	7e-6 (16.7%)	0.53
Remaining thresholds	1.63	1.64	0.2 (12.2%)	0.05
Total	85.7	85.6	1.3 (1.5%)	0.16
		^{56}Fe		
Elastic	54.4	54.4	1.7 (3.1%)	0.26
Inelastic	10.5	10.4	0.26 (2.5%)	-0.02
(n, γ)	1.2e-2	1.2e-2	9.3e-5 (0.8%)	0.60
(n, 2n)	2.18e-3	2.15e-3	1.7e-4 (8.1%)	0.04
Remaining thresholds	0.04	0.0412	7.3e-3 (17.7%)	0.28
Total	64.9	64.9	1.7 (2.6%)	0.22
		^{57}Fe		
Elastic	66.8	66.5	2.8 (4.2%)	0.01
Inelastic	30.4	30.2	1 (3.3%)	-0.1
(n, γ)	5.9e-2	4.9e-2	2.2e-3 (4.5%)	-0.03
(n, 2n)	5.8e-2	5.7e-2	3.7e-3 (6.5%)	-0.14
Remaining thresholds	3.2e-2	3.4e-2	8.8e-3 (25.9%)	0.56
Total	94.8	94.3	2.7 (2.9%)	-0.07
		^{58}Fe		
Elastic	97.8	97.4	3 (3.1%)	0.12
Inelastic	13.4	13.4	0.3 (2.2%)	-0.67
(n, γ)	9.4e-3	9.4e-3	1.8e-4 (1.9%)	0.66
(n, 2n)	1.2e-2	1.2e-2	7.4e-4 (6.2%)	-0.05
Remaining thresholds	2.3e-3	2.4e-3	8e-4 (33.3%)	0.58
Total	106.8	106.3	2.7 (2.5%)	0.16
		Fe		
Elastic	56.2	56.2	1.7 (3%)	0.61
Inelastic	10.7	10.6	0.3 (2.8%)	-0.74
(n, γ)	1.4e-2	1.4e-2	1.7e-4 (1.2%)	2.04
(n, 2n)	3.3e-3	3.2e-3	2.4e-4 (7.5%)	0.38
Remaining thresholds	0.13	0.13	1.8e-2 (13.8%)	1.47
Total	66.9	66.8	1.7 (2.5%)	0.47

3.3e-2 may be read as 3.3×10^{-2}.

5.4.2 Comparison of dpa cross sections of structural isotopes between libraries

The total neutron dpa cross sections of the isotopes of iron, ^{58}Ni, ^{28}Si and ^{48}Ti are computed from JENDL-4.0, ENDF/B-VII.1, TENDL-2014, TENDL-2015 and TENDL-2017 using the CRaD code [99]. The dpa cross sections in ^{57}Fe, ^{58}Fe and ^{58}Ni computed using the data from different libraries are presented in Fig. 5.6, for illustrations. In each case the uncertainties in

the cross sections calculated from random TENDL data files are also shown with respect to the mean dpa cross sections. The dpa cross sections from different evaluated nuclear data libraries are found to vary appreciably among each other for some of these materials. The convergence between them is better for the major isotopes like ^{56}Fe, ^{58}Ni, ^{28}Si and ^{48}Ti, but for less abundant isotopes, such as ^{54}Fe, ^{57}Fe, ^{58}Fe, etc., they do not compare well [99].

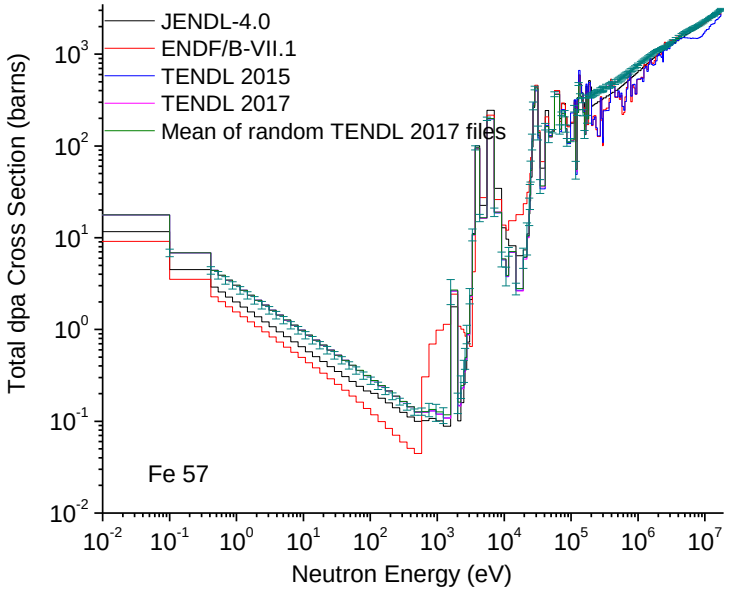

Fig. 5.6 (a)

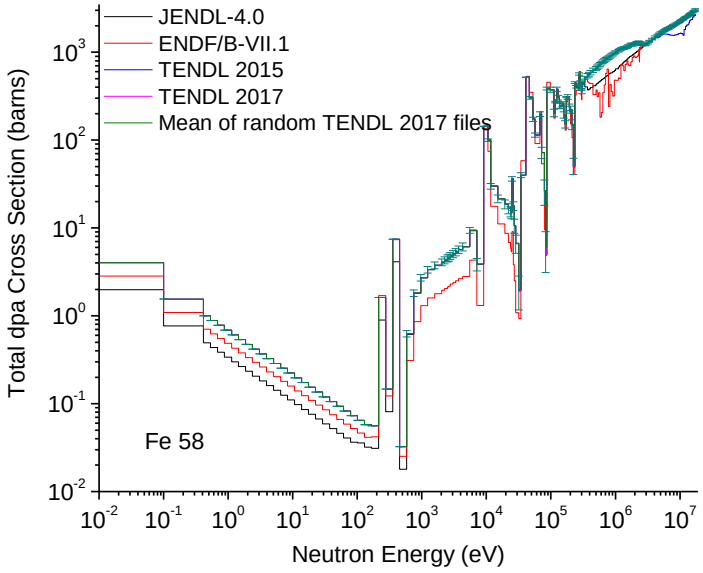

Fig. 5.6 (b)

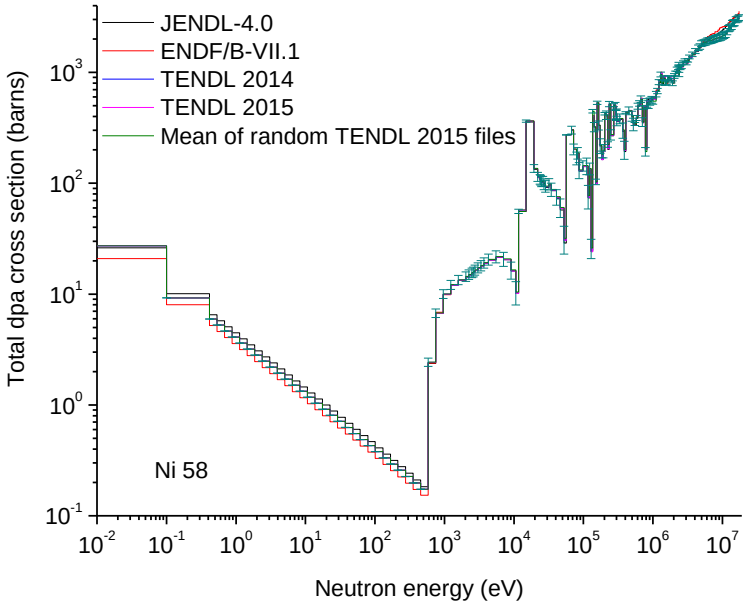

Fig. 5.6 (c)

Fig. 5.6: Total neutron dpa cross sections and nuclear data uncertainties calculated at 300 K from different evaluated nuclear data libraries by using the CRaD code; (a): ^{57}Fe; (b): ^{58}Fe; (c): ^{58}Ni.

Some of the important causes for these variations have been meticulously investigated from different basic evaluated nuclear data files [99]. Significant differences are observed among different libraries in the contribution from elastic scattering to the dpa cross sections in ^{57}Fe and ^{58}Fe. Since the abundances of these isotopes in natural iron are low, these differences do not affect the overall estimates of dpa in iron obtained by using different libraries. The elastic scattering angular distributions of secondary neutrons in ^{57}Fe and ^{58}Fe from different basic evaluated nuclear data libraries are shown in Fig. 5.7 (a) and (b). In these figures, the quantity plotted in the y-axis is $f(\cos\theta, E)$ calculated from Eq. (2.2), with $\mu = \cos\theta$. Here E is the incident neutron energy and θ is the scattering angle of the outgoing neutron. In the computation of elastic scattering dpa cross sections, the damage energy is calculated from the recoil energy that is transferred to the target nucleus due to scattering of the neutron at various angles. Hence, this scattering distribution must be calculated correctly for each incident neutron for the correct estimation of the number of displacements of atoms. The angular distributions at a few incident

neutron energies (100 keV, 600 keV, 1 MeV and 2 MeV) are shown here as examples. Large discrepancies are observed when the data from ENDF/B-VII.1 are compared to the data from JENDL-4.0 and TENDL-2015. The deviations observed between the dpa cross sections obtained using ENDF/B-VII.1 and other libraries in the energy region of elastic contribution in Fig. 5.6 (a) and (b) can be due to these differences in the angular distributions of scattered neutrons. The differences in the basic neutron interaction cross sections in different libraries also contribute (comparatively to a lesser extent in this particular case) to the observed differences in dpa cross sections.

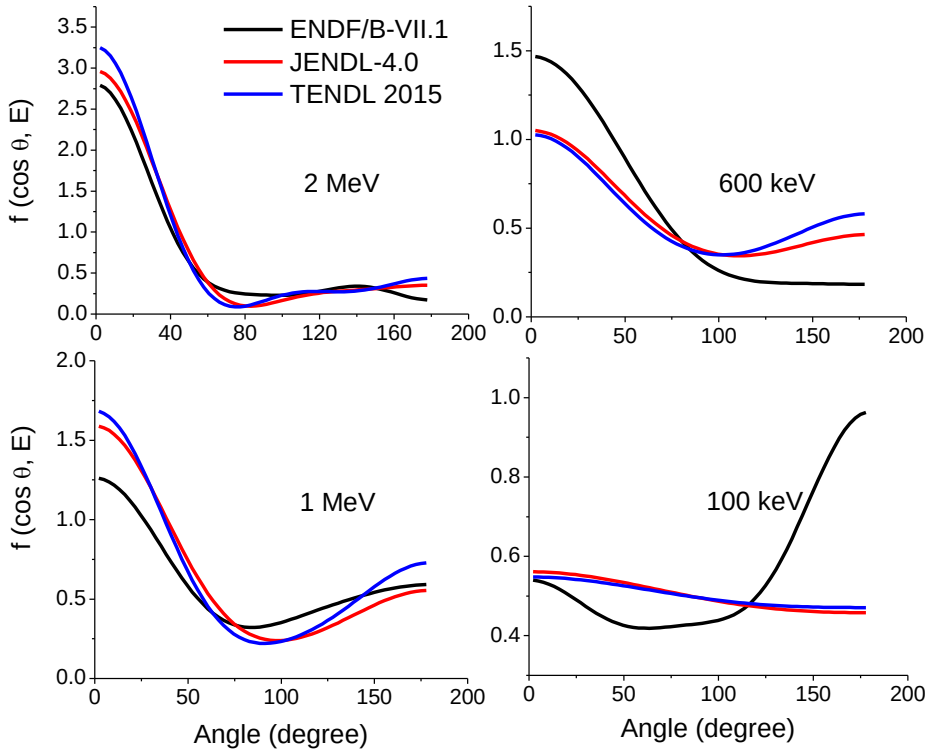

Fig. 5.7 (a)

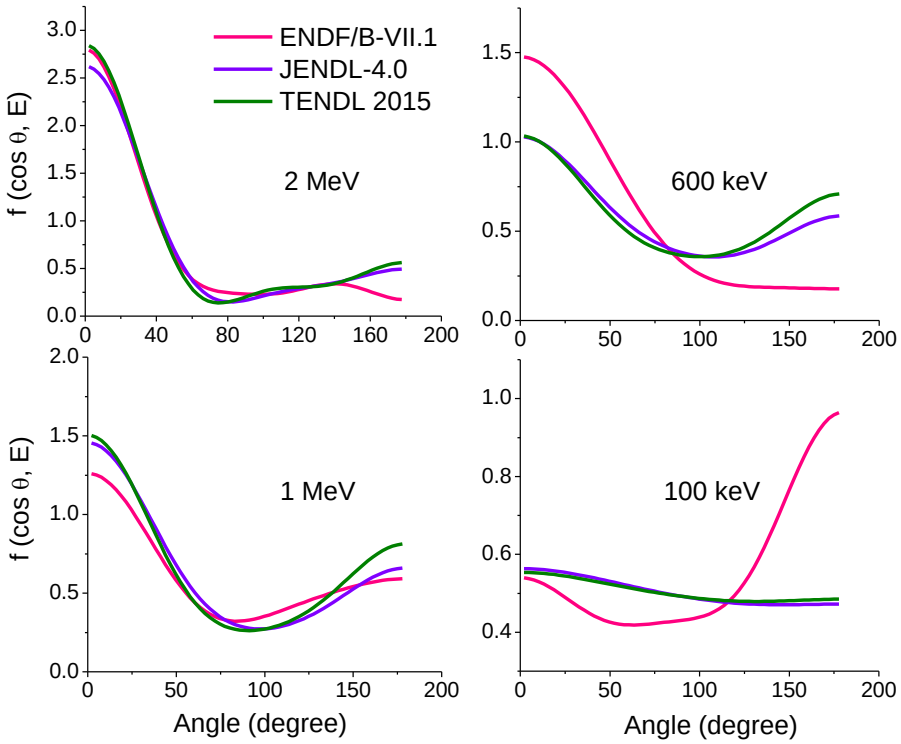

Fig. 5.7 (b)

Fig. 5.7: Angular distributions of the secondary neutrons in (n, n) reaction computed by CRaD using the ENDF/B-VII.1, JENDL-4.0 and TENDL-2015 data; (a): ^{57}Fe; (b): ^{58}Fe.

5.4.3 Comparison of neutron spectra integrated total dpa from different libraries

The total dpa/efpy computed in^{56}Fe, ^{58}Ni and ^{28}Si for irradiation in PWR-RPV spectrum, fast neutron fission and fusion spectra [106-107] by using different basic evaluated nuclear data libraries are compared in Table 5.3. The uncertainties in total dpa are calculated with the help of random data files available in TENDL-2017 (for ^{56}Fe) and in TENDL-2015 (for ^{58}Ni and ^{28}Si). The uncertainties in the total dpa in ^{56}Fe, ^{58}Ni and ^{28}Si are found to be around 3%, 6% and 4% respectively. The uncertainty in total dpa in ^{48}Ti is found to be about 5% and that in other isotopes of Fe is about 3% [99]. The total dpa in each of these spectra from different libraries are different, but these differences may not be practically significant. In this context, the TMC concept indicates that the mean of all the random evaluations along with its associated

uncertainty can be chosen when a single value for the predicted dpa parameter is required to be known for design purposes.

Table 5.3a: Comparison of total neutron dpa/efpy in **^{56}Fe** in various neutron spectra calculated using different basic evaluated nuclear data libraries

Reactor	dpa/efpy				
	JENDL-4.0	ENDF/B-VII.1	TENDL-2015	TENDL-2017	mean ± uncertainty*
PFBR: core centre	63.9	63.6	64.7	64.9	64.9±1.7
JAEA-FNS	8.7e-4	9.4e-4	7.2e-4	9.1e-4	9.1e-4±1.8e-5
DEMO-HCPB-FW	12.3	12.8	10.6	12.6	12.6±0.21
ITER D–D	1.8e-2	1.7e-2	1.8e-2	1.8e-2	1.8e-2±4.4e-4
ITER D–T	4.98	5.22	4.26	5.13	5.13±0.09
PWR-RPV	1.2e-3	1.2e-3	1.2e-3	1.2e-3	1.2e-3±2.1e-5

*From TENDL-2017 random files

Table 5.3b: Comparison of total neutron dpa/efpy in **^{58}Ni** in various neutron spectra calculated using different basic evaluated nuclear data libraries

Reactor	dpa/efpy				
	JENDL-4.0	ENDF/B-VII.1	TENDL-2014	TENDL-2015	mean ± uncertainty*
PFBR: core centre	83.1	83.5	82.9	83	82.8±3.9
JAEA-FNS	1e-3	1e-3	9.2e-4	9.3e-4	9.2e-4±5.6e-5
DEMO-HCPB-FW	14.7	14.8	13.8	13.8	13.7±0.6
ITER D–D	1.9e-2	1.9e-2	1.9e-2	1.9e-2	1.9e-2±7e-4
ITER D–T	5.82	5.90	5.44	5.44	5.40±0.26
PWR-RPV	1.4e-3	1.4e-3	1.4e-3	1.4e-3	1.4e-3±5.5e-5

*From TENDL-2015 random files

Table 5.3c: Comparison of total neutron dpa/efpy in **^{28}Si** in various neutron spectra calculated using different basic evaluated nuclear data libraries

Reactor	dpa/efpy				
	JENDL-4.0	ENDF/B-VII.1	TENDL-2014	TENDL-2015	mean ± uncertainty*
PFBR: core centre	97.1	103	96.1	96.1	97.5± 3.5
JAEA-FNS	6.1e-4	6.2e-4	5.9e-4	5.9e-4	5.8e-4±1.9e-5
DEMO-HCPB-FW	11.7	12.2	11.4	11.4	11.5±0.26
ITER D–D	2.2e-2	2.2e-2	2.1e-2	2.1e-2	2.1e-2±5.8e-4
ITER D–T	4.51	4.72	4.45	4.45	4.46±0.10
PWR-RPV	1.6e-3	1.7e-3	1.6e-3	1.6e-3	1.7e-3±5.4e-5

*From TENDL-2015 random files

5.5 Uncertainty in PKA spectra and average energy of PKAs due to nuclear data

5.5.1 Uncertainty in PKA spectra

The spectra of PKAs resulting from neutron interactions are calculated from the basic evaluated nuclear data in energy multi-grouped format (as 175×175, 198×198, etc. matrices) according to the methods described in Chapter 2. All the nuclear data libraries do not give sufficient information on the distributions of recoil nucleus (particularly for the threshold type of reactions) to compute the PKA spectra from each of all the possible reaction channels. As for examples, PKA spectra cannot be computed realistically for isotopes of Fe and ^{28}Si from JENDL-4.0 and isotopes of Fe from the random files in TENDL-2017. In these instances, the computation of PKA spectra is performed in the CRaD code by assuming an isotropic emission of recoil nucleus after (n, p), (n, α), etc. type of reactions and by using evaporation models for emitted neutrons in continuum inelastic and (n, 2n) reactions. These approximations do not yield very accurate results and better methods need to be developed within CRaD code to cope up with such instances. In general, all the partial neutron reactions contribute dominantly to the recoils in the keV energy range. The (n, α) and (n, p) reactions give large contributions to the recoils in 1 to 3 MeV energy range [99].

The uncertainties in all the recoil groups from each incident neutron group are computed, which are also in a matrix form of the same dimensions as the PKA matrix. For simplicity, the uncertainties in nuclear data for the elastic, inelastic and (n, 2n) channels are calculated explicitly and for the remaining threshold type of reactions, calculations are performed after adding them all together as (n, remaining threshold). Finally, the uncertainties are calculated in the "sum" PKA spectra after combining all these partial PKA contributions (using Eq. (5.4)). The PKA

spectra and their uncertainties due to nuclear data in ^{56}Fe and ^{58}Ni isotopes, obtained by using the ENDF-6 random data files in TENDL-2015, are illustrated in Fig. 5.8. A high incident neutron energy (14.5 MeV) is chosen for illustration so that contributions from a larger number of reaction channels can be observed. Both unperturbed and the mean (with its uncertainty) PKA spectra are shown here. The uncertainties in PKA spectra vary from low energy to high energy recoil groups. For the 14.5 MeV neutrons in cases of both ^{56}Fe and ^{58}Ni, the uncertainties are found to be around 12% in the low energy recoil groups, 5-7% around the 100 to 200 keV recoil groups and about 50% in the vicinity of 1 MeV recoil groups [99]. It is to be noted that the absolute values of the PKA spectra in the higher energy recoil groups (~ 1 MeV) are very small and their contributions to the overall neutron spectrum integrated quantities are also very less.

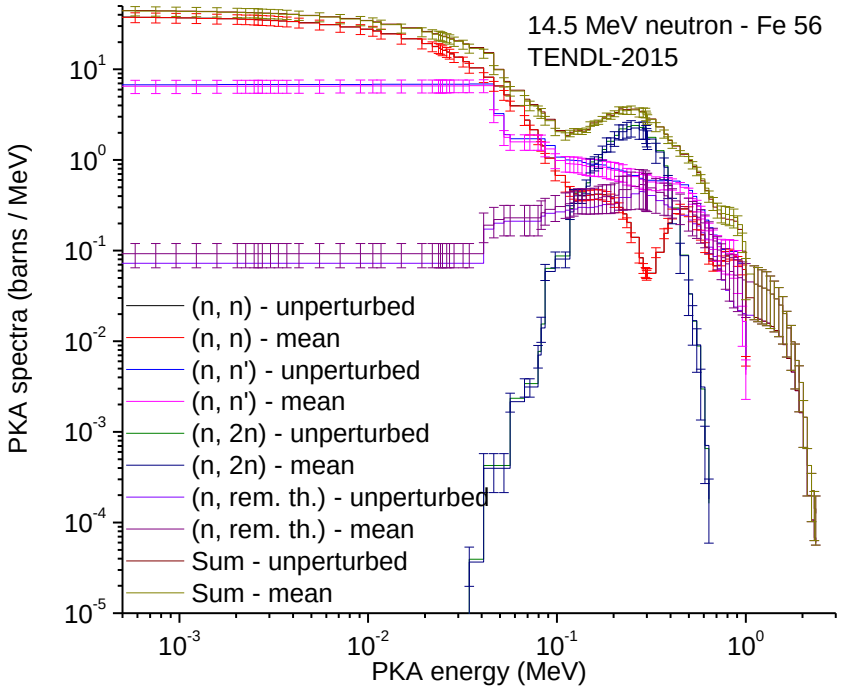

Fig. 5.8 (a)

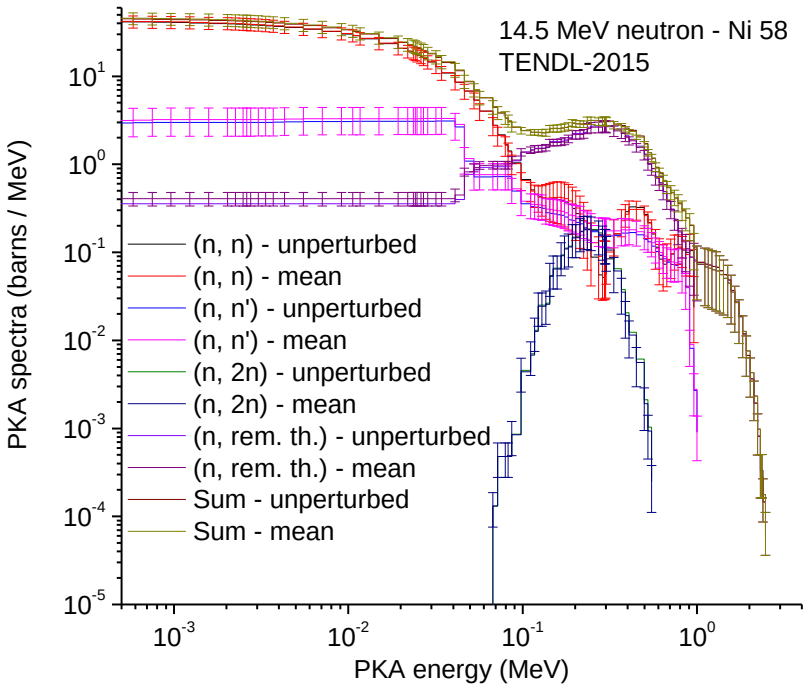

Fig. 5.8 (b)

Fig. 5.8: The nuclear data uncertainties in the spectra of PKAs for interactions of 14.5 MeV neutrons, calculated by CRaD using the random data files in TENDL-2015; (a): ^{56}Fe; (b): ^{58}Ni.

5.5.2 Contributions of partial neutron reactions to PKA uncertainty

The PKA spectrum-averaged recoil energies in Fe and its isotopes are calculated from the ENDF-6 random files in TENDL-2017 using Eqs. (4.2) and (4.3). The reaction-wise average PKA energies corresponding to a neutron spectrum φ are then calculated using Eq. 5.6,

$$(\overline{E}_R)_\varphi = \frac{\sum_{g_n=1}^{G} (\overline{E}_R)_{g_n} (E_{g_n+1} - E_{g_n}) \varphi_{g_n}}{\sum_{g_n=1}^{G} (E_{g_n+1} - E_{g_n}) \varphi_{g_n}} \quad . \tag{5.6}$$

The reaction-wise uncertainty in PKA energies for the PFBR core centre spectrum is found to be within 3%. The distributions of average PKA energies are also found to be skewed [99]. The ENDF-6 random files in TENDL-2015 contain more complete information on energy

distribution of recoil nuclei and similar estimations from this library have yielded the overall nuclear data uncertainty of around 6-7% [99].

5.5.3 Neutron spectra integrated average PKA energies from different libraries

The PKA energies averaged over the PKA spectrum for each neutron group (Eq. 4.3) and average energies of PKAs in Fe corresponding to various neutron spectra (Eq. 5.6) are estimated using the ENDF/B-VII.1, JENDL-4.0 and TENDL-2017 databases. The uncertainties in recoil energies contributed from (n, γ) reaction are not quantified from the random files. However, the absolute contributions from (n, γ) recoils are estimated using ENDF/B-VII.1 data and accounted in all the central values of average PKA energies. The spectrum averaged PKA energies in Fe from (n, γ) reaction as calculated using ENDF/B-VII.1 are 0.533, 0.972, 0.834, 0.569, 0.833, 0.564 keV respectively for the PFBR core centre, JAEA-FNS, DEMO-HCPB-FW, ITER-DD, ITER-DT and PWR-RPV spectra [99]. The variation of average PKA energy in Fe with neutron energy is shown in the top plot in Fig. 5.9. The PKA energy of about 0.5 keV below 10 keV neutron energy is mainly due to the (n, γ) reaction. The uncertainties are found to be about 3% only when compared to the absolute mean values of PKA energies. The PKA energies calculated from different libraries up to about 5 MeV neutrons are very similar, but at higher neutron energies, the predictions obtained using JENDL-4.0 and TENDL-2017 random files are higher by about 50 to 80 keV when compared to those obtained using the ENDF/B-VII.1 data. This is because, approximations (mentioned in Section 5.5.1) are used in the CRaD code to compute the PKA spectra resulting from continuum inelastic and threshold reactions, which leads to higher values of the average energies of PKAs [99]. The ratios of mean to unperturbed average PKA energies (plot below in Fig. 5.9) are found to be very close to 1 for the full energy range.

The neutron spectra integrated average PKA energies in Fe are shown in Fig. 5.10. The nuclear data uncertainties (using TENDL-2017) are estimated to be within 3% in all the spectra. The shape of the neutron spectrum and the fractions of neutrons in each energy group dictate the average energy of PKAs. The DEMO and ITER-DT spectra being very similar, results in almost same PKA energies. The ITER-DD spectrum has peaks at 2.5 MeV and 14 MeV and decreasing trend in between. The JAEA-FNS spectrum has an increasing trend towards high energy with a peak at 14 MeV, which greatly increases the share of the PKA energy coming from high energy threshold reactions. Due to the reasons discussed above, in the fusion neutron spectra, the average PKA energies estimated using JENDL-4.0 and TENDL-2017 random files are higher by about 50 keV as compared to those estimated using the ENDF/B-VII.1. In the other three spectra, the PKA energies estimated from all these libraries are similar.

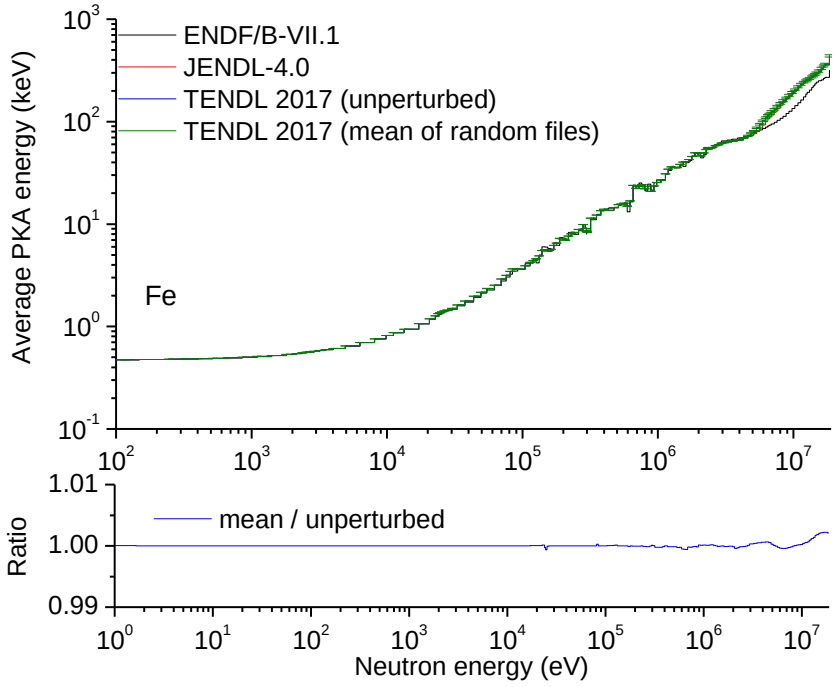

Fig. 5.9: The PKA spectrum average energy in Fe (including all reactions) calculated using different evaluated nuclear data libraries (top). The ratios of the mean to unperturbed PKA energies (not including (n, γ)) are shown below [99].

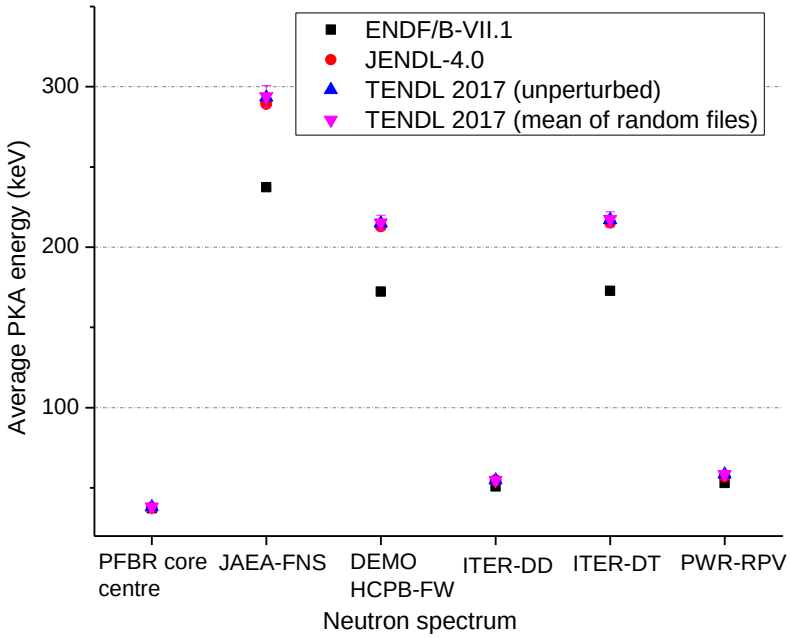

Fig. 5.10: The average energies of PKAs in Fe for various neutron spectra. The uncertainties are calculated using TENDL-2017 random database; all the central values are plotted after adding the contributions from (n, γ) reaction. However, the uncertainties include uncertainties in all nuclear reactions, except the (n, γ) reaction.

5.6 Uncertainty in damage energy and number of vacancy defects due to nuclear data

The use of ion irradiation to emulate neutron radiation damage phenomena is well known [2]. The source term of primary radiation damage by neutrons in the units of dpa can be equivalently determined by self-ion simulations using SRIM-2013 [114]. The damage energy T_{dam} and number of vacancies $\nu(T_{\mathrm{dam}})$ produced in the material is uncertain due to uncertainties in nuclear data using which the PKA energies are estimated. Hence, it is vital to quantify these uncertainties. The uncertainties in T_{dam} and $\nu(T_{\mathrm{dam}})$ are quantified here with the help of the outputs from CRaD code to simulate Fe self-ions using the SRIM-2013 software according to the procedure described in Chapter 4.

The damage energies and number of vacancies simulated using the PKA energies estimated from different nuclear data libraries and for different irradiation spectra are presented

in Table 5.4. In case of average PKA energies calculated using nuclear data from TENDL-2017, the simulations are performed only with the mean energy and the upper and lower bounds of energies after accounting their uncertainties. No simulations are performed with the average PKAs from unperturbed data. Both the upper and lower bounds of the damage energy are calculated as it depends non-linearly on the PKA energy, but within the range of PKA energies and their uncertainties estimated here, the uncertainties in the damage energies are found to vary approximately linearly. The uncertainties in damage energy and formation of primary defects are estimated to be around 3% based on the random nuclear database in TENDL-2017. Since the predictions of number of vacancies (defects) formed in the irradiated material can differ depending on the nuclear data library used and the spectrum of irradiation, knowing their mean values along with the nuclear data uncertainty is of significance.

Table 5.4: The nuclear data uncertainties in damage energy and defect production parameters for Fe self-ion irradiations using SRIM-2013

Reactor	PFBR core centre	JAEA-FNS	DEMO-HCPB-FW	ITER D–D	ITER D–T	PWR-RPV
			ENDF/B-VII.1			
PKA energy (keV)	37.2	237.4	172.3	50.8	172.8	53
Damage energy (keV)	26.7	142.2	108	35.7	108.3	37.1
vacancies	267	1422	1080	357	1083	371
			JENDL-4.0			
PKA energy (keV)	37.7	289.2	213	54.7	215.2	57.2
Damage energy (keV)	27	167.7	129.8	38.2	131	39.8
vacancies	270	1677	1298	382	1310	398
			TENDL-2017			
PKA energy (keV)[a]	38.1	293.4	214.9	54.9	217.1	58.5
PKA energy (keV)[b]	38.2±0.2	293.9±6.8	215.3±4.6	54.9±0.4	217.4±4.7	58.5±0.3
Damage energy (keV)	27.4±0.2	167 170.1 173.1	128.6 131 133.5	38.3±0.3	129.7 132 134.5	40.6±0.2
vacancies	274±2	1670 1701 1731	1286 1310 1335	383±3	1297 1320 1345	406±2

[a] From unperturbed data; [b] From random data files

The absolute values of the number of vacancies will be smaller if arc-dpa model (Eq. 2.18) is used instead of NRT model, but the estimated nuclear data uncertainties will be similar. The predictions of nuclear data uncertainties in the above parameters of primary radiation damage, viz. dpa cross sections, PKA spectra, etc. depend on the availability of complete information in the random nuclear data files which are used to propagate the uncertainties. The random nuclear data files available as a part of TENDL-2015 provide more complete information on the spectra of the recoil nucleus compared to the recent TENDL-2017 random nuclear data. The nuclear data uncertainties in dpa/efpy, average PKA energy and the vacancies are estimated to be about 6 to 7% by using the TENDL-2015 random files [99].

The PKA spectra and average PKA energies reflect the differential nuclear data more directly than the dpa cross sections and the integrated dpa parameter, where, in the latter quantities more functions like the calculations of damage energy and number of vacancies and integration over them are involved. The correlations and uncertainties in these material physics parameters also have effects in the estimation of the overall uncertainty of the dpa faced by the material, which are not quantified in the present study. These can give rise to an additional 5 to 20% uncertainty component in the atom displacement rates [72]. The uncertainties in neutron spectra (which are not considered here) also affect the overall uncertainty in the integrated parameters, viz. integrated dpa and neutron spectra-averaged PKA energy.

5.7 Uncertainty in the production of gases due to nuclear data

The neutron cross sections for the production of charged particles in different libraries differ from each other in many aspects, such as content of the data, their representations, absolute

magnitudes, etc. Therefore, a survey is made from different basic evaluated nuclear data libraries [100] in order to know the scope of theoretical predictions of gas production.

5.7.1 Survey of (n, CPO) cross sections from different basic evaluated nuclear data libraries

The sum of all the cross sections of neutron reactions producing hydrogen, deuterium, tritium, helium-3 and helium-4are estimated using the data in different evaluated nuclear data libraries such as ENDF/B-VII.1, JENDL-4.0, TENDL-2017 and ENDF/B-VIII.0in a multi-grouped form using the CRaD code by following the procedure described in Chapter 2. A summary of the cross sections available in various basic evaluated nuclear data files for these gas production reactions in a few structural isotopes are presented in Table 5.5. The presence of data in a database for the total production of a particle is represented by 'Y' for available and 'N' for absence. The number of different channels for which the particle production cross sections are given separately differs from one library to another. As an example, it is observed that one library indicates the production of protons by giving only (n, p) reaction channel separately and remaining in the lumped data in MT = 5, whereas, another library indicates that its total production is due to contributions coming separately from (n, p), (n, n p) and (n, p α) etc., reaction channels. In another instance, it may be observed that one such basic evaluated nuclear data library does not provide the numerical data of cross sections for the production of a particular particle from any identified reaction channel, whereas, another such library provides a non-zero production of that particle coming fully from at least one of the many possible reaction channels. Note that, for most of the isotopes presented in Table 5.5, the production cross section of ^{3}He is absent from ENDF/B-VII.1 and ENDF/B-VIII.0, but in JENDL-4.0 and TENDL-2017, the same is non-zero for many of these isotopes. Also, there can be large differences in some activation reaction channels such as total deuteron, triton and ^{3}He productions among the data in

different basic evaluated nuclear data libraries [100]. Note for example, the cross section data for the productions of deuteron, triton and ^{3}He in ^{56}Fe are not present in JENDL-4.0, but they are present in the other three nuclear data libraries (see Table 5.5). Hence, the differences in the content of data and the absolute magnitudes of reaction cross sections in different nuclear data libraries can lead to variations in the theoretical estimates of gas production from neutron induced transmutation reactions.

Table 5.5: The summary of total charged particle production cross section data in different basic evaluated nuclear data libraries

Target	Availability of total particle production cross section data																			
	Proton				Deuteron				Triton				^{3}He				Alpha			
	A1*	A2	A3	A4	A1	A2	A3	A4	A1	A2	A3	A4	A1	A2	A3	A4	A1	A2	A3	A4
^{54}Fe	Y	Y	Y	Y	Y	N	Y	Y	N	N	Y	Y	N	N	Y	Y	Y	Y	Y	Y
^{56}Fe	Y	Y	Y	Y	Y	N	Y	Y	Y	N	Y	Y	Y	N	Y	Y	Y	Y	Y	Y
^{57}Fe	Y	Y	Y	Y	N	N	Y	Y	N	N	Y	Y	N	N	Y	Y	Y	Y	Y	Y
^{58}Fe	Y	Y	Y	Y	N	N	Y	Y	N	N	Y	Y	N	N	Y	Y	Y	Y	Y	Y
^{58}Ni	Y	Y	Y	Y	Y	Y	Y	Y	N	Y	Y	Y	N	Y	Y	N	Y	Y	Y	Y
^{59}Ni	Y	Y	Y	Y	Y	Y	Y	Y	Y	Y	Y	Y	Y	Y	Y	Y	Y	Y	Y	Y
^{60}Ni	Y	Y	Y	Y	Y	Y	Y	Y	N	Y	Y	Y	N	Y	Y	N	Y	Y	Y	Y
^{61}Ni	Y	Y	Y	Y	N	Y	Y	Y	N	Y	Y	Y	N	Y	Y	N	Y	Y	Y	Y
^{62}Ni	Y	Y	Y	Y	Y	Y	Y	Y	N	Y	Y	Y	N	Y	Y	N	Y	Y	Y	Y
^{64}Ni	Y	Y	Y	Y	Y	Y	Y	Y	N	Y	Y	Y	N	Y	Y	N	Y	Y	Y	Y
^{50}Cr	Y	Y	Y	Y	Y	Y	Y	Y	N	Y	Y	N	N	Y	Y	N	Y	Y	Y	Y
^{52}Cr	Y	Y	Y	Y	N	Y	Y	N	N	Y	Y	N	N	Y	Y	N	Y	Y	Y	Y
^{53}Cr	Y	Y	Y	Y	N	Y	Y	N	N	Y	Y	N	N	Y	Y	N	Y	Y	Y	Y
^{54}Cr	Y	Y	Y	Y	N	Y	Y	N	N	Y	Y	N	N	Y	Y	N	Y	Y	Y	Y
^{55}Mn	Y	Y	Y	Y	Y	Y	Y	Y	Y	Y	Y	Y	Y	Y	Y	Y	Y	Y	Y	Y
^{12}C	-	-	Y	Y	-	-	Y	Y	-	-	N	N	-	-	N	N	-	-	Y	Y
^{13}C	-	-	N	N	-	-	N	N	-	-	N	N	-	-	N	N	-	-	Y	Y
nat. C	Y	Y	-	-	Y	Y	-	-	N	N	-	-	N	N	-	-	Y	Y	-	-
^{28}Si	Y	Y	Y	Y	Y	N	Y	Y	N	N	Y	N	N	N	Y	N	Y	Y	Y	Y
^{29}Si	Y	Y	Y	Y	N	N	Y	N	N	N	Y	N	N	N	Y	N	Y	Y	Y	Y
^{30}Si	Y	Y	Y	Y	N	N	Y	N	N	N	Y	N	N	N	Y	N	Y	Y	Y	Y
^{10}B	Y	Y	Y	Y	Y	Y	Y	Y	Y	Y	Y	Y	N	N	N	N	Y	Y	Y	Y
^{11}B	Y	Y	Y	Y	N	Y	N	N	Y	Y	Y	Y	N	N	N	N	Y	Y	Y	Y
^{92}Mo	Y	Y	Y	Y	Y	Y	Y	Y	Y	Y	Y	Y	Y	Y	Y	Y	Y	Y	Y	Y
^{94}Mo	Y	Y	Y	Y	Y	Y	Y	Y	Y	Y	Y	Y	Y	Y	Y	Y	Y	Y	Y	Y
^{95}Mo	Y	Y	Y	Y	N	Y	Y	N	N	Y	Y	N	N	Y	Y	N	Y	Y	Y	Y
^{96}Mo	Y	Y	Y	Y	Y	Y	Y	Y	Y	Y	Y	Y	N	Y	Y	N	Y	Y	Y	Y
^{97}Mo	Y	Y	Y	Y	Y	Y	Y	Y	Y	Y	Y	Y	Y	Y	Y	Y	Y	Y	Y	Y
^{98}Mo	Y	Y	Y	Y	Y	Y	Y	Y	Y	Y	Y	Y	N	Y	Y	N	Y	Y	Y	Y
^{99}Mo	Y	Y	Y	Y	Y	Y	Y	Y	Y	Y	Y	Y	N	Y	Y	N	Y	Y	Y	Y
^{100}Mo	Y	Y	Y	Y	Y	Y	Y	Y	Y	Y	Y	Y	N	Y	Y	N	Y	Y	Y	Y

* A1, A2, A3, A4 means, respectively, ENDF/B-VII.1, JENDL-4.0, TENDL-2017, ENDF/B-VIII.0

5.7.2 Comparison of concentrations of gases in structural elements between libraries

The concentrations of hydrogen and helium gases produced in some elements due to irradiation in PFBR core centre, ITER-DT and PWR-RPV neutron spectra are calculated by the CRaD code from different libraries (see Table 5.6).In general, good agreement can be observed, apart from some exceptions. As for examples, note the differences in the predictions from different libraries in the amounts of total helium produced in Cr in PFBR core centre and ITER-DT spectra [100]. Also note the differences in the production of helium in Fe (in PFBR core centre spectrum) and in Si (in ITER-DT spectrum). These differences are due to large variations in helium production cross sections in some energy regions when data from different libraries are used.

Table 5.6: Production of hydrogen and helium due to neutron interactions in structural elements

Element	Nuclear data	Gas produced in ~ 6.3 years (appm)					
		Hydrogen			Helium		
		PFBR core centre	ITER-DT	PWR-RPV	PFBR core centre	ITER-DT	PWR-RPV
Fe	E7.1*	934	1680	4.3e-2	65.4	408	6.5e-3
	J4.0	938	1860	4.38e-2	50.6	366	4.94e-3
	T17	915	1760	4.43e-2	39.2	401	4.19e-3
	E8.0	912	1550	4.37e-2	44.7	405	4.51e-3
Ni	E7.1	13600	6630	0.46	927	954	4e-2
	J4.0	13500	6790	0.459	1100	922	4.24e-2
	T17	13400	7140	0.472	885	836	3.57e-2
	E8.0	13100	6560	0.462	1000	913	4.23e-2
Cr	E7.1	468	1240	2.74e-2	48.1	270	3.98e-3
	J4.0	326	1270	2.05e-2	18.5	337	2.17e-3
	T17	464	1430	2.81e-2	18.1	331	2.2e-3
	E8.0	468	1240	2.74e-2	48.1	270	3.98e-3
C	E7.1	2.71e-2	0.741	0	146	667	0
	J4.0	2.48e-2	1.69	0	163	719	0
	T17	2.68e-2	0.733	0	145	664	0
	E8.0	2.68e-2	0.733	0	145	664	0
Si	E7.1	940	2940	7.91e-2	448	1700	4.03e-2
	J4.0	788	2740	7.22e-2	379	1950	4e-2
	T17	788	2840	7.2e-2	456	2420	4.79e-2
	E8.0	940	2940	7.91e-2	448	1700	4.03e-2

* E7.1, J4.0, T17, E8.0 respectively means ENDF/B-VII.1, JENDL-4.0, TENDL-2017 and ENDF/B-VIII.0

5.7.3 Uncertainty in gas production and activation cross sections

The gas production and total activation cross sections in $^{54, 56, 57, 58}$Fe are calculated by the CRaD code using the random ENDF-6 files in TENDL-2017. The corresponding random cross sections in elemental Fe are then computed from these isotopic cross sections (by weighing with their abundances). The ratios of the mean to the unperturbed cross sections for the gas production reaction channels in ^{56}Fe are found to deviate up to a maximum of about 20% from unity and the energy-wise distributions of these cross sections are skewed [100]. In case of total activation reaction channel in ^{56}Fe, the energy-wise uncertainties, the deviations of the ratios of mean to unperturbed cross sections from unity and the distributions of the cross sections from Gaussian behavior are found to be smaller, as compared to the gas production reaction channels. In ^{56}Fe, the correlations in cross sections between different activation reaction channels are moderate. The correlations in (n, p), (n, α) and (n, total activation) cross sections between the four isotopes of Fe are small [100].

The neutron spectra averaged activation cross sections in Fe, their uncertainties and the skewness values are presented in Table 5.7. The reference cross sections obtained by using the unperturbed data sets are also presented here. The maximum uncertainties in spectrum averaged one-group hydrogen, helium, deuterium, tritium and helium-3 production cross sections in various neutron spectra are found to be around 16%, 31%, 54%, 56% and 30% respectively. The uncertainties in total activation cross sections in Fe subjected to irradiation in PFBR core centre, ITER-DT and PWR-RPV neutron spectra are found to be 1%, 3.7% and 4.3% respectively. These uncertainties are less compared to the uncertainties seen in the partial activation cross sections. In fact, the total cross sections as well as the total activation cross sections of neutrons (sum of all partial activation channels) can be determined relatively more accurately as compared

to the production of charged particles in individual reactions, at higher energies. Also, the uncertainties and the deviations from linearity (i.e. unity value of the ratio of mean to unperturbed data) and Gaussian behavior are smaller in the total activation cross sections.

Table 5.7: Unperturbed, mean values and nuclear data uncertainties in neutron spectra-averaged activation cross sections in Fe estimated using random data files in TENDL-2017

Particle production	Statistical parameter	Spectrum-averaged one group cross section (barns)		
		PFBR core centre	ITER-DT	PWR-RPV
(n, x p)	Unperturbed	5.82e-4	4.06e-2	1.95e-3
	Mean ± uncertainty	5.91e-4 ± 7.64e-5 (12.9%)	4.14e-2 ± 6.46e-3 (15.6%)	1.97e-3 ± 2.07e-4 (10.5%)
	Skewness	0.133	0.468	0.04
(n, x d)	Unperturbed	7.66e-8	8.49e-4	2e-6
	Mean ± uncertainty	8.77e-8 ± 2.49e-8 (28.4%)	9.83e-4 ± 3.03e-4 (30.8%)	2.3e-6 ± 6.8e-7 (29.6%)
	Skewness	0.737	0.782	0.74
(n, x t)	Unperturbed	2.3e-10	5.44e-7	5.02e-9
	Mean ± uncertainty	2.77e-10 ± 1.21e-10 (43.6%)	6.74e-7 ± 3.62e-7 (53.7%)	6.04e-9 ± 2.41e-9 (39.9%)
	Skewness	0.757	0.809	0.682
(n, x ^{3}He)	Unperturbed	3.71e-12	7.71e-9	7.02e-11
	Mean ± uncertainty	5.04e-12 ± 2.8e-12 (55.7%)	8.98e-9 ± 3.7e-9 (41.2%)	9.32e-11 ± 4.77e-11 (51.2%)
	Skewness	1.24	1.02	1.26
(n, x α)	Unperturbed	3.13e-5	8.31e-3	2.1e-4
	Mean ± uncertainty	3.22e-5 ± 5.55e-6 (17.2%)	8.69e-3 ± 2.6e-3 (29.9%)	2.17e-4 ± 3.79e-5 (17.5%)
	Skewness	0.36	0.656	0.434
(n, total activation)	Unperturbed	1.21e-2	0.21	7.42e-2
	Mean ± uncertainty	1.2e-2 ± 1.15e-4 (1%)	0.21 ± 7.7e-3 (3.7%)	7.41e-2 ± 3.22e-3 (4.3%)
	Skewness	0.87	-0.045	-0.085

5.7.4 Uncertainty in the concentrations of produced gases

The five different species of gases produced in Fe and their nuclear data uncertainties for different irradiation times in PFBR core centre, ITER-DT and PWR-RPV spectra are estimated from TENDL-2017 by the CRaD code. The uncertainties in the productions of hydrogen and

helium are found to be lower compared to those in the production of deuterium, tritium and helium-3. The distributions of concentrations of gases produced at each time are also found to be skewed. The predicted values of the concentrations of these gases in Fe after about 6.3 years of irradiation in various spectra, along with their associated uncertainties and values of skewness are presented in Table 5.8. The uncertainties and skewness for other time periods of irradiations are also in the similar ranges. The maximum uncertainties in the production of hydrogen, helium, deuterium, tritium and helium-3 are about 16%, 31%, 54%, 56% and 30% respectively. Note that the uncertainties in the concentrations of produced gases and those in the spectra averaged one-group cross sections are comparable to each other.

Table 5.8: Unperturbed, mean values and nuclear data uncertainties in concentrations of gases produced in Fe for 6.3 years of irradiation, estimated using random data files in TENDL-2017

Gas	Statistical parameter	Concentration of gas (appm)		
		PFBR core centre	ITER-DT	PWR-RPV
Hydrogen	Unperturbed	913	1700	4.36e-2
	Mean ± uncertainty	927 ± 119 (12.8%)	1730 ± 270 (15.6%)	4.42e-2 ± 4.64e-3 (10.5%)
	Skewness	0.138	0.453	0.11
Deuterium	Unperturbed	0.121	35.5	4.55e-5
	Mean ± uncertainty	0.139 ± 3.95e-2 (28.4%)	41.1 ± 12.7 (30.8%)	5.16e-5 ± 1.52e-5 (29.5%)
	Skewness	0.737	0.784	0.748
Tritium	Unperturbed	3.62e-4	2.27e-2	1.14e-7
	Mean ± uncertainty	4.38e-4 ± 1.91e-4 (43.7%)	2.81e-2 ± 1.51e-2 (53.7%)	1.36e-7 ± 5.41e-8 (39.9%)
	Skewness	0.754	0.81	0.674
Helium-3	Unperturbed	5.82e-6	3.22e-4	1.56e-9
	Mean ± uncertainty	7.9e-6 ± 4.39e-6 (55.6%)	3.75e-4 ± 1.54e-4 (41.2%)	2.09e-9 ± 1.07e-9 (51.1%)
	Skewness	1.24	1.02	1.27
Helium-4	Unperturbed	49.5	347	4.77e-3
	Mean ± uncertainty	51 ± 8.8 (17.2%)	363 ± 109 (29.9%)	4.86e-3 ± 8.5e-4 (17.5%)
	Skewness	0.334	0.652	0.466

5.8 Uncertainty in neutron kerma coefficients due to nuclear data

The uncertainties in neutron kerma coefficients due to the uncertainties in nuclear data are estimated by using the random ENDF-6 nuclear data files in TENDL-2015. The choice of TENDL-2015 over TENDL-2017 for the present study is decided based on the fact that more detailed data on the distribution of the secondary particles and recoil nuclei are available as a part of TENDL-2015, but not in TENDL-2017 random files (as mentioned earlier in Section 5.5 and 5.6). The neutron kerma cross sections are computed in 175 and 198 energy group structures by using the CRaD code and integrated neutron heating rates for PFBR core centre, ITER-DT and PWR-RPV neutron spectra are estimated (using Eq. 3.8). The integrated neutron heating rates obtained by using the nuclear data from different libraries, such as ENDF/B-VII.1, JENDL-4.0, TENDL-2014 and TENDL-2015 are also compared.

5.8.1 Contributions of partial neutron reactions to kerma uncertainty

Similar to the study described in Section 5.4.1, the uncertainties of nuclear data in the partial reaction-wise neutron kerma coefficients are estimated by using the random files in TENDL-2015. An illustration for the case of irradiation of ^{56}Fe in the PFBR core centre neutron spectrum is presented in Table 5.9 [113]. The unperturbed and mean values of the contributions from different reactions to the neutron heating rates, along with their uncertainties due to nuclear data are calculated. Note, for the PFBR core centre spectrum, most of the neutron heating is due to elastic scattering and inelastic scattering reaction (about 82% and 16% respectively). The uncertainties in neutron heating from these two reactions are about 6% each. The contribution of all other CPO reactions (remaining thresholds) to total neutron heating is only about 1.2%, but it has an uncertainty of about 41%. The uncertainty in total neutron heating in ^{56}Fe is found to be

about 5% for this spectrum. The distribution of neutron heating parameter is also found to be skewed.

Table 5.9: Uncertainties of nuclear data in the partial reaction-wise contributions to neutron kerma in ^{56}Fe for irradiation at PFBR core centre calculated by CRaD using the TENDL-2015

Neutron Heating (W / kg)				
Reactions	Unperturbed value	Mean of random data*	Nuclear data uncertainty	Skewness
Elastic	427	427	23.7(5.55%)	1.3e-3
Inelastic	89.5	86.4	4.89 (5.66%)	-0.54
(n, γ)	5.20e-2	5.35e-2	1.88e-3 (3.51%)	0.17
(n, 2n)	1.81e-2	1.71e-2	3.75e-3 (21.93%)	0.31
Remaining thresholds	4.83	6.17	2.51 (40.68%)	1.66
Total	522	520	24.2 (4.65%)	-1.3e-2

*using random files in TENDL-2015

5.8.2 Comparison of neutron kerma coefficients from different libraries

The uncertainties of nuclear data in the neutron kerma coefficients of a few structural isotopes, viz. ^{56}Fe, ^{58}Ni, ^{28}Si and ^{48}Ti for irradiations in PFBR core centre, ITER-DT and PWR-RPV neutron spectra are calculated by the CRaD code. Approximately, 300 random files (see Table 5.1) for each of these isotopes are used here for propagating the uncertainties. The unperturbed neutron kerma coefficients, their mean values and uncertainties of these isotopes are presented in Table 5.10. The unperturbed values of the neutron kerma coefficients from other basic evaluated nuclear data libraries are also presented here. The uncertainties are found to vary with the neutron spectrum under consideration. The maximum uncertainties estimated are as follows: 28.7% in ^{56}Fe (for ITER-DT), 12.6% in ^{58}Ni (for ITER-DT and PWR-RPV), 9% in ^{28}Si (for ITER-DT) and 20.7% in ^{48}Ti (for ITER-DT). In most of the cases presented here, the estimated neutron kerma coefficients from different libraries are found to be within the uncertainties of nuclear data. However, the neutron kerma coefficients in ^{58}Ni, ^{28}Si and ^{48}Ti in some spectra from ENDF/B-VII.1 and JENDL-4.0 libraries are found to be slightly outside the

ranges of calculated uncertainties. Note, unlike in case of dpa cross sections, material physics parameters are not involved in neutron heating, but the required basic evaluated nuclear data in this case is more in terms of the distributions of charged particles. An estimation of neutron heating rates in ^{56}Fe in PFBR core centre and ITER-DT spectra using the TENDL-2017 random files (where energy distributions of the recoil nucleus are not available) has yielded the nuclear data uncertainties as 2.5%and 12% respectively [127]. This is comparatively lower than the respective uncertainties obtained using the TENDL-2015 random files.

Table 5.10a: Comparison of total neutron kerma coefficient in **^{56}Fe** in various neutron spectra calculated using different basic evaluated nuclear data libraries

Reactor	Neutron Heating (W / kg)				
	E7.1	J4.0	T14[a]	T15	Mean ± uncertainty[b]
PFBR: core centre	518	519	523	522	520 ± 24.2
ITER D–T	136	121	113	112	141 ± 40.5
PWR-RPV	1.06e-2	1.05e-2	1.02e-2	1.02e-2	1.03e-2 ± 4.29e-4

[a]T14 = TENDL 2014, T15 = TENDL-2015; [b] from random files in TENDL-2015

Table 5.10b: Comparison of total neutron kerma coefficient in **^{58}Ni** in various neutron spectra calculated using different basic evaluated nuclear data libraries

Reactor	Neutron Heating (W / kg)				
	E7.1	J4.0	T14	T15	Mean ± uncertainty
PFBR: core centre	1110	915	1090	1090	1070 ± 111
ITER D–T	487	495	492	494	490 ± 61.4
PWR-RPV	3.32e-2	2.45e-2	3.15e-2	3.15e-2	3.10e-2 ± 3.90e-3

Table 5.10c: Comparison of total neutron kerma coefficient in **^{28}Si** in various neutron spectra calculated using different basic evaluated nuclear data libraries

Reactor	Neutron Heating (W / kg) (mean ± uncertainty)				
	E7.1	J4.0	T14	T15	Mean ± uncertainty
PFBR: core centre	2170	2030	2020	2020	2050 ± 70.6
ITER D–T	565	613	583	582	579 ± 52.2
PWR-RPV	4.60e-2	4.09e-2	4.29e-2	4.29e-2	4.33e-2 ± 1.47e-3

Table 5.10d: Comparison of total neutron kerma coefficient in **^{48}Ti** in various neutron spectra calculated using different basic evaluated nuclear data libraries

Reactor	Neutron Heating (W / kg) (mean ± uncertainty)				
	E7.1	J4.0	T14	T15	Mean ± uncertainty
PFBR: core centre	784	837	769	769	756 ± 51.8
ITER D–T	129	147	99.4	99.4	107 ± 22.2
PWR-RPV	1.44e-2	1.49e-2	1.33e-2	1.33e-2	1.30e-2 ± 9.41e-4

5.9 Summary

The TMC methodology is applied with the help of the CRaD code to propagate the uncertainties in nuclear data to the uncertainties in the parameters of primary radiation damage. It is observed that predictions of these parameters by using different basic evaluated nuclear data libraries differ from one another. In such instances, it will be wise to use the mean value of the parameters along with their nuclear data uncertainties which are calculated according to the TMC methodology by using a large number of ENDF-6 random nuclear data files.

The nuclear data uncertainties in total integrated dpa, average PKA energy, damage energy and number of vacancies produced in the material are estimated to be around 6 to 7%. However, the uncertainties in energy-wise variations of dpa cross sections (with neutron energy) and PKA spectra (with recoil energy) are found to be larger and vary with energy. The TMC methodology propagates uncertainty in a non-linear way by incorporating correlations between different nuclear physics parameters. Hence, when applied in a similar way, it can help to understand how the non-negligible correlations between various parameters of the damage energy function and atom-displacement models affect their final uncertainties [119]. The uncertainties in the gas production cross sections and concentrations of gases in elemental Fe are found to vary in the range between 16% and 56%, with the larger uncertainties being observed in

case of tritium and helium-3 gases. The uncertainties in neutron kerma coefficients are found to be in the range of 9 to 29%. The distributions of the parameters of primary radiation damage obtained by using the random ENDF-6 files are found to be non-Gaussian. The energy-energy correlation coefficients of these parameters are found to be non-negligible is some cases, which can be used to fine-tailor basic evaluated nuclear data.

Chapter 6

Summary and Future Scope

6.1 Summary of the thesis

The primary radiation damage phenomena occur in materials in about first 100 picoseconds of the interaction between incoming radiations with matter. It is generally quantified by estimating the damage metrics, viz. PKA spectra, dpa cross sections, gas production cross sections and heating cross sections, by using neutron interaction data from evaluated nuclear data libraries. This study is very important to enable accurate assessment of radiation damage of core structural materials in a nuclear reactor for ensuring its safe and economic operation.

There have been continuous efforts worldwide towards improving the basic evaluated nuclear data, particularly focusing on comprehensive evaluation of the covariances of data and making the evaluations more complete and general purpose. Several collaborative efforts have also been made to model the displacement damage phenomena more realistically and achieve consistency with the observations made in irradiation experiments. These collective efforts and improvements in the basic evaluated nuclear data and modeling of displacement damage quite essentially demand of investigating their effects on the estimation of the metrics of primary radiation damage. There exist a number of basic evaluated nuclear data libraries such as ENDF/B-VII.1, JENDL-4.0, ENDF/B-VIII.0, JEFF-3.3, TENDL-2017, etc. which result from the evaluations using different fundamental nuclear physics models, computer codes, subjective assessments and methodologies by the evaluators of nuclear data. The metrics of primary radiation damage estimated using different such basic evaluated nuclear data libraries show differences among them and have associated uncertainties which are due to nuclear data. The

recently proposed and widely applied TMC methodology is realized as feasible to apply for the propagation of these uncertainties from nuclear data to the metrics of primary damage. It is also observed that the dpa cross sections in polyatomic materials are generally computed unrealistically by weighted addition of individual elemental contributions and alternatively, in a pragmatic approach by considering databases of interactions between different sub-lattices in the Parkin-Coulter method. The latter method is however limited to application only in case of few-component polyatomic materials. Thus, a need is perceived to devise a computationally viable method to estimate dpa cross sections in polyatomic structural materials. However, it is appreciable that a dedicated computational tool is necessary in order to perform the above noted investigations in a detailed manner. There has been a long-standing lack of availability of such a tool. Hence, the requirement of these investigations being self-inspiring, it is targeted to overcome the challenge of developing the computer code needed for the study. In this thesis, the following works are performed to address the above objectives and challenges:

(a) Development of a computer code CRaD

A computer code CRaD is developed to quantify the metrics of primary radiation damage of structural materials by neutrons, viz. PKA spectra, dpa cross sections, production of gases, heating cross sections and their respective spectra-integrated quantities, by using the data in latest basic evaluated nuclear data libraries. It post-processes the neutron cross sections from pre-processed File 3 and other necessary data from Files 1, 4, 5, 6, 12 and 15 of the raw evaluated nuclear data file to estimate the metrics according to the ENDF-6 standard procedures. The databases of these metrics generated using the CRaD code are compiled into a library named as CRaD-PRDL 1.0 for future fast reactor design purposes.

(b) Comparison of CRaD results with standard codes and data

The results of CRaD code are compared with the reported data such as ASTM E693-12 standard dpa cross sections in iron, JEFF-3.3 dpa database, etc.; reported data in literature and other standard codes such as NJOY-2016, NJOY21, RECOIL and SPECTER. The agreements observed in these exercises are satisfactory.

While performing validation of CRaD code with the NJOY-2016 code, a discrepancy is noted in the computation of dpa cross sections using NJOY-2016 code with respect to the application of the complete NRT model. This is illustrated in case of ^{56}Fe. In some cases, it is observed that NJOY-2016.31 and NJOY21 codes generate the (n, p) and (n, α) cross sections (which are incomplete, not containing the continuum contributions), even though they are not completely disentangled in the original evaluation. These are noted in case of isotopes of Fe from ENDF/B-VIII.0 and ^{55}Mn from ENDF/B-VII.1 and ENDF/B-VIII.0.

The neutron heating cross sections computed by applying the direct method in the CRaD code are found to differ with the values obtained from the energy balance method applied in NJOY-2016 code in the incident energy region where contributions from both recoil nucleus and light charged particles to the heating by direct method are important. The direct method as used in CRaD code is found to be advantageous because the heating values are always positive and damage cross sections due to atom-displacement phenomena (where only heavy recoil nuclei are considered) can be compared to the heating cross sections in a more apparent way.

(c) Neutron spectrum dependence of primary radiation damage metrics

The dependences of the damage metrics on neutron spectra are investigated in detail by using the recent basic evaluated nuclear data libraries. The effect of fast and thermal fission and

fusion neutron spectra on the four metrics of primary radiation damage are demonstrated elaborately. The incident neutron spectrum at the location of application of the structural material plays an important role in the determination of the integrated damage parameter. In addition to the neutron spectrum, the neutron energy-wise variations of PKA spectra, dpa cross sections, gas production cross sections and heating cross sections in the particular material also determine the magnitudes of the corresponding spectrum integrated parameters.

(d) Development of a novel method to estimate dpa in polyatomic materials

A new method is proposed to compute neutron dpa cross sections in elemental and polyatomic materials by performing simulations with self-ions using the SRIM-2013 code. This method is envisaged to be useful in correlating the primary radiation damage due to neutrons by using corresponding energy self-ions in the irradiation experiments and modern simulation techniques like MD, BCA, MC, etc. It is shown that the source term of neutron-induced primary radiation damage, i.e. dpa can be determined equivalently by applying the self-ion simulations.

(e) Implementation of arc-dpa model in regular applications

Apart from the NRT model, the improved arc-dpa model is also implemented in the CRaD code to estimate the primary displacement damage in materials. It is shown that the arc-dpa model along with its set of parameters can reproduce the primary damage phenomena as observed in irradiation experiments and realistic simulations. Hence, it is established that this model can be used in regular applications to predict primary radiation damage more realistically, without having to depend on the extensive MD simulations each time.

(f) Proposal for rescaling of measured damage to the improved dpa predictions

The rescaling of experimentally observed changes in the properties of materials (such as hardness, electrical resistivity, swelling, etc.) with the improved values of dpa obtained using the improved nuclear data and displacement damage modeling of materials is necessary in order to be consistent with the recent improvements. The measured parameters of radiation damage can be rescaled with the improved dpa without affecting their designed time limits of operation in the radiation environment.

(g) Nuclear data uncertainties and statistical parameters for primary radiation damage metrics by TMC methodology

The uncertainties of nuclear data in the metrics of primary radiation damage are quantified for a few important structural isotopes by applying the TMC methodology in the indigenously developed code, CRaD. The large number of ENDF-6 random files in TENDL-2015 and TENDL-2017 are used to propagate the uncertainties and random databases of the derived damage metrics are generated. The statistical quantities such as mean, standard deviation, skewness and correlation coefficients of the damage metrics are estimated. The metrics computed using other basic evaluated nuclear data libraries are compared with their corresponding mean values obtained using the random files. In most cases the estimations using different libraries are found to be within the quantified nuclear data uncertainties, with some exceptions. The distributions of the metrics are found to be non-Gaussian. The non-negligible inter-channel and inter-isotope energy-energy correlations of the metrics can be used to adjust and fine-tailor nuclear data to achieve the desired accuracy of derived quantities.

To conclude, this thesis work has successfully developed and validated an indigenous computer code CRaD, which has helped to extensively investigate the effects of improvements in the evaluated nuclear data and displacement damage modeling on the metrics of primary radiation damage. These improvements are found to hold significant impacts in the estimation of the damage metrics. The study has also logically justified the necessity to rescale the measured damage with the improved values of dpa, proposed a new method to compute dpa cross sections in polyatomic materials using self-ion simulations and quantified the nuclear data uncertainties in the damage metrics by applying the TMC methodology.

6.2 Scope of future study

(a) The computer code CRaD can be made to perform calculations in a more efficient manner. The features that can be included to improve its capabilities are as follows:

(i) A detailed study to calculate the spectra of recoil atoms from the nuclear reaction models and measured experimental data in various reactions induced by neutrons and other particles can be made.

(ii) Methodologies to simulate displacement damages in polyatomic targets can be revisited and developed further. The dpa cross sections in materials such D-9 steel, Eurofer97 ferritic steel, etc can be computed by the proposed method of self-ion simulations using the SRIM-2013 code and compared with the existing data from standard method.

(iii) The metrics of primary radiation damage due to other incident particles like proton, deuteron, alpha and gamma can be estimated from the respective nuclear data libraries.

(iv) Methodologies to compute primary radiation damage due to higher (> 20 MeV) energy particles can be developed.

(v) The time-dependent transmutation effects of structural nuclides under various irradiation spectra and the build-up of inventories can be simulated in a detailed manner.

(vi) The effect of energy self-shielding can be included in the calculation of the dpa cross sections, kerma cross sections and gas production rates.

(vii) The energy balance method to compute neutron heating cross sections can be developed.

(b) The library CRaD-PRDL 1.0 can be extended further by performing computation of the metrics of primary radiation damage for more materials from different ENDF-6 libraries and also by developing the methodologies discussed in points (a) (i) to (vii).

(c) The uncertainties in dpa cross sections due to uncertainties in the parameters of PKA energy partition function and in the parameters of atom displacement damage models can be rigorously quantified. The knowledge of the probability distributions of these material physics model parameters can help to perform the propagation of these uncertainties by an approach similar to that of the TMC methodology.

(d) Experiments to measure the heating, production of gases and displacement damage due to interactions of neutrons in structural materials can be carried out to validate the theories and models that are developed in the CRaD code.

(e) The self-ion plus arc-dpa methodology can be extended for the important polyatomic materials by finding their corresponding model parameters.

Appendix A: Typical Energy Group Structure

The point cross sections data have been multigrouped into various energy group structures for applications in different neutron spectra. A typical energy group structure used in the study is presented in Table A.1, for illustration.

Table A.1: The 100 energy group structure [43]

Group Number	Neutron energy (eV)	Group Number	Neutron energy (eV)	Group Number	Neutron energy (eV)	Group Number	Neutron energy (eV)
1	1.00E-04	31	5.70E+02	61	4.00E+05	91	1.00E+07
2	1.00E-03	32	7.60E+02	62	4.50E+05	92	1.10E+07
3	1.00E-02	33	9.60E+02	63	5.00E+05	93	1.20E+07
4	2.30E-02	34	1.28E+03	64	5.50E+05	94	1.30E+07
5	5.00E-02	35	1.60E+03	65	6.00E+05	95	1.40E+07
6	7.60E-02	36	2.00E+03	66	6.60E+05	96	1.50E+07
7	1.10E-01	37	2.70E+03	67	7.20E+05	97	1.60E+07
8	1.70E-01	38	3.40E+03	68	7.80E+05	98	1.70E+07
9	2.50E-01	39	4.50E+03	69	8.40E+05	99	1.80E+07
10	3.80E-01	40	5.50E+03	70	9.20E+05	100	1.90E+07*
11	5.50E-01	41	7.20E+03	71	1.00E+06		
12	8.40E-01	42	9.20E+03	72	1.20E+06		
13	1.28E+00	43	1.20E+04	73	1.40E+06		
14	1.90E+00	44	1.50E+04	74	1.60E+06		
15	2.80E+00	45	1.90E+04	75	1.80E+06		
16	4.20E+00	46	2.50E+04	76	2.00E+06		
17	6.30E+00	47	3.20E+04	77	2.30E+06		
18	9.20E+00	48	4.00E+04	78	2.60E+06		
19	1.30E+01	49	5.20E+04	79	2.90E+06		
20	2.10E+01	50	6.60E+04	80	3.30E+06		
21	3.00E+01	51	8.80E+04	81	3.70E+06		
22	4.50E+01	52	1.10E+05	82	4.10E+06		
23	6.90E+01	53	1.30E+05	83	4.50E+06		
24	1.00E+02	54	1.60E+05	84	5.00E+06		
25	1.30E+02	55	1.90E+05	85	5.50E+06		
26	1.70E+02	56	2.20E+05	86	6.00E+06		
27	2.20E+02	57	2.50E+05	87	6.70E+06		
28	2.80E+02	58	2.90E+05	88	7.40E+06		
29	3.60E+02	59	3.20E+05	89	8.20E+06		
30	4.50E+02	60	3.60E+05	90	9.00E+06		

*upper limit = 2.00E+07

References

[1] H. Ullmaier, W. Schilling, In: Physics of Modern Materials, vol. I; IAEA, Vienna, 1980.

[2] G.S. Was, In: *Fundamentals of Radiation Materials Science*; Springer: New York, 2007.

[3] F. A. Garner, *Comprehens. Nucl. Mater.* 4 (2012) 33 – 95.

[4] L.R. Greenwood, D.W. Kneff, R.P. Skowronski, *J. Nucl. Mater.* 122 & 123 (1984) 1002 – 1010.

[5] R.V. Nandedkar, W. Kesternich, *J. Nucl. Mater.* 62 (1989) 329

[6] D.W. Kneff, et al., *J. Nucl. Mater.* 141 – 143 (1986) 824 – 828.

[7] R.C. Haight, et al., *Nucl. Sci. Engg*. 124 (1996) 219 – 227.

[8] Y. Ikeda, et al., *Fus. Tech.* 21 (1992) 2190 – 2196.

[9] Y. Ikeda, et al., *Fus. Engg. Des.* 42 (1998) 289 – 297.

[10] A. Kumar, et al., *Fus. Engg. Des.* 18 (1991) 397 – 405.

[11] U.J. Schrewe, et al., *Phys. Med. Biol.* 45 (2000) 651 – 683.

[12] F. Seitz, *Discussions Faraday Soc.* 5 (1949) 271 – 282.

[13] W.S. Snyder and J. Neufeld, *Phys. Rev.* 97 (1955) 1636 – 1646.

[14] G.H. Kinchin, R.S. Pease, *Rep. Prog. Phys.*18 (1) (1955) 1 – 51.

[15] J. Lindhard, V. Nielsen, M. Scharff, P.V. Thomsen, *Mat. Fys. Medd. Dan. Vid. Selsk.* 33 (10) (1963).

[16] J. Lindhard, M. Scharff, H. E. Schiøtt, *Mat. Fys. Medd. Dan. Vid. Selsk*. 33 (14) (1963) 1 – 42.

[17] M.T. Robinson, I.M. Torrens, *Phys. Rev. B* 9 (1974) 5008 – 5024.

[18] M.J. Norgett, M.T. Robinson, I.M. Torrens, *Nucl. Engg. Des.* 33 (1975) 50 – 54.

[19] ASTM E693-12, Standard Practice for Charactersing Neutron Exposures in Iron and Low Alloy Steels in Terms of Displacements Per Atom (DPA), E 706 (ID).

[20] K. Nordlund, et al., "Primary Radiation Damage in Materials", *Report Nuclear Science NEA/NSC/DOC (2015) 9*, OECD/NEA, 2015.

[21] V. Kumar, Nagendra Singh Raghaw, H.S. Palsania, *Nucl. Sci. Engg.* 172 (2012) 151 – 163.

[22] K. Nordlund, et al., *Nature Communications* (2018) 9:1084. DOI: 10.1038/s41467-018-03415-5.

[23] K. Nordlund, et al., *J. Nucl. Mater.* 512 (2018) 450 – 479.

[24] C.H.M. Broeders, A.Yu. Konobeyev *J. Nucl. Mater*. 328 (2004) 197 – 214.

[25] A.Yu. Konobeyev et al., *Nuclear Energy and Technology* 3 (2017) 169 – 175.

[26] T.A. Gabriel, J.D. Amburgey, N.M. Greene, "Radiation Damage Calculations: Primary Recoil Spectra, Displacement Rates, and Gas Production Rates", *Report ORNL/TM – 5160*, Oak Ridge National Laboratory, 1976.

[27] L.R. Greenwood, R.K. Smither, "SPECTER: Neutron Damage Calculations for Materials Irradiations", *Report ANL/FPP/TM-197*, Argonne National Laboratory, 1985.

[28] L.R. Greenwood, *J. Nucl. Mater*. 216 (1994) 29 – 44.

[29] A.C. Kahler (Ed.), "The NJOY Nuclear Data Processing System, Version 2016", *Report LA-UR-17-20093*, Los Alamos National Laboratory, 2016.

[30] M. Harada et al., *J. Nucl. Mater*. 343 (2005) 197 – 204.

[31] M.R. Gilbert, J. Marian, J.-Ch. Sublet, *J. Nucl. Mater*. 467 (2015) 121 – 134.

[32] M.R. Gilbert, J.-Ch. Sublet, *J. Nucl. Mater*. 504 (2018) 101 – 108.

[33] J.-Ch. Sublet, et al., *Nuclear Data Sheets* 139 (2017) 77 – 137.

[34] M.A. Abdou, C.W. Maynard, *Nucl. Sci. Engg.* 56 (1975) 360 – 380.

[35] Li Zhang, M.A. Abdou, *Fus. Engg. Des.* 36 (1997) 479 – 503.

[36] D.J. Mazey, *J. Nucl. Mater.* 174 (1990) 196 – 209.

[37] C. Abromeit, *J. Nucl. Mater.* 216 (1994) 78 – 96.

[38] C. David, et al., *J. Nucl. Mater.* 383 (2008) 132 – 136.

[39] G.S. Was, et al., *Scripta Mater.* 188 (2014) 33 – 36.

[40] J.F. Ziegler, J.P. Biersack, U. Littmark, *The Stopping and Range of Ions in Solid;* Pergamon Press: New York, 1985. http://www.srim.org/SRIM/SRIMLEGL.htm

[41] R.E. Stoller, et al., *Nucl. Instrum. Methods* B310 (2013) 75 – 80.

[42] R. Devanathan, W.J. Weber, *J. Nucl. Mater.* 278 (2000) 258 – 265.

[43] H.L. Heinisch, et al., *J. Nucl. Mater.* 327 (2004) 175 – 181.

[44] D.M. Parkin, C.A. Coulter, *J. Nucl. Mater*. 85 – 86 (1979) 611 – 615.

[45] D.M. Parkin, C.A. Coulter, *J. Nucl. Mater*. 101 (1981) 261 – 276.

[46] D.M. Parkin, C.A. Coulter, *J. Nucl. Mater*. 103 – 104 (1981) 1315 – 1318.

[47] D.M. Parkin, C.A. Coulter, *J. Nucl. Mater*. 117 (1983) 340 – 344.

[48] L. R. Greenwood, *J. Nucl. Mater.* 115 (1983) 137 – 142.

[49] L. R. Greenwood, et al., *J. Nucl. Mater.* 122 & 123 (1984) 1002 – 1010.

[50] V. Gopalakrishnan, R.V. Nandedkar, S. Ganesan, *J. Nucl. Mater.* 228 (1996) 207 – 214.

[51] IAEA Summary documentation: IAEA-NDS-11, Rev. 5.

[52] IAEA Summary documentation: IAEA-NDS-23, Rev. 3.

[53] B. Goel and B. Krieg, Status of the Nuclear Data Library KEDAK-4, October 1984, *Report KFK-3838* (1985), IAEA Summary documentation: IAEA-NDS-21, Rev. 4.

[54] IAEA Summary documentation: IAEA-NDS-100, Rev. 3.

[55] IAEA Summary documentation: IAEA-NDS-18, Rev. 3.

[56] L. K. Mansur, et al., *J. Nucl. Mater.* 139 (1986) 228 – 236.

[57] D. Rochman, et al., *EPJ Web of Conferences* 146, 02006 (2017).

[58] D.A. Brown, et al., *Nuclear Data Sheets* 148 (2018) 1 – 142.

[59] A.J. Koning, D. Rochman, *Nuclear Data Sheets* 113 (2012) 2841 – 2934.

[60] A.J. Koning, S. Hilaire and M.C. Duijvestijn, "TALYS-1.0", Proceedings of the International Conference on Nuclear Data for Science and Technology, April 22-27, 2007, Nice, France, Editors O. Bersillon, F. Gunsing, E. Bauge, R. Jacqmin and S. Leray, EDP Sciences, 211 (2008). www.talys.eu.

[61] D.L. Smith, "Covariance Matrices for Nuclear Cross Sections Derived from Nuclear Model Calculations", *Report ANL/NDM-159*, Argonne National Laboratory, 2004.

[62] A.J. Koning, D. Rochman, *Ann. Nucl. Energy* 35 (2008) 2024 – 2030.

[63] R. Capote et al., *Nuclear Data Sheets* 110 (2009) 3107 – 3214.

[64] N. Otuka et al., *Nuclear Data Sheets* 120 (2014) 272 – 276.

[65] D. Rochman, A.J. Koning, S.C. van der Marck, *Ann. Nucl. Energy* 36 (2009) 810 – 831.

[66] D. Rochman et al., *J. Korean Phys. Soc.* 59 (2011) 1236 – 1241.

[67] D. Rochman, A.J. Koning, S.C. van der Marck, *J. Korean Phys. Soc.* 59 (2011) 1386 – 1389.

[68] D. Rochman et al., *Nucl. Instrum. Methods. A* 612 (2010) 374 – 387.

[69] D. Rochman, A.J. Koning, D.F. Da Cruz, *J. Nucl. Sci. Tech.*48 (2011) 1193 – 1205.

[70] Mihaela Ionescu-Bujor, Dan G. Cacuci, *Nucl. Sci. Eng.*147 (2004) 189 – 203.

[71] P. Griffin, D. Rochman, A.J. Koning, *EPJ Web of Conferences* 146, 02008 (2017). DOI: 10.1051/epjconf/201714602008

[72] S.P. Simakov, A.J. Koning, A.Yu. Konobeyev, *EPJ Web of Conferences* 146, 02012 (2017). DOI: 10.1051/epjconf/201714602012

[73] https://www-nds.iaea.org/CRPdpa/

[74] The Joint Evaluated Fission and Fusion File, JEFF-3.3. https://www.oecd-nea.org/dbdata/jeff/

[75] https://www-nds.iaea.org/

[76] K. Shibata, et al., *J. Nucl. Sci. Technol.* 48(1) (2011) 1 – 30.

[77] A.Yu. Konobeyev, U. Fischer, P.E. Pereslavtsev, *KERNTECHNIK* 80 (2015) 1, 7 – 12.

[78] Uttiyoarnab Saha, K. Devan, *Materials Today: Proceedings* 5 (2018) 16501–16508.

[79] M. Herman, A. Trkov (Eds.), ENDF-6 Formats Manual, *CSEWG Document ENDF-102, Report BNL-90365-2009 Rev.1*, Brookhaven National Laboratory, 2010.

[80] V. Gopalakrishnan, "Tools in RPD for the computation of DPA", *Report RPD/NDS/96*, Indira Gandhi Centre for Atomic Research, 2001.

[81] https://github.com/njoy/NJOY2016

[82] Koji Niita et al., *Radiation Measurements* 41 (2006) 1080 – 1090.

[83] Uttiyoarnab Saha, K. Devan, *Proceedings of the DAE-BRNS Symp. on Nucl. Phys*. 61 (2016) 644 – 645.

[84] Uttiyoarnab Saha, K. Devan, *Proceedings of the DAE-BRNS Symp. on Nucl. Phys.* 62 (2017) 1142 – 1143.

[85] Jeremy Lloyd Conlin, et al., *EPJ Web of Conferences*146, 09040 (2017). DOI: 10.1051/epjconf/201714609040

[86] D.E. Cullen, "PREPRO 2018: 2018 ENDF/B Pre-processing Codes", report IAEA-NDS-39, Rev. 18, June 20, 2018.

[87] Junhyun Kwon, Yong Hee Choi, Gyeong-Geun Lee, "Calculation of Primary Radiation Damage Parameters using ENDF/B-VII: Recoil Spectra &Damage Cross Section", 2nd Research Coordination Meeting on Primary Radiation Damage Cross-Section, Vienna, Austria, June 29 – July 2, 2015.

[88] G. H. Kinchin and R. S. Pease, *J. Nucl. Energy* 1 (1955) 200 – 202.

[89] K. Nordlund et al., *Phys. Rev. B* 57 (1998) 7556 – 7570.

[90] R.S. Averback, R. Benedek, K.L. Merkle, *Phys. Rev. B* 18 (1978) 4156 – 4171.

[91] D.J. Bacon, F. Gao, Yu.N. Osetsky, *Nucl. Instrum. Methods* 153 (1999) 87 – 98.

[92] P. Jung, *J. Nucl. Mater.* 117 (1983) 70 – 77.

[93] J.H. Kinney, M.W. Guinan, Z.A. Munir, *J. Nucl. Mater.* 123 (1984) 1028 – 1032.

[94] S.J. Zinkle, B.N. Singh, *J. Nucl. Mater.* 199 (1993) 173 – 191.

[95] L. Malerba, *J. Nucl. Mater*. 351 (2006) 28 – 38.

[96] M. Herman, et al., *Nuclear Data Sheets* 108 (2007) 2655 – 2715.

[97] Lahey / Fujitsu Fortran 95 User's Guide, Revision C.

[98] Uttiyoarnab Saha, et al., *Pramana – J. Phys.* 90 (2018) 46.

[99] Uttiyoarnab Saha, K. Devan, S. Ganesan, *J. Nucl. Mater.* 510 (2018) 43 – 60.

[100] Uttiyoarnab Saha, K. Devan, S. Ganesan, *J. Nucl. Mater.* 519 (2019) 88 – 103.

[101] Uttiyoarnab Saha, K. Devan, "Validation of Neutron DPA Cross Sections, Heating Cross Sections and PKA Spectra computed using the CRaD code", *Report: IGC-RDG/RND/CPS/198, 2019.*

[102] M. Kiritani, *J. Nucl. Mater*. 191 – 194 (1992) 125 – 131.

[103] M.T. Robinson, *J. Nucl. Mater*. 216 (1994) 1 – 28.

[104] S.J. Zinkle, (2012). Radiation-induced effects on microstructure. In *Comprehensive Nuclear Materials* (Vol. 1, pp. 65 – 98). Elsevier Ltd.

[105] G.S. Was and R.S. Averback, (2012). Radiation damage using ion beams. In *Comprehensive Nuclear Materials* (Vol. 1, pp. 195 – 221). Elsevier Ltd. DOI: 10.1016/B978-0-08-056033-5.00007-0.

[106] P. Puthiyavinayagam et al., *Prog. Nucl. Eng.* 101 (2017) 19 – 42.

[107] http://fispact.ukaea.uk/wiki/Reference_input_spectraX

[108] Uttiyoarnab Saha, K. Devan, S. Ganesan, *J. Nucl. Mater.* 522 (2019) 86 – 96.

[109] K.L. Merkle et al., *J. Nucl. Mater.* 117 (1983) 4 – 11.

[110] Jeremie Lefevre, et al., *J. Appl. Phys.* 105 (2009) 023520.

[111] G.L. Montet and G.E. Meyers *Carbon* 9 (1971) 179 – 183.

[112] Uttiyoarnab Saha, K. Devan, "Processing of gas production cross sections of isotopes of Fe from ENDF/B-VIII.0 using CRaD, NJOY-2016.31 and NJOY21 codes", *Report: IGC-RDG/RND/CPS/192, 2019.*

[113] Uttiyoarnab Saha, K. Devan, "An Estimation of the Neutron Heating Rates in Structural Materials and their Uncertainties due to Basic Evaluated Nuclear Data", *(under review in Progress in Nuclear Energy).*

[114] Uttiyoarnab Saha, K. Devan, S. Ganesan, *J. Nucl. Mater.* 503 (2018) 30 – 41.

[115] F. Gao and W. J. Weber, *Phys. Rev. B* 63 (2001) 054101.

[116] W.A. Rhoads and R.L. Childs, *Nucl. Sci. Engg.* 99 (1988) 88 – 89.

[117] P. Mohanakrishnan, *Ann. Nucl. Energy* 35 (2008) 158 – 166.

[118] https://www-nds.iaea.org/public/download-endf/DXS/

[119] P. Griffin, "A rigorous treatment of uncertainty quantification for Silicon damage metrics", In *Summary Report of the Technical Meeting*, "Nuclear Reaction Data and Uncertainties for Radiation Damage", INDC (NDS)-0719, IAEA Headquarters, Vienna, Austria, June 2016.

[120] S.P. Simakov et al., Damage Cross Sections and Uncertainties for Natural Iron. https://www-nds.iaea.org/CRPdpa/RCM3_Presentations/5_Simakov.pdf

[121] D. Rochman et al., *Ann. Nucl. Energy* 38 (2011) 942 – 952.

[122] D. Rochman et al., *Ann. Nucl. Energy* 112 (2018) 236 – 244.

[123] P. Helgesson, H. Sjöstrand, D. Rochman, *Nuclear Data Sheets* 145 (2017) 1 – 24.

[124] H. Sjöstrand et al., *Radiation Protection Dosimetry* 161 (1 - 4) (2014) 312 – 315.

[125] M.B. Chadwick et al., *Nuclear Data Sheets* 112 (2011) 2887 – 2996.

[126] B. Efron, *The Canadian Journal of Statistics* 9 (1981) 139 – 172.

[127] Uttiyoarnab Saha, K. Devan, *Proceedings of the DAE-BRNS Symp. On Nucl. Phys.* 63 (2018) 1116 – 1117.